

**BIOMECHANICAL CHARACTERISTICS  
OF THE OSTEOARTHRITIS KNEE**

James Naim

Bachelor of Engineering  
Mechatronic Engineering Major



Department of Mechatronic Engineering  
Macquarie University

November 6, 2017

Supervisor: Dr Dane Turner



## **ACKNOWLEDGMENTS**

I would like to acknowledge the guidance of both Dr. Dane Turner and Dr. Joseph Cadman for their ongoing support throughout my research thesis project. Further to this I would like to give a special thank you to Jeffrey Min, a colleague at my industry experience, who has provided consistent direction and improvements of the results yielded. All participants and patients who were a part of this research project are also greatly appreciated for their efforts and allowing the scientific community to broaden their knowledge in this area of study. I would like to thank Peter Thoms and Quoc Nguyen who have played a major role as part of the team at the Faculty of Medicine and Health Sciences and have been a source of tremendous and invaluable help and support. Finally, to my family for supporting me since the beginning and continuing to be the foundation of strength which allowed me to make it all the way to completing my university studies, thank you endlessly.





## **STATEMENT OF CANDIDATE**

I, James Naim, declare that this report, submitted as part of the requirement for the award of Bachelor of Engineering in the Department of Mechatronic Engineering, Macquarie University, is entirely my own work unless otherwise referenced or acknowledged. This document has not been submitted for qualification or assessment at any academic institution.

Student's Name: James Naim

Student's Signature: James Naim (electronic)

Date: 6 November, 2017



## **ABSTRACT**

Biomechanical characteristics of the osteoarthritis knee joint is an area of increasing interest in clinical studies. Prevalence of knee osteoarthritis is on the rise across the globe, a statistic particularly shared in Australia. The biomechanical characteristics include the joint angles and joint moments of the knee that can be measured from a subject by the process of gait analysis. Gait analysis requires a motion capture system and a force plate system where the inverse kinematics and the inverse dynamics of the gait data obtained can be calculated. Data processing is a key element of this report which requires the relevant information to be accurately and efficiently processed. Filtering techniques are implemented within this study to reduce the noise and increase the accuracy of the results.



# Contents

Acknowledgments	iii
Abstract	vii
Table of Contents	ix
List of Figures	xiii
List of Tables	xvii
<b>1 Abbreviations</b>	<b>1</b>
<b>2 Introduction</b>	<b>3</b>
2.1 Gait Analysis Motion Capture Method . . . . .	3
2.2 Project Outline . . . . .	4
<b>3 Literature Review</b>	<b>7</b>
3.1 Knee Osteoarthritis . . . . .	7
3.2 Gait . . . . .	7
3.2.1 Gait Events . . . . .	8
3.3 Gait Analysis . . . . .	10
3.3.1 Skin Reflective Marker Setup . . . . .	10
3.3.2 Bone Pin Setup . . . . .	11
3.3.3 Inertial Measurement Units . . . . .	12
3.3.4 Microsoft Kinect v2 . . . . .	13
3.4 Optimal Marker Sets . . . . .	14
3.4.1 Helen Hayes . . . . .	14
3.4.2 Modified Helen Hayes . . . . .	14
3.4.3 Clustered Marker set . . . . .	15
3.5 Biomechanics of the Knee . . . . .	15
3.6 Biomechanics Results . . . . .	16
3.6.1 Joint Angles . . . . .	16
3.6.2 Joint Moments . . . . .	17
3.7 Signal Processing . . . . .	18

3.7.1	Butterworth Filter . . . . .	18
3.7.2	Exponential Filter . . . . .	19
<b>4</b>	<b>Methodology . . . . .</b>	<b>21</b>
4.1	Subjects . . . . .	21
4.2	Gait Analysis Data Collection . . . . .	21
4.2.1	Motion Capture Method . . . . .	21
4.2.2	Retro-reflective Marker Placement . . . . .	22
4.2.3	Gait Events . . . . .	24
4.3	Biomechanical Calculations . . . . .	25
4.3.1	Kinematics . . . . .	25
4.3.2	Kinetics . . . . .	30
4.4	Data Processing . . . . .	34
4.4.1	Vicon Nexus . . . . .	34
4.4.2	OpenSim . . . . .	36
4.5	Data Processing Automation . . . . .	37
4.5.1	Matlab . . . . .	37
4.6	Signal Processing . . . . .	38
4.6.1	Butterworth Filter . . . . .	38
4.7	Flow Chart . . . . .	39
<b>5</b>	<b>Results . . . . .</b>	<b>41</b>
5.1	Inverse Kinematics . . . . .	42
5.1.1	Walking . . . . .	42
5.1.2	Stair Ascent . . . . .	44
5.1.3	Stair Descent . . . . .	46
5.2	Inverse Dynamics . . . . .	48
5.2.1	Walking . . . . .	48
5.2.2	Stair Ascent . . . . .	50
5.2.3	Stair Descent . . . . .	51
5.3	Temporal Spatial Parameters . . . . .	52
5.4	Signal Processing . . . . .	53
5.4.1	Marker Trajectories . . . . .	53
5.4.2	Ground Reaction Forces . . . . .	56
<b>6</b>	<b>Discussion . . . . .</b>	<b>59</b>
6.1	Walking . . . . .	59
6.2	Stair Ascent . . . . .	60
6.3	Stair Descent . . . . .	61
6.4	Signal Processing . . . . .	62
6.4.1	Butterworth Filter . . . . .	62
6.5	Data Processing . . . . .	66
6.6	Problems and Solutions . . . . .	67

<i>CONTENTS</i>	<b>xi</b>
6.7 Limitations . . . . .	69
<b>7 Conclusion</b>	<b>71</b>
<b>8 Future Work</b>	<b>73</b>
<b>A Data Processing Automation</b>	<b>75</b>
A.1 Overview . . . . .	75
A.2 TRC File - Automated File Format Reconstruction . . . . .	75
A.3 CSV to GRF Converter - Unfiltered Force Plate Data . . . . .	79
A.4 CSV to GRF Converter - Filtered Force Plate Data . . . . .	85
A.5 Signal Processing - TRC File BW Filter . . . . .	92
A.6 Filtered TRC - Final Format Reconstruction . . . . .	94
A.7 Signal Processing - CSV to GRF BW Filter . . . . .	96
A.8 Post Processing Automation . . . . .	103
<b>B Marker Sets</b>	<b>111</b>
B.1 Overview . . . . .	111
B.2 Helen Hayes . . . . .	111
B.3 Modified Helen Hayes . . . . .	112
<b>C Results</b>	<b>113</b>
C.1 Inverse Kinematics . . . . .	113
C.1.1 Walking . . . . .	113
C.1.2 Stair Ascent . . . . .	118
C.1.3 Stair Descent . . . . .	123
C.2 Inverse Dynamics . . . . .	128
C.2.1 Walking . . . . .	128
C.2.2 Stair Ascent . . . . .	133
C.2.3 Stair Descent . . . . .	137
<b>D Attendance Form</b>	<b>143</b>
D.1 Overview . . . . .	143
D.2 Consultation Meeting Attendance Form . . . . .	143
<b>Bibliography</b>	<b>143</b>





## List of Figures

3.1	Complete gait cycle [9]. . . . .	8
3.2	Stair ascent stance phase [6]. . . . .	9
3.3	Retro-reflective markers placed on anatomical positions of subject. . . . .	11
3.4	Biomechanics of the knee joint [23]. . . . .	15
3.5	OA vs Healthy Knee Flexion Angle for walking trial [24]. . . . .	16
3.6	OA vs Healthy EKAM for walking trial [24]. . . . .	17
4.1	Modified Helen Hayes marker set. . . . .	23
4.2	Portable stair case with portable force plate. . . . .	25
4.3	Gait2392 Model with muscles attached. . . . .	26
4.4	Gait2392 Model with no muscles attached. . . . .	26
4.5	Knee joint centre [29]. . . . .	28
4.6	Joint centre locations [29]. . . . .	29
4.7	Knee flexion angle. . . . .	30
4.8	Kistler force plate centre of pressure [30]. . . . .	31
4.9	GRF characteristics. . . . .	32
4.10	Cardan transformation of three rotations about the x,y,z axes [30]. . . . .	33
4.11	Vicon Nexus software platform capture space with virtual markers of subject before labelling. . . . .	35
4.12	Final Vicon Nexus labelled virtual model of subject. . . . .	35
4.13	Final scaled OpenSim model. . . . .	36
4.14	Process flow chart which displays all the steps taken to complete the gait data collection and analysis of a single subject. . . . .	39
5.1	Walking KFA plot for OA vs Control subjects. Contains one representative walking trial from each subject. Skeleton models demonstrate the gait events occurring at 0, 60 and 100% of gait cycle, indicated by red lines. Orange lines represent control data while the black lines denote OA data. Displays the max, min and RoM regions. . . . .	43
5.2	Mean and SD of walking KFA for OA and control individuals. Mean is represented by the rectangle box and SD is shown by an error bar. Red asterisk denotes statistical significance. OA and control subjects are identified as the blue and orange box, respectively. . . . .	44

5.3	Stair Ascent KFA plot for OA vs Control subjects. Contains one representative stepping up trial from each subject. Skeleton models demonstrate the gait events occurring at 0, 25, 85 and 100% of stance phase, indicated by red lines. Orange lines represent control data while the black lines denote OA data. . . . .	45
5.4	Mean and SD of stepping up KFA for OA and control individuals. Mean is represented by the rectangle box and SD is shown by an error bar. Red asterisk denotes statistical significance. OA and control subjects are identified as the blue and orange box, respectively. . . . .	46
5.5	Stair Descent KFA plot for OA vs Control subjects. Contains one representative stepping down trial from each subject. Skeleton models demonstrate the gait events occurring at 0, 25, 85 and 100% of stance phase, indicated by red lines. Orange lines represent control data while the black lines denote OA data. . . . .	47
5.6	Mean and SD of stepping down KFA for OA and control individuals. Mean is represented by the rectangle box and SD is shown by an error bar. Red asterisk denotes statistical significance. OA and control subjects are identified as the blue and orange box, respectively. . . . .	47
5.7	Walking KFM plot for OA vs Control subjects. Contains one representative walking trial from each subject. Skeleton models demonstrate the gait events occurring at 0 and 100% of stance phase, indicated by red lines. Orange lines represent control data while the black lines denote OA data. . . . .	49
5.8	Stair Ascent KFM plot for OA vs Control subjects. Contains one representative stepping up trial from each subject. Skeleton models demonstrate the gait events occurring at 0, 25, 85 and 100% of stance phase, indicated by red lines. Orange lines represent control data while the black lines denote OA data. . . . .	50
5.9	Stair Descent KFM plot for OA vs Control subjects. Contains one representative stepping down trial from each subject. Skeleton models demonstrate the gait events occurring at 0, 15, 85 and 100% of stance phase, indicated by red lines. Orange lines represent control data while the black lines denote OA data. . . . .	51
5.10	Mean and SD of walking TSPs for OA and control individuals. Mean is represented by the rectangle box and SD is shown by an error bar. Red asterisk denotes statistical significance. OA and control subjects are identified as the blue and orange box, respectively. . . . .	52
5.11	Plot of filtered vs UF marker trajectory data in the x direction at different cut-off frequencies. . . . .	53
5.12	Plot of filtered vs UF marker trajectory data in the y direction at different cut-off frequencies. . . . .	54
5.13	Plot of filtered vs UF marker trajectory data in the z direction at different cut-off frequencies. . . . .	55

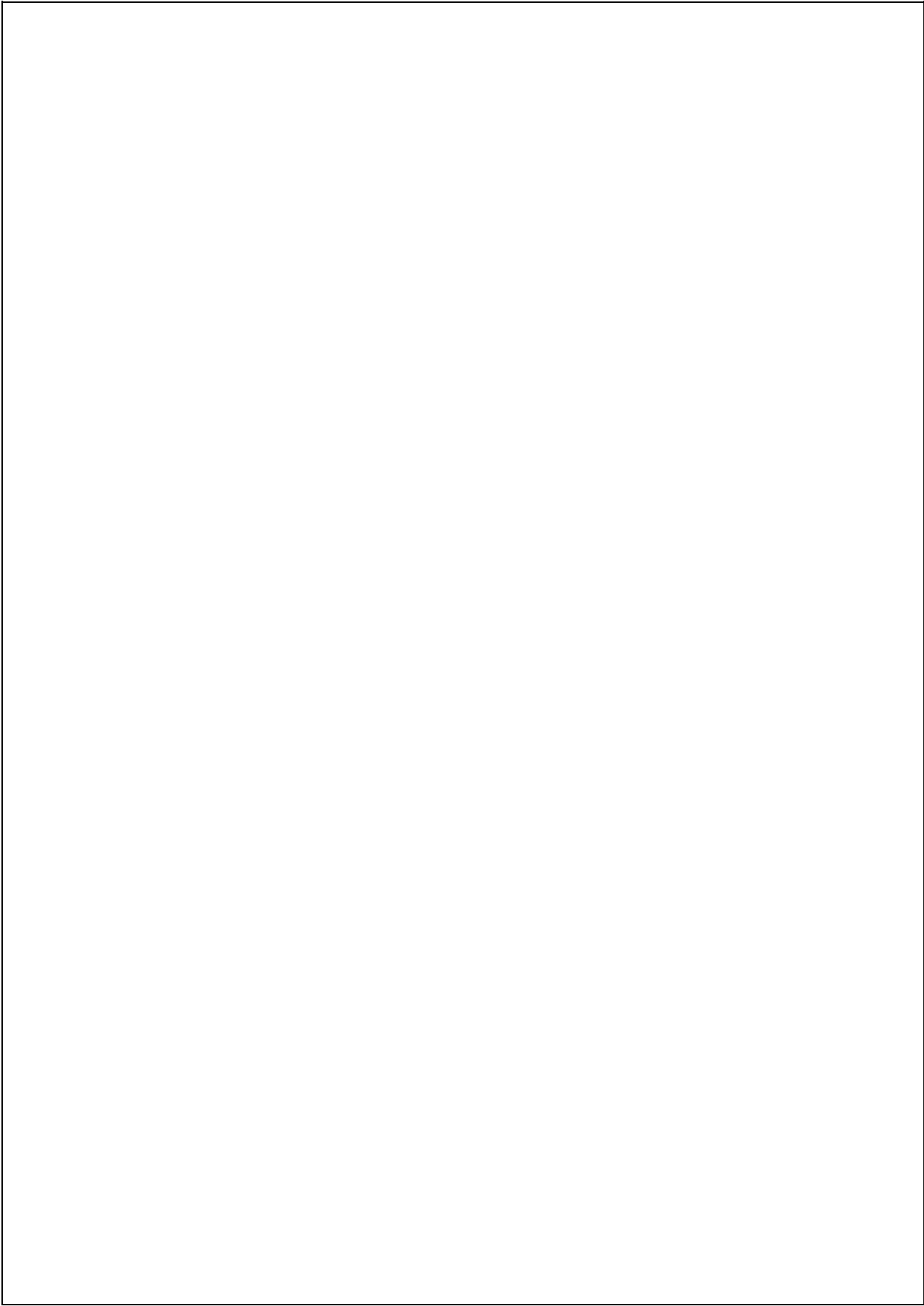
---

5.14	Plot of filtered vs UF GRF data in the x direction at different cut-off frequencies. . . . .	56
5.15	Plot of filtered vs UF GRF data in the y direction at different cut-off frequencies. . . . .	57
5.16	Plot of filtered vs UF GRF data in the z direction at different cut-off frequencies. . . . .	58
6.1	Vicon Nexus displaying a rippled or zig-zag like marker trajectory. . . . .	62
6.2	Plot of filtered vs UF GRF data in the z direction at different cut-off frequencies over a short time frame. . . . .	65



# List of Tables

5.1	Comparison of walking KFA characteristics between OA and control subjects. A bold font p-value signifies statistical significance. . . . .	43
5.2	Comparison of stepping up KFA characteristics between OA and control subjects. A bold font p-value signifies statistical significance. . . . .	45
5.3	Comparison of stepping down KFA characteristics between OA and control subjects. A bold font p-value signifies statistical significance. . . . .	46
5.4	Comparison of walking TSPs between OA and control subjects. A bold font p-value signifies statistical significance. . . . .	52



# Chapter 1

## Abbreviations

OA	Osteoarthritis
BW	Butterworth
UF	Unfiltered
STA	Soft Tissue Artefact
IR	Infra-red
COP	Centre of Pressure
ROM	Range of Motion
MAX	Maximum
MIN	Minimum
TSP	Temporal Spatial Parameters
GRF	Ground Reaction Force
TUG	Timed Up and Go
BMI	Body Mass Index
FP	Force Plate
FS	Foot Strike
FO	Foot Off
IMU	Inertial Measurement Unit
AHRS	Attitude and Heading Reference System
HJC	Hip Joint Centre
KJC	Knee Joint Centre
AJC	Ankle Joint Centre
KFA	Knee Flexion Angle
KFM	Knee Flexion Moment
DOF	Degree of Freedom
HH	Helen Hayes
ASIS	Anterior Superior Iliac Spine
PSIS	Posterior Superior Iliac Spine
EKAM	External Knee Adduction Moment
KAAI	Knee Adduction Angular Impulse
HH	Helen Hayes

ASIS	Anterior Superior Iliac Spine
PSIS	Posterior Superior Iliac Spine
KAM	Knee Adduction Moment
$f_c$	Cut-Off Frequency
TKA	Total Knee Arthroplasty



# Chapter 2

## Introduction

Osteoarthritis (OA) is the most common chronic condition of the joints in the human body [1]. It is important due to the large number of people who deal with this degenerative joint disease which progressively worsens over time [2]. The causes of knee OA include age, heredity, gender, stress injuries, athletics and other illnesses [3]. This condition is widespread and requires increased understanding and attention. People with severe forms of knee OA often resort to surgical solutions such as total knee arthroplasty (TKA). Australia's ageing population has demonstrated an increase in the prevalence of OA, with 8 percent of Australia's population known to have OA [4]. The rate of knee replacements has increased from 107 to 156 per 100,000 people from 2012-13, due to diagnosis of knee OA [4]. Knee OA affects half the world's population aged 65 years or older, making it the most common disorder of articulating joints in humans [3].

Producing an in-depth biomechanical analysis of a patient's OA knee and a healthy participant's knee, will help enhance our current understanding of contemporary surgical applications in terms of knee OA. This paper explores the biomechanical approach of detecting the level of knee OA as a contrast to the general X-ray method. The question under investigation is, How does an OA knee differ biomechanically to a healthy knee joint? The patient questionnaire results are compared to the biomechanical data collected in the gait laboratory. Relationships can be established between the severity of OA the patient identifies in the questionnaires, opposed with the results obtained from the biomechanical analysis of the gait activities completed.

### 2.1 Gait Analysis Motion Capture Method

Gait analysis is an increasingly popular method of measuring the biomechanics of various human movements. It provides as a less invasive alternative to the more conservative x-ray method. Gait analysis yields results of the investigation from a different perspective to that of an x-ray. It takes into account a number of factors of the subject's under investigation, providing an increased understanding as to the extent of the subjects OA. These results are obtained by implementing a motion capture system, known as the

gold standard in collecting gait data. The motion capture system tracks skin reflective markers placed on specific anatomical locations on the subject's body, using infra-red (IR) technology. As motion capture technology has rapidly advanced, gait analysis has emerged as a prominent technique utilised in clinical studies, particularly at investigating knee OA.

Vicon Nexus software and hardware is utilised, which is comprised of eight IR cameras, a sync box and the program which translates the data collected live onto the computer screen. The cameras only detect the reflected IR light off the skin reflective markers, each equipped with a filter which blocks other waveforms of light such as visible light. The reflective markers are placed on the skin above the anatomical bone location, in order for the appropriate joint centres to be calculated. Reflective markers are utilised due to being non-invasive in comparison to invasive methods such as bone pin markers. Vicon Nexus provides a three-dimensional volume space, where the reflective markers are virtually shown in correspondence with their coordinates calculated in the gait laboratory. This virtual skeleton produces a live viewing of the activity completed by the subject, allowing further processing in the program OpenSim. OpenSim is used to formulate the biomechanical characteristics of the subject's gait data for further statistical analysis. This data allows for an increased understanding of knee OA in terms of the location the OA is affecting the most, the different physiological loads experienced, and how the co-activation of muscles are stimulated for various severities and locations of knee OA.

## 2.2 Project Outline

This research project is divided into various key components which provides a basis, procedure, result and thorough explanation that illustrate the findings of the areas under investigation. Each chapter serves a distinct purpose in terms of the key parts explored for the biomechanical analysis of the OA knee joint.

Chapter 3 recognises the relevant literature in relation to the biomechanical analysis of the osteoarthritis knee joint. The various methods and experimental procedures are explained which are applicable to completing this study. Each component of the investigation of the biomechanical analysis is described in terms of their unique advantages and limitations, in order for the most appropriate processes to be chosen. The review of literature describes in detail common errors found by studies when implementing certain procedures and how to overcome them in order to produce accurate results. Furthermore, this chapter illustrates various optimisation techniques for each part of the process, providing increased confidence in the results obtained.

Chapter 4 explores the methodological procedures which take place, in order to yield the required results for this particular study. The methodology is explained in detail following the sequence of events in which each step is executed. The procedures chosen in this section are those that have been researched extensively in the literature review to be the most favorable and beneficial for this particular study. The specifics of the study are explained in this chapter comprising of the demographics of the study followed by the tools and practices carried out to achieve the required results.

Chapter 5 illustrates the results obtained in this study. The results have been processed through different programs and displayed visually in terms of graphs and tables. The results represent the findings of this study which allow the investigation of the different biomechanical characteristics to be established between OA and control subjects.

Chapter 6 provides an in-depth explanation about the outcome of the results and any problems, limitations and solutions that emerged throughout the project. The results are justified in this section which determine the differences viewed between OA and healthy subjects.



# Chapter 3

## Literature Review

### 3.1 Knee Osteoarthritis

Knee OA is known to have a leading effect on increasing the rates of disabilities among the ageing population [5]. Knee OA is a degenerative disorder which progressively reduces the amount of cartilage between articulating bones, in turn increasing the friction between bones [6]. This rubbing effect gradually worsens over time, damaging the bone [6]. The loads experienced by the knee are recognised as one of the most profound factors in determining the onset and extent of the disease [2]. The load is ascertained by a number of aspects which include the effect of the surrounding muscles on the knee joint [2]. The co-activation of muscles such as the hamstring and quadriceps fluctuate the forces experienced by the knee joint, hence the moments of the knee need to be calculated [2]. Gait analysis involves the collection of biomechanical data, which can aid in the understanding of the differences demonstrated by the healthy and OA knee joint.

### 3.2 Gait

The gait cycle is comprised of the stance and swing phase as shown in figure 3.1 [6]. The first element which studies determine is the part of the gait cycle that is to be investigated [3]. A number of studies specifically look at the swing phase or the stance phase, while more recent research focuses on both components of the gait cycle [6]. The stance phase includes the region of the complete gait cycle from approximately 0-60% [6]. The stance phase begins with initial contact by an event known as foot strike (FS) [6]. The stance phase ends with foot off (FO) of the same initial contact leg, demonstrated in figure 3.1 [6]. As a result, ground reaction forces (GRF's) are generated and measured during the stance phase, allowing the joint moments to later be calculated [7]. The swing phase comprises of the complete gait cycle region from approximately 60-100%, a period where the initial contact leg has no contact with the ground [6]. The swing phase begins at the time where FO occurs of the initial contact leg, up until the next FS of the same leg [8]. During the swing phase which includes initial, mid and terminal swing periods,

the marker trajectory data is tracked by the motion capture cameras and recorded [8]. The marker coordinates enable the joint centres and angles to later be computed [7].

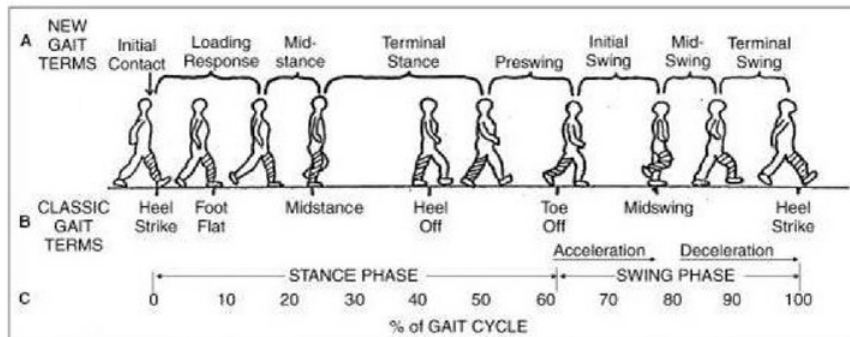


Figure 3.1: Complete gait cycle [9].

### 3.2.1 Gait Events

Gait events undertaken by the subject are designed in a way to replicate certain activities that occur in the daily life of the average person [9]. These events, such as walking or stair ascent, yield biomechanical results that provide different understandings of a subjects gait style. A number of these activities are investigated in contemporary clinical research [1]. As a result of the activities a new understandings of the physiological loads experienced by the knee joint and how the surrounding structures interact to stabilise this joint can be developed [10].

#### Walking

Normal gait or walking is among the most contemporary methods of analysing the subject's biomechanical characteristics [1-3, 10, 11]. The subject is instructed to walk at their regular speed along a 10m walkway [10-12]. A successful trial is defined by the FS to FS contact on force plate 1 and 3 by the operative leg for OA subjects, and a randomly selected leg for control participants [1-3, 10-12]. Walking trials are conducted for gait analysis, however the subjects are directed to complete the trials at a comfortable speed followed by a fast-paced speed [13]. The various physiological loads can be compared for the same task with a change in speed [13].

#### Timed Up and Go

Participants performed 5 metre timed up and go (TUG) activities at different speeds [14]. The TUG task comprises of a sit-to-stand action followed by a walk and finally a turn to sit back down at the original position [14]. TUG is a highly complex task, making it less common in knee joint clinical studies as most subjects suffer from a form of OA [14].



### Stair Ascent

Figure 3.2 illustrates a custom-built staircase with two steps, each of height 18 cm, a common height for steps [6]. The subject is to begin the activity from the floor and step up until reaching the end point on the second step, this is completed with both legs separately [6]. Due to a limitation of only having two steps, the subject was required to interchange legs for stair ascension gait analysis [6]. The interchanging of legs allowed a complete gait cycle to be formed, which includes both the stance and swing phase [6]. Figure 3.2 demonstrates the different events to be completed for each leg, to make up the complete gait cycle for stair ascension [6].

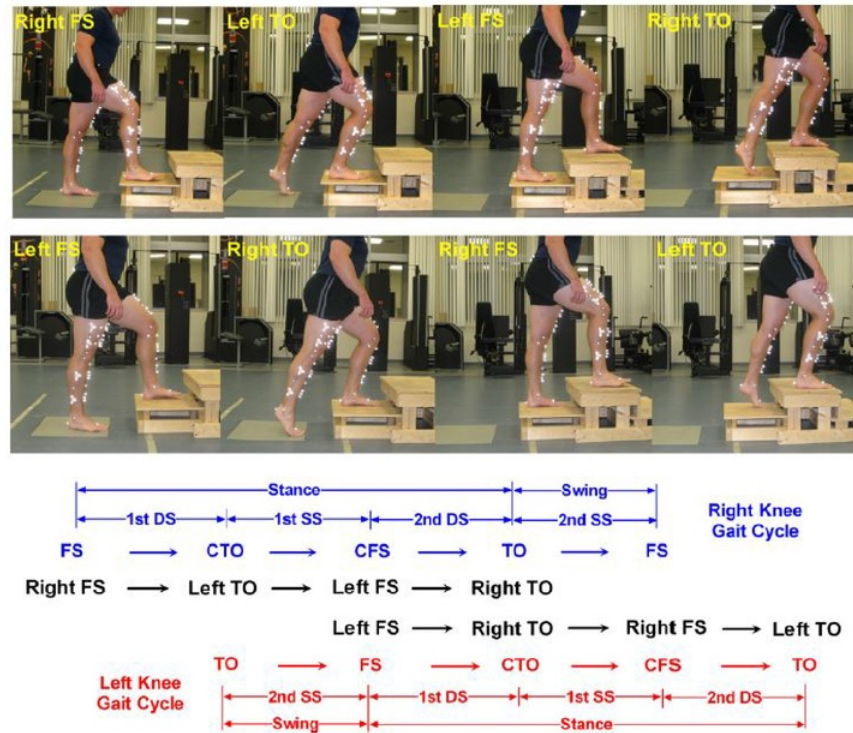


Figure 3.2: Stair ascent stance phase [6].

### Stair Descent

Stair descent or stepping-down is a common gait activity completed by subjects [6, 15]. A wooden step of 20 cm height is utilised, whereby the subject stepped down onto the force plate mounted in the first step, with the elevated leg and then stepped forward with

the opposite leg [6, 15]. The individual landed with both legs in front of the force plate in a quiet stance [6, 15]. In order to minimise the line of sight error with the reflective markers, the subject was to flex their arms across the chest for the duration of the gait event [15]. The data was collected during the stance phase of the stepping down task, that is from FS until FO from the same force plate with the elevated leg [6, 15].

### Cutting Manoeuvre

Participants were instructed to perform lateral cutting manoeuvres in addition to normal gait trials [12]. The technique is made up of the subject beginning in a stationary standing position, followed by pushing off using the left leg and just before landing on the right foot, immediately pushed off the platform, cutting to the left at an angle of approximately 45 degrees [12]. The FS, mid-stance point and FO were the three events under investigation, for each lateral cutting cycle trial [12]. The cutting motion is a complex technique for subjects to execute successfully, especially those suffering from severe OA, hence it is rarely used in clinical studies [12].

### Instrumented Treadmill

Determining biomechanical characteristics of the knee joint by utilising an instrumented treadmill is an alternative practice in comparison to standard gait [16, 17]. GRF data is collected while the subject walks on the treadmill, instrumented with tandem piezo-electric force plates [16, 17]. The subject's kinematics are also collected whilst walking on the treadmill [16, 17]. This technique is not common in contemporary clinical studies due to the high cost of the instrumented treadmill, line of sight issues with motion capture and also not replicating the daily activity as sufficiently as walking on the ground [17].

## 3.3 Gait Analysis

Gait analysis techniques include methods of obtaining motion data from a subject, which can be invasive or non-invasive [6].

### 3.3.1 Skin Reflective Marker Setup

Non-invasive techniques of tracking bone motion such as external skin markers shown in figure 3.3 have demonstrated strong evidence of accurate results, comparable to that of the invasive bone-pin marker setup [12]. 59 female participants were divided into three groups and investigated [7]. Group one contained healthy subjects, group two had patients with early medial knee OA and group three consisted of patients with established medial knee OA [7]. The three groups with similar body mass index (BMI) demonstrated soft tissue artefacts (STA) which had the same effect on each group, meaning the variations measured between groups were not likely a resultant of the STA error [7]. STA is the relative movement between markers on the skin and bones, which has been shown to



increase the joint angle error [7]. The biomechanical analysis of 44 OA patients compared with 40 healthy participants was examined [11]. Error values of 3.4 to 4.4 degrees were detected, for OA and healthy individuals respectively [11]. The skin marker method was utilised to obtain the error value quantities [11]. The results produced were not significantly different from the outcomes obtained in studies which utilised the bone-pin marker setup [12]. The skin marker setup is a non-invasive method, that is more commonly used in contemporary studies on knee biomechanics, rapidly overtaking the highly invasive bone-pin method [18].



**Figure 3.3:** Retro-reflective markers placed on anatomical positions of subject.

### 3.3.2 Bone Pin Setup

Bone pins have demonstrated results of higher accuracy compared to that of external skin markers [11]. Reported errors of 5.7-15.5 degrees for external skin markers compared to that of 2.5-4.4 degrees for bone pin markers when measuring knee adduction angles have been shown [11]. Eight healthy male subjects had bone-pin markers implanted in the leg, while skin markers were placed on the leg, both placed on anatomically specific locations

[12]. The knee joint kinematics computed demonstrated the precision of the measurement to be effected by an increased error that occurs due to skin movement [12]. The overall error is found to be lower for bone-pin-markers compared to skin markers [18]. The errors detected for bone-pins include being potentially due to the movement of pins in the bone, the pin oscillating and/or bending or perhaps the markers attached on the pin could move [18]. The average errors detected during walking and stepping movements for the bone pin method, yielded an average joint rotation error of 4.4 degrees and a translational error of 13 millimetres [12]. On the other hand, the external skin markers produced errors of 13.1 degrees and 16.1 mm for the same tasks [12]. Bone pin investigations are difficult to conduct, as it is an invasive form of experimental analysis, which requires strict ethics and rules [12]. Limited applications of the bone pin method occur primarily due to the invasiveness of the procedure, the ethical considerations and the errors consistently found with the femoral pin [18].

### 3.3.3 Inertial Measurement Units

Inertial Measurement Units (IMUs) have recently emerged as a more innovative system of measuring motion data [19]. IMUs comprise of accelerometers that measure linear acceleration and gyroscopes which calculate the angular velocity [14]. This alternative includes a number of advantages which more traditional systems do not offer such as portability and being usable outside of a laboratory environment [19]. IMUs are increasingly being used in contemporary research, which identifies various movement disorders and assesses surgical outcomes [19]. Due to the recent emergence of IMUs, they have had limited exposure in the research field to understand whether the devices consistently produce more accurate data than more conventional systems [19]. Optical motion capture systems are recognised as the premium standard for collecting motion data [19]. Optical motion capture systems are result dependent on a diverse range of factors which include the type of equipment, number of cameras, configuration, and biomechanical models utilised [19]. An accurate set of metrics have been established for a currently used IMU under specific conditions [19]. Current IMUs have demonstrated excellent characteristics in terms of utility and reliability [19]. Accuracy and Precision was on par with the premium standard system for static trials, with an average of plus or minus 1 degree [19]. The commercial grade IMU investigated, illustrated similarly accurate and precise results for the dynamic trials with minimal percentage errors for low velocity tasks [19]. The percentage error grew slightly for tasks of higher velocities in excess of 2000 degrees per second (dps), a speed reached by extreme sporting activities such as sprinting [19]. Daily activities such as stair descent and sit to stand express velocities of hip and knee extension of less than 210 dps [19]. This demonstrates that for tasks such as measuring a subjects gait to determine the biomechanical characteristics of the OA knee joint, these IMU devices are a suitable alternative.

Limitations are found where the motions detected were all in the planar region, unable to show the errors determined in a realistic three-dimensional environment [19]. Tech-

niques such as the attitude and heading reference system (AHRS) have been implemented whereby magnetic sensors are incorporated with the IMUs. This fusion of data from both devices yields a three-dimensional orientation of the volume space, with respect to a reference inertial frame based on magnetic North and Gravity [14]. Although AHRS is a promising technique for three-dimensional orientation, the limitations currently far outweigh its advantages [14]. A number of factors still negatively impose on the AHRS technique, which include the conditions of motion for example during a sit to stand gait task, the magnetic environment interfering with the sensors, the positioning of the sensors forming inaccurate estimations of location, soft tissue artefacts and anatomical referencing process errors [14]. Future work and advancements on IMU technology is required for this method to become a serious contender in biomechanical gait analysis clinical studies [14].

### 3.3.4 Microsoft Kinect v2

The financial cost and technical expertise required to utilise optoelectronic methods of motion capture data are unrealistic for many clinical studies [17]. The emergence of the Microsoft Kinect v2 sensors has allowed for a publically available, cost-effective and user-friendly motion capture system, demonstrating precise results in terms of kinematic data collection [17]. The Microsoft Kinect v2 provides a multitude of data streams which include, colour, infrared, depth images, body index images and skeletal information for every subject tracked [20]. These tracking sensors are limited in distance with the depth image able to sense between 0.5-4.5 metres, while the volume space has a constrained field of view being 70 degrees horizontally and 60 degrees vertically [17]. Microsoft utilises a software development kit (SDK) which assigns indices to the joint locations that are required to be tracked [20]. Defining the position and orientation of the sensors in reference to the marker is another weak point, as extra mathematical transformations need to be applied as not all sensors can see the marker at the same time depending on the gait setup [20]. The Microsoft Kinect v2 was tested against the gold standard VICON motion capturing system with 10 motion capture cameras [20]. The statistical results displayed a close correlation between the two methods, however it was found that the Microsoft Kinect v2 could only produce these excellent results when the spatial calibration of the sensors was perfected [20]. This perfection of calibration included a number of complex steps such as Euclidean transformations and custom algorithms [20]. A test of the lower extremities was conducted using a single Kinect v2 sensor opposed with the VICON motion capture system [17]. The results demonstrated the effectiveness of the Microsoft Kinect v2 sensor with statistical data in accordance with the VICON results, however displayed profound limitations when assessing ankle joint kinematics [17]. The inability of the Microsoft Kinect v2 to precisely measure lower body kinematics during gait is considered to be a huge disadvantage [13]. Due to the low cost of the Microsoft Kinect v2 sensors and its usability, being able to be utilised in most environments, it has resulted in an increase in use in clinical studies especially in the area of gait analysis [13, 17].



## 3.4 Optimal Marker Sets

Kinematic gait analysis is commonly based on body markers located in reference to a set arrangement known as a marker set [21]. Various marker sets have been developed over the years, however the majority of clinical studies implement a modified model of the Helen Hayes set [21].

### 3.4.1 Helen Hayes

The original Hospital Helen Hayes marker set was specifically developed for a low resolution capture system which is why it has so few markers, whilst being as far apart as possible [21]. The Helen Hayes marker set is comprised of 15 markers, shown in appendix B.2 [7]. The Helen Hayes marker set comprises of three rotational degrees-of-freedom (DoF), a joint motion constraint that is known to introduce errors in terms of joint angle computations [21]. The Helen Hayes set defines the three DoF by the following: “thigh segment definition relies on hip joint centre (HJC) approximated from pelvis markers, shank definition relies on a knee marker shared with the thigh, and foot definition relies on an ankle joint centre estimated from shank markers” [21]. The errors and limitations that arise from this marker placement system include causing errors to spread to more distal joints and requires the entire model to be utilised even if it is only a subcomponent of interest, such as the knee [21].

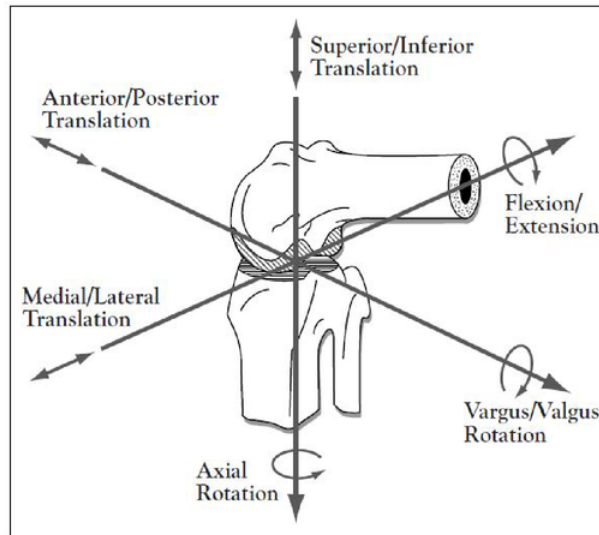
### 3.4.2 Modified Helen Hayes

The lower extremities of the subjects are examined by using thirty-seven markers placed in eight defined body segments in the lower limb region [11]. Three retro-reflective markers were placed on the thigh and shank, which defined the alignment and position of the lower limb segments [11]. Anatomical measurements were taken on the marked up subject, similar to the locations measured in the hospital HH method [11]. The measurements were required as inputs for Harrington equations which are used to calculate the HJC [11]. The placement of skin markers is in accordance with an extended Helen Hayes protocol, comprised of 27 markers [7]. The number of markers used in the gait analysis method were increased, compared to the generic Helen Hayes model to reduce errors caused by STA [6]. The reflective markers were placed on defined bony landmarks and segmental surfaces, specifically attached on the anterior superior iliac spine (ASIS), posterior superior iliac spines (PSIS), the sacrum, the medial and lateral malleoli, the second metatarsal head, and the heel [6]. Extended versions of the Helen Hayes marker set have demonstrated increased effectiveness and accuracy in measurements of knee biomechanics, while utilising the skin marker method [6]. This ensures markers are placed on anatomical areas where soft tissue does not deform and is less likely to move, while enhancing the definition of the body segments [6].

### 3.4.3 Clustered Marker set

Placing three or more skin markers in clusters, located across the thigh and shank has proven to be a common measurement technique of knee joint motion [12]. Five groups of markers in clusters of three were used, attaching the markers to the lateral thighs, lateral shanks and posterior pelvis [7]. Spacing of markers and orientation are two key factors when implementing the cluster technique, ensuring minimal obstruction and optical crosstalk [12]. Markers in the same cluster were spaced between 10-15cm away from each other, while making sure the orientation of the cluster was non-coplanar for a minimum of two camera views for the total duration of the motion capture gait trial [12]. The cluster marker set method is preferred in clinical studies, primarily due to the difficulty of finding the anatomical landmarks if the single marker approach is undertaken [21]. Further research is required in terms of finding the optimal placements of marker clusters, to best define the various axes of the body, in turn reducing cross-talk [21].

## 3.5 Biomechanics of the Knee



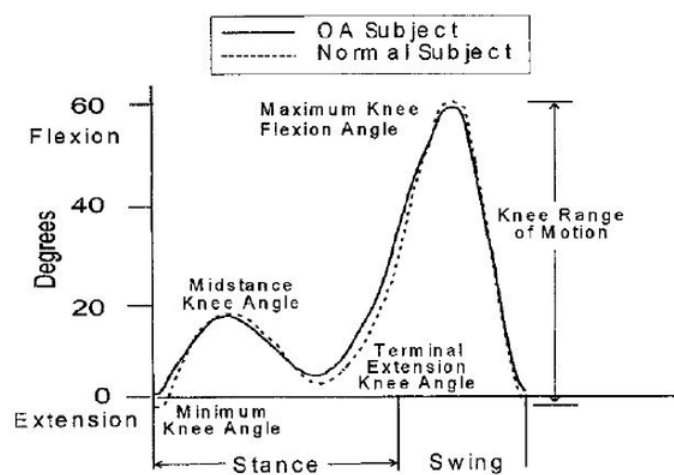
**Figure 3.4:** Biomechanics of the knee joint [23].

The combined motion of the bones, muscles, tendons and ligaments define the movement of the human body [22]. The science of human movement is referred to as biomechanics [22]. Various components of the knee joint such as the menisci, cartilages, ligaments and muscles react in mechanically complex ways to different types of physiological loads [22]. Ligaments are the fundamental support structures for the knee joint in terms of stabilising

the joint during motion [22]. Each ligament provides support to the knee joint in more than one DoF, however the complete stability is determined by the interaction of the stability produced from the ligaments [22]. Due to knee OA being so prevalent around the globe, the pressure distribution experienced by the knee joint in various daily activities needs to be determined [22]. The knee joint is comprised of six DoF which include three rotational and three translational as shown in figure 3.4 [23].

## 3.6 Biomechanics Results

### 3.6.1 Joint Angles



**Figure 3.5:** OA vs Healthy Knee Flexion Angle for walking trial [24].

No significant variation could be determined in knee flexion angle during the stance phase for a stepping-down gait task between the knee OA and healthy groups [15]. Small, however significant differences during the full gait cycle between the knee OA group and the healthy participants in terms of knee adduction angle were detected [7]. The defined knee axis of rotation is determined to be a major factor in the results that are produced in terms of knee adduction angle [7]. The minimum knee angle of the knee OA subjects was shown to be substantially greater compared to that of the healthy participants displayed in figure 3.5 [24]. Figure 3.5 further demonstrates the increased range of motion (RoM) of the knee joint for healthy subjects opposed to knee OA subjects. The RoM was calculated by subtracting the maximum extension angle from the maximum flexion angle while walking, resulting in a much lower knee range of motion for knee OA patients compared with healthy participants [24]. Further findings demonstrated the stride length for OA

knee patients to be shortened greatly during walking [24]. Similar understandings are established, which denote the step length and top walking speed of the knee OA patients to be reduced profoundly as opposed to healthy participants [16, 24]. The findings of multiple experiments have provided stronger understandings in that knee OA subjects have an increased adduction knee angle during early and mid-stance, compared with the healthy participants [11].

### 3.6.2 Joint Moments

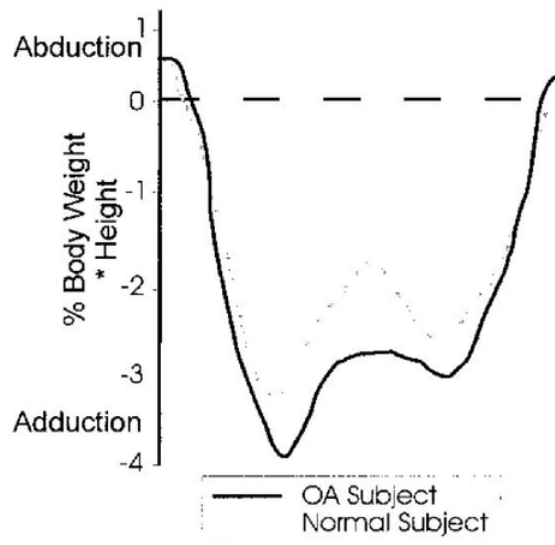


Figure 3.6: OA vs Healthy EKAM for walking trial [24].

The peak external knee adduction moment (EKAM) during walking is investigated, by analysing the biomechanical characteristics of patients with knee OA ranging from mild to severe conditions [24]. A higher peak EKAM for subjects with knee OA compared to healthy participants is illustrated in figure 3.6 [24]. Interestingly, no significant variation between the healthy and knee OA subjects was found in terms of sagittal plane moments which include: the initial knee extension moment, early mid-stance knee moment, terminal stance knee moment and pre-swing knee flexion moment (KFM) [24]. The GRF's link to gait speed is explored, revealing that the ground reaction outcomes comprised of the push-off forces and impulses were significantly worse for knee OA patients compared to healthy participants [16]. Knee OA subjects were found to have a higher knee adduction angular impulse (KAAI) compared to healthy participants [2]. KAAI is defined to be the integral of EKAM, hence a higher KAAI dictates a higher EKAM [2]. The results demonstrated that knee OA subjects had larger first and second peaks of EKAM during

walking trials shown in figure 3.6 [2]. Interestingly, it was shown that the knee OA subjects had similar KFMs to the healthy group [2]. A relationship between the gait activity measured and pain recorded by the patient was established [3]. Knee OA patients who reported moderate to severe gait related knee pain walked with an increased KFM during the mid-stance phase of a walking trial compared to patients with mild or no knee pain [3]. The majority of severely affected OA patients were more inclined to produce a varus (adduction) thrust, compared to the healthy participants during a walking trial [11]. Moreover, poorer biomechanical characteristics were seen in severely affected OA patients with a varus thrust, as opposed to OA subjects with a valgus (abduction) thrust [11]. In addition, an increased peak knee adduction moment (KAM) and KAM impulse were detected in the OA varus thrust group, in comparison to controls with varus thrust [11].

## 3.7 Signal Processing

### 3.7.1 Butterworth Filter

Butterworth filters are commonly implemented in data collection procedures such as high speed video, force platforms, accelerometers and strain gauges [25]. The Butterworth filter is utilised to provide the most flat frequency response within the pass band that is mathematically sound [26]. The simplicity and consistent performance of Butterworth filters have made them a popular choice for signal processing in clinical studies, which require the removal of high-frequency noise [27]. Butterworth filter can be set at high-pass, low-pass or band pass depending on the result required [25]. Low-pass Butterworth filters allow safe passage of sinusoids with frequencies less than that of a specified cut-off frequency ( $f_c$ ) [25]. The output signal will not contain any sinusoids with frequencies above the set  $f_c$  level, as they are effectively eliminated in the filter by extreme attenuation [25]. The  $f_c$  cannot be set too low even though it will significantly reduce the high-frequency noise, as the low frequency components will become blurred and inaccurate [28]. Should the  $f_c$  be set too high, the low-frequency components will be accurate, however the high frequency components will not be stopped from entering the output signal [28]. Therefore, the  $f_c$  that is required for optimal results is when it is equal to the largest frequency in the low-frequency component, enabling all the required frequencies to pass through the filter correctly [28]. The mathematical transfer function of a Butterworth filter is given by equation 3.1

$$G^2(\omega) = |H(j\omega)|^2 = \frac{G_0^2}{1 + \frac{j\omega}{j\omega_c}^{2n}} \quad (3.1)$$

where  $n$  = order of filter,  $\omega_c$  = cutoff frequency (-3dB) and  $G_0$  is the DC gain

Motion capture systems are responsible for tracking and recording the trajectories of markers [27]. This process is prone to errors, due to the derivative estimation process which detects noises that are neither accurate nor required [27]. The sinusoids collected



to be processed are assumed to be stationary in order for a Butterworth filter to be utilised [27]. Gait analysis is a significant example of when the signals detected are not always stationary [27]. Body markers placed on distal areas of the lower extremity such as the ankle marker, demonstrate this vertical displacement shift in the signal [27]. "After heel-strike occurs the ankle marker remains stationary, almost completely motionless until toe-off, after which it swings in the air" [27]. This shows the sinusoid to hold more high-frequency components than others, illustrating the power of the signal changing in time [27]. This is a limiting factor of the Butterworth filter, as it is unable to accurately process changes in local signal structure [27].

### 3.7.2 Exponential Filter

Exponential filters like Butterworth filters are also regularly utilised when high frequency noise is required to be eliminated [28]. Digital speckle interference fringes is a common area where the exponential filter demonstrates its effectiveness in signal processing [28]. Sparse fringes evident in speckle interference fringe patterns is specifically filtered using a low-pass exponential or Butterworth filter, however dense fringes require improved versions of these filters in order to obtain accurate results in reducing the speckle noise [28]. Fourier transforms are incorporated to transform the speckle interference fringe pattern from the time domain to the frequency domain [28]. This process allows the low-frequency and high frequency components to be categorised as the interference fringes and the speckle noise respectively [28]. For this reason a low-pass exponential filter is employed, in order for the interference fringes to pass completely through the filter while the speckle noise is stopped by the filter [28].

$$H(u, v) = \exp\left(-\left(\frac{D(u, v)}{D_0}\right)^n\right) \quad (3.2)$$

Equation 3.2 defines a common low-pass exponential filter where,  $H(u, v)$  is the transfer function of the exponential low-pass filter,  $D_0$  is the cutoff frequency of the filter and  $n$  is the attenuation coefficient of the filter [28]. The attenuation coefficient ( $n$ ) is chosen to reduce as much as possible the high-frequency components (speckle noise) in the input signal which coincide with the low-frequency (interference fringes) components [28].



# Chapter 4

## Methodology

### 4.1 Subjects

Knee OA patients between the ages of 45-75 years old, both male and female, are investigated. The patients were recruited from a surgical waiting list awaiting primary TKA. Healthy participants between the ages of 45-75 years old, both male and female, with no prior or present knee injuries, disease, pain or surgery were chosen for the control group. The healthy participants were recruited through various advertisements around the University campus. Informed consent was required by each subject and the approval of the study was obtained by the Macquarie University Human Research Ethics Committee.

### 4.2 Gait Analysis Data Collection

#### 4.2.1 Motion Capture Method

The gait analysis motion capture method comprises of eight infrared (IR) motion capture cameras. Settings can be adjusted to determine the number of cameras required, to sense and capture the retro-reflective markers in the capture volume. It is recommended that at least three of the IR cameras can view the target space with the retro-reflective markers. This technique is called optical-passive motion capture, known to be the most flexible and common method utilised in gait analysis. The optical-passive system contains IR LED's around the camera lens, in addition with IR pass filters placed over the camera lens. This ensures the motion capture cameras only sense the reflected IR from the retro-reflective markers, and cannot pickup any other wavelength of light such as visible light. Without this IR pass filter the IR would not be able to be detected due to increased noise from visible light, compromising the purpose of the system. The process of triangulation captures the centre of the markers, yielding the frame-to-frame positions in three-dimensional space. The animation of the markers which are placed on the skin above the anatomical landmarks of the patient, are displayed in real time on the simulation computer, via the Vicon Nexus software platform. Vicon Nexus is utilised to control the motion capture

camera system through the use of a sync box. This allows the real-time display of the virtual space on the computer screen, which reflects the experimental space where the capture volume is located. Specific to this research project, eight motion capture cameras are employed, connected to one simulation computer operated by an experienced user. The key objective for this method is to measure the kinematics experienced by the subject, in turn allowing the calculations of the joint angles to be made.

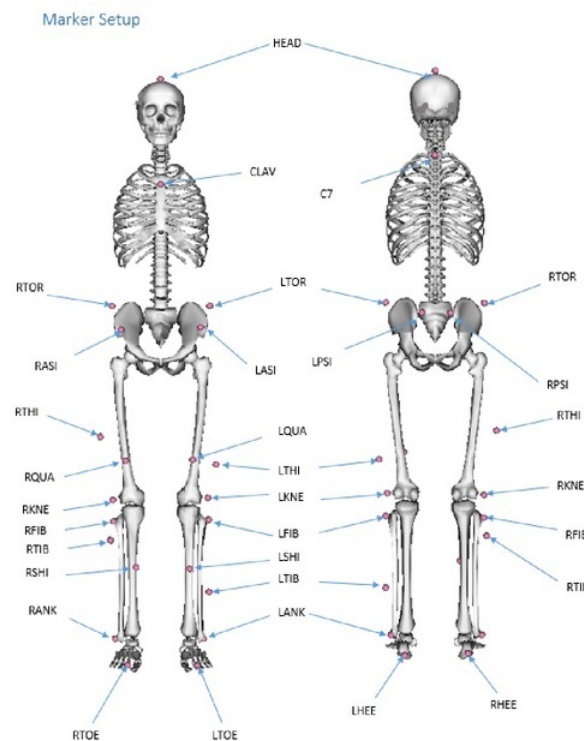
The gait analysis also comprises of collecting the kinetic data exerted by the subject, through the use of piezoelectric force plates. Specific to this research project, three Kistler piezoelectric force plates are embedded in the ground in the gait laboratory. In addition, a portable Kistler piezoelectric force plate is also used for the portable staircase where activities are performed. These force plates ensure accurate measurements of forces and moments produced by the subject are recorded. Kistler Bioware is the software which reads the data measured by the force plates, by plugging each force plate into the Kistler data acquisition (DAQ) system box. The force plates embedded into the gait laboratory floor define where the motion capture cameras should be placed, as this space is set to be the capture volume. Similarly, when the portable force plate is mounted onto the portable stair case, it is also placed in the same capture volume space. The dynamics measured are recorded into Vicon Nexus so that the inverse dynamics can later be calculated in OpenSim.

#### 4.2.2 Retro-reflective Marker Placement

The subject has 27 retro-reflective markers placed on their body. The markers are manufactured and distributed by Logemas, each with a diameter of 14 millimetres. The locations where the markers are placed are derived from an adaptation of the HH marker set. The HH marker set does not take into account any upper body segments such as the head, which is important for more accurate virtual scaling in the processing stages. Due to the limitations of the HH marker set, an additional 12 markers are utilised for this particular research project. The modified Helen Hayes marker set is shown in figure 4.1, where the pink spheres are the reflective markers. In reference to figure 4.1, the anatomical locations where the extra markers are placed on the subject are shown which include the head, C7, clavicle, left and right shin, left and right fibula, left and right PSIS, left and right torso and the left and right quadriceps. Appendix B.3 presents the details and corresponding anatomical locations of the individual markers which make up the modified HH marker set. The extra markers define each segment of the body more distinctly, increasing the accuracy of the results where in-depth measurements are required. This can be demonstrated when a marker is placed on the right ASIS and the right femoral lateral epicondyle, the motion capture camera can easily mix up the two markers when the subject is in motion. The added marker on the right quadriceps enhances the definition of this segment, enabling the motion capture system to correctly track each marker in motion. As a result, this helps the operator to produce a more precise scaled model through the use of OpenSim software. In turn, this ensures the results calculated from

the virtual scaled model are more closely aligned to the expected results. Accounting for the misplacement of body markers is much more effective and efficient with the modified HH marker set, as the extra markers provide more defined segments of the various body regions.

Anthropometry is required for each subject, to determine the parameters for Vicon Nexus enabling the required calculations to be made. The anatomical measurements taken for each subject is aligned with the traditional Helen Hayes protocol. The measurements include the height (mm), body mass (kg), inter-asis distance (mm), left and right leg length (mm), left and right knee width (mm) and left and right ankle width (mm). Including the anatomical measurements yields a more accurate and precise virtual model of the subject. As a result, the joint centre calculations will be more accurate which positively effects the joint angle results.



**Figure 4.1:** Modified Helen Hayes marker set.

### 4.2.3 Gait Events

The activities which the subject is instructed to complete include walking, stair ascent and stair descent trials. The tasks selected allow different investigations to take place about the variations which occur in stance and swing phase of the knee. These various activities which replicate daily tasks enable the joint angles and joint moments to be determined. Depending on the gait activity, certain OA patients will struggle. This will allow observations of how the participants overcome the struggle to be made.

#### Walking

Embedded in the floor of the gait laboratory along a straight line are three Kistler piezo-electric force plates. The force plates are covered with the same rubber flooring which surfaces the whole room, meaning the subject does not know where they are positioned. The subject begins at a stationary point within a range of three metres before the first force plate in the gait laboratory. The subject walks normally in a straight line at a comfortable speed. The subject is not told to aim for the force plate locations as this would compromise the study by altering the walking style of the subject. In order for a trial to be successful, the subject must make heel strike contact with a single foot on each force plate. The gait cycle is taken from heel strike of the designated leg on the first force plate to the heel strike of the same leg on the third force plate. During this time, the Vicon Nexus motion capture system is controlled by an operator who starts and stops each trial of motion capture. Each marker for the course of the trial is tracked and the forces experienced are recorded. The results are saved onto a separate file for each trial for further processing. The subject is to complete several trials with both the left and right leg being the first contact point, to obtain specific results for each individual leg.

#### Stair Ascent

A portable stair case shown in figure 4.2 has been specifically built by the METS department for this research project. The stair case is comprised of two steps with a step height and depth which replicates that of an average step on a stair case. The portable stair case is placed at the end of force plate 1, where the capture space is more easily defined for the motion capture system. The portable Kistler force plate is installed on the first step of the portable stair case, in order for moments to be calculated for stair ascent and descent. Each trial is recorded on Vicon Nexus by the operator. The subject begins in a stationary position on force plate 2. The subject steps onto force plate 1 with a designated foot, and then onto the portable force plate with the opposite leg, finally stepping onto the top of the stair case and holding in a stationary position. The subject completes several trials, firstly with either the right or left leg to make contact with the portable force plate and then the opposite leg. The gait cycle for a single stair ascent trial is taken to be from heel strike to toe off of the leg which first makes contact with ground force plate 1 as well as the heel strike to toe off of the opposite leg designated to make contact with the portable force plate.

### Stair Descent

Stair descent is a similar process to that of stair ascent, only in this case the subject will start at the top of the portable stair case in a stationary position. The subject steps down onto the portable force plate with a designated leg, followed by stepping onto the ground force plate 1 with the opposite leg. The subject is to keep walking straight after landing on the first force plate for a short distance, after reaching the third ground force plate. The gait cycle for a single stair descent trial is taken to be from heel strike to toe off of the leg which first makes contact with the portable force plate on step one as well as the heel strike to toe off of the opposite leg designated to make contact with the ground force plate 1.



Figure 4.2: Portable stair case with portable force plate.

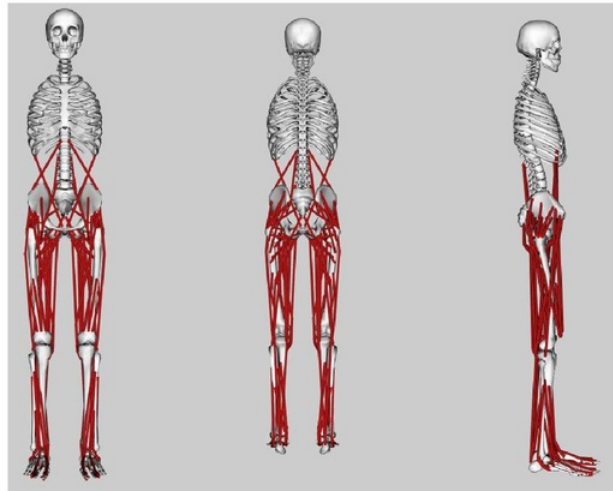
## 4.3 Biomechanical Calculations

### 4.3.1 Kinematics

#### Gait2392 Model

In this study the kinematics of the knee joint is investigated. The kinematic data consists of body marker positions in terms of a three-dimensional Cartesian coordinate system, denoted by  $(x,y,z)$ . In order to utilise the marker position data, a program such as OpenSim is required for efficient and effective calculation methods. OpenSim requires a virtual model to be imported in order for the body marker data to be applied allowing calculations to take place. The virtual model utilised in this study is the Gait2392 model which is a three-dimensional, 23 DoF model of the human musculoskeletal system. “The





**Figure 4.3:** Gait2392 Model with muscles attached.



**Figure 4.4:** Gait2392 Model with no muscles attached.



Gait2392 model was created by Darryl Thelen (University of Wisconsin-Madison) and Ajay Seth, Frank C. Anderson, and Scott L. Delp (Stanford University)" [29]. "The model comprises of lower extremity joint definitions adopted from Delp, low back joint and anatomical dimensions given from Anderson and Pandey, and a 2D knee model adopted from Yamaguchi and Zajac" [29]. The Gait2392 model is comprised of 92 musculotendon actuators to define the 76 muscles in the lower limbs and torso shown in figure 4.3 [29]. For the purpose of this study only the skeletal structure of the model is required so the muscles and tendons are removed in OpenSim displaying a model shown in figure 4.4 [29].

The default Gait2392 virtual model illustrates a subject of height 1.8m with a mass of 75.16kg [29]. A scaling tool is implemented in OpenSim which incorporates the marker position data, allowing the default Gait2392 model to be manipulated in order to represent the unique subjects dimensions. The Gait2392 model consists of seven lower extremity body segments which include the pelvis, femur, patella, tibia/fibula, talus, foot and toes [29]. The patella was removed from the original Delp model of the knee by Ajay Seth from the Gait2392 model to minimise kinematic restrictions [29]. This means the modified Gait2392 model used in this study comprises of six body segments, with reference frames fixed in each body segment [29]. For the Gait2392 model the locations of the reference frames are as follows:

- PELVIS: The pelvic reference frame is fixed at the midpoint of the line connecting the two ASIS's.
- FEMUR: The femoral frame is fixed at the centre of the femoral head.
- TIBIA: The tibial segment is located at the mid point of the line between the medial and lateral femoral epicondyles.
- TALUS: The talar frame is located at the midpoint of the line between the apices of the medial and lateral maleoli.
- CALCANEUS: The calcaneal frame is located at the most distal, inferior point on the posterior surface of the calcaneus.
- TOES: The toe frame is located at the base of the second metatarsal.

### Joint Centres

Reference frames are more commonly known as joint centres. Specifically the femur, tibia and talus reference frames are denoted as the hip joint centre (HJC), knee joint centre (KJC) and ankle joint centre (AJC), respectively. "Models of the hip, knee, ankle, subtalar, and metatarsophalangeal joints define the relative kinematics of the aforementioned

segments” [29]. This study is focussed on the kinematics of the knee joint which is defined by the Delp model shown in figure 4.5. Figure 4.5 is utilised without the patella as Ajay Seth adapted the Delp model to remove kinematic constraints [29]. The modified model only comprises of a single DoF which consists of the tibiofemoral joint, allowing only knee flexion and extension to be determined [29]. The 2D model was constructed in a way where the motion between the femur and tibia are defined by there relative joint centres as functions of the angle of the knee [29]. This was geometrically determined in the Delp model whereby the femoral condyles are represented as ellipses, while the tibial plateau is denoted as a line segment [29]. For the entirety of the knee RoM the model depicts the femoral condyles to remain in contact with the tibial plateau, as this determines the transformation of the femoral reference frame (HJC) to the tibial reference frame (KJC) [29]. The tibiofemoral contact point shown in figure 4.5 is dependent on the angle of the knee [29]. The Gait2392 adapted model by Ajay Seth was later modified into a version that is utilised in this study. This new virtual model resembles the knee joint in a three dimensional, six DoF model replicating the three rotational and three translational motions the knee joint can make. This is illustrated in figure 4.6 where a three dimensional view is shown of the pelvis and lower extremities denoting the femoral reference frame (HJC), the tibial reference frame (KJC) and the talus reference frame the (AJC). Joint angles can be found about the x, y and z axis meaning flexion/ extension, internal/external rotation and ab-adduction can be determined in the updated model. The scope of this study focusses only on the knee joint angles in terms of flexion/extension as the results obtained for adduction and rotation were not sufficient. Future work is directed at improving the process of gathering adduction and rotation for further analysis.

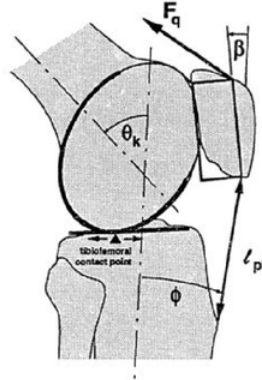


Figure 4.5: Knee joint centre [29].

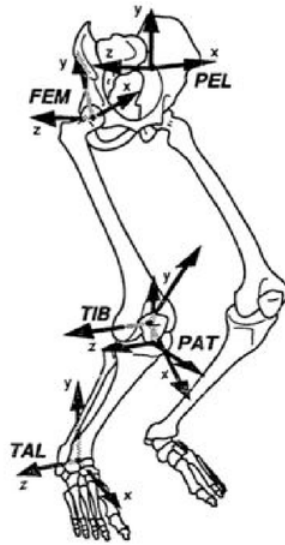


Figure 4.6: Joint centre locations [29].

### Joint Angles

To determine the knee joint angles a process known as inverse kinematics (IK) is used to compute the joint angles for a desired pose of the subject. This process is executed in OpenSim which imports the body marker trajectory data. The model is scaled to suit the unique subjects dimensions. The scaled model with the new and more accurately placed body marker coordinates is then used for IK calculations. The IK process in OpenSim first defines the joint centres of the lower extremities (refer to joint centres section). Resultantly, the joint centre locations are given by three dimensional Cartesian coordinates. Geometric techniques are used to determine the hip, knee and ankle joint angles. For the purpose of this study the interest is of the knee only, however joint centres of the ankle and hip are required in order to calculate the knee joint angles (KJA). Figure 4.5 can be extrapolated with the two lines forming  $\Theta_k$  extending to the HJC for the superior located line while the inferior line is extended to the AJC. The extended version is displayed in figure 4.7 with less detail. The intersection of these two lines is defined as the (x,y,z) coordinates of the KJC. The knee flexion angle is calculated between the continuation of the AJC and HJC axis shown in figure 4.7.



**Figure 4.7:** Knee flexion angle.

### 4.3.2 Kinetics

Kinetics is defined by analysing and understanding the forces that cause the movement to be made [30]. The reaction forces and moments are calculated by utilising the kinematic data, anthropometric measures and external forces detected [30]. The method of finding kinetic data from the previously obtained variables is known as inverse dynamics [30]. To perform ID in two dimensions a number of assumptions must be made which include the following:

1. Each segment has a fixed mass located as a point mass at its centre of mass (CoM).
2. The location of each segment's CoM remains fixed during the movement.
3. The joint are represented by either hinge or ball and socket joints.
4. The mass moment of inertia of each segment is constant during movement.
5. The length of each segment remains constant during the movement.

To perform ID in three dimensions which this study requires, changes in calculation techniques need to be made. The primary difference is utilising Euler's equation in three dimensions, followed by being able to mathematically show vectors in local and global coordinate systems [30]. Euler's equation of motion for two dimensions is comparable to that of Newton's Second Law where the sum of the moments is equal to the product of the mass moment of inertia ( $I$ ) and the angular acceleration ( $\alpha$ ) at one moment in time [30]. Mathematically Euler's two dimensional equation of motion is shown in equation 4.1.

$$\sum M = I\alpha \quad (4.1)$$

Euler's basic 2D equation evolves into a complex form when three dimensional analysis is required. Euler's equation of motion in three dimensions calculates the moments in the local coordinate system, whereby general motion is experienced by the rigid-body segment [30]. The general motion experienced is both translation and rotation [30]. Euler's equation of motion in three dimensions is expressed mathematically in 4.2.

$$\sum \vec{M} = I\vec{\alpha} + \vec{\omega} * I\vec{\omega} \quad (4.2)$$

In order to utilise Euler's three dimensional formula to obtain the moments in the local coordinate system for a given system, a number of variables must first be defined [30]. The centre of pressure (CoP) is an important factor which is used to calculate the mass moment of inertia. External forces or ground reaction forces (GRF's) are assumed to act at a single point of contact, known as the centre of pressure (CoP) [30]. The Kistler force plate calculates the CoP using four in-built triaxial transducers shown in figure 4.8. The coordinates of the transducers are shown in figure 4.8 to be (0,0), (0,Z), (X,0) and (X,Z) [30]. The CoP location is defined by the vertical forces experienced at each transducer [30]. Figure 4.8 denotes the vertical forces as  $F_{00}$ ,  $F_{X0}$ ,  $F_{0Z}$  and  $F_{XZ}$ . The resultant vertical force is given by  $F_Y$  equal to the sum of the four vertical forces. An example of the resultant GRF is shown in figure 4.9, where it is located at the CoP. The CoP location is given by the following equations:

$$x = \frac{X}{2} \left[ 1 + \frac{(F_{X0} + F_{XZ}) - (F_{00} + F_{0Z})}{F_Y} \right] \quad (4.3)$$

$$z = \frac{Z}{2} \left[ 1 + \frac{(F_{0Z} + F_{XZ}) - (F_{00} + F_{X0})}{F_Y} \right] \quad (4.4)$$

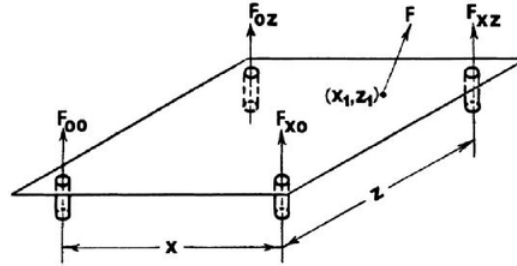


Figure 4.8: Kistler force plate centre of pressure [30].

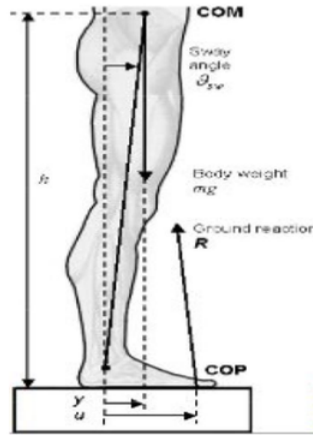
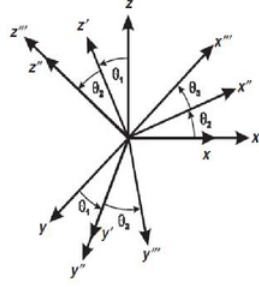


Figure 4.9: GRF characteristics.

The kinematic data includes a TRC file with the  $x, y, z$  coordinates of the marker trajectories at every sample time point [30]. The coordinates collected are defined in the global coordinate system (GCS), set in the gait laboratory. The GCS is defined as  $X$  in the forward/backward direction,  $Z$  is the vertical axis and  $Y$  is the left/right axis. The Kistler force plate coordinate system also utilises the GCS. The first local coordinate system (LCS) is used to define each body segment which follows an anatomical axis system with the origin located at the COM of the segment [30]. The second LCS is a marker axis system which defines the body markers [30]. Two transformations are required to get from the GCS to the marker coordinate system and then to the anatomical coordinate system. The first rotational transformation is shown in figure 4.10. The Cardan sequence is performed by firstly rotating about the  $x$  axis then the new  $y$  axis and finally about the new  $z$  axis. The first rotation in the transformation is denoted by  $\Theta_1$  which rotates about the  $x$  axis and yields  $x', y', z'$  [30]. The next two rotations then produce  $\Theta_2$  and  $\Theta_3$ . Euler rotational sequences are also used depending on the coordinate system requirements. Matrix transformations are then used to define  $\Theta_1$ ,  $\Theta_2$  and  $\Theta_3$  from the given  $x, y, z$  coordinates. Angular velocities and accelerations are then required to be derived from the three time varying angular positions previously mentioned. The first derivative of angle  $\Theta_1$ ,  $\Theta_2$  and  $\Theta_3$  is taken with respect to the change in time. The derivation of the angles provides the angular velocities denoted by  $\omega_1$ ,  $\omega_2$  and  $\omega_3$ . Finally the angular accelerations  $\alpha_1$ ,  $\alpha_2$  and  $\alpha_3$  are obtained by deriving the angular velocities with respect to the change in time. The kinematic variables have all been defined after this point and hence the 3D kinetics can be calculated.





**Figure 4.10:** Cardan transformation of three rotations about the x,y,z axes [30].

Euler's three dimensional rotational equations of motion are broken into the x,y and z components, defined in equations 4.5-4.7.

$$I_x \alpha_x + (I_z - I_y) \omega_y \omega_z = \sum M_x = R_{zd} l_d + R_{zp} l_p + M_{xp} - M_{xd} \quad (4.5)$$

$$I_y \alpha_y + (I_x - I_z) \omega_x \omega_z = \sum M_y = M_{yp} - M_{yd} \quad (4.6)$$

$$I_z \alpha_z + (I_y - I_x) \omega_x \omega_y = \sum M_z = -R_{xd} l_d - R_{xp} l_p + M_{zp} - M_{zd} \quad (4.7)$$

where  $I_x, I_y, I_z$  = Moments of inertia about x-y-z axes

$\omega_x, \omega_y, \omega_z$  = Angular velocities

$\alpha_x, \alpha_y, \alpha_z$  = Angular accelerations

$M_{xd}, M_{yd}, M_{zd}$  = Distal moments

$R_{xd}, R_{xp}, R_{yd}, R_{yp}, R_{zd}, R_{zp}$  = Joint reaction forces

$l_p, l_d$  = Distances from COM to proximal and distal joints.

The joint reaction forces are calculated by equation 4.8.

$$\sum F_X = ma_{X,Y,Z} \text{ or } R_{X,Y,ZP} - R_{X,Y,ZD} = ma_{X,Y,Z} \quad (4.8)$$

$M_{xp}, M_{yp}$  and  $M_{zp}$  are the three unknowns in equations 4.5-4.7. All known variables listed are substituted into the 3D Euler equation of motion to find the three unknown moments.

## 4.4 Data Processing

The data processing stage is a lengthy and timely task if it is completed manually without the assistance of Matlab code automation. Each subject completes an average range of 30-60 trials during the gait laboratory data collection session. Each trial requires the exportation of two distinct files known as Trace (TRC) and Comma Separated Value (CSV) files for further processing.

### 4.4.1 Vicon Nexus

Vicon Nexus records all the motion capture and force plate data collected in the gait laboratory from each individual trial. Each trial requires further processing before the files can be exported into OpenSim. Each trial is selected in Vicon Nexus to label and gap fill the captured markers. The markers are labelled in accordance with their respective anatomical location as shown in figure 4.11. This labelling process defines each marker for the duration of the trial, so Vicon Nexus can calculate the exact coordinates of each respective marker at every time point. Gap filling is the process which defines markers that are obstructed from the camera's vision for a number of frames. The user selects an appropriate marker with a similar trajectory to the missing marker, whereby Vicon Nexus fills the gap with the new trajectory. The final model displays the markers connected in accordance with their anatomical locations as shown in figure 4.12. Two files are exported for each trial as a result of completing the Vicon Nexus process, which include a TRC and CSV file. The TRC file contains the time, frame number and the 3D Cartesian coordinates of each of the 27 body markers. The CSV file contains the GRF's and moments detected by the force plates. The files require format reconstruction for OpenSim to be able to read the data correctly.



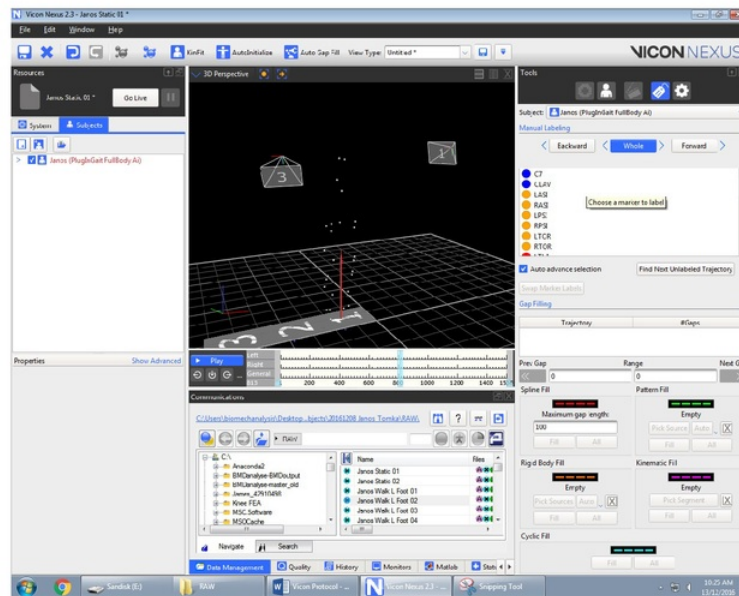


Figure 4.11: Vicon Nexus software platform capture space with virtual markers of subject before labelling.

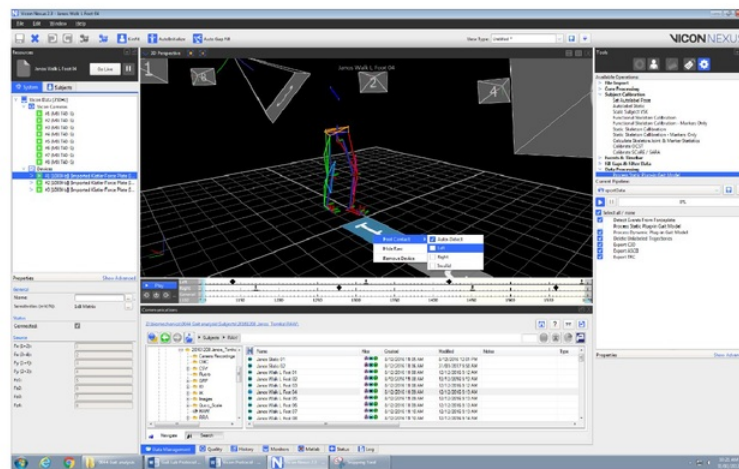
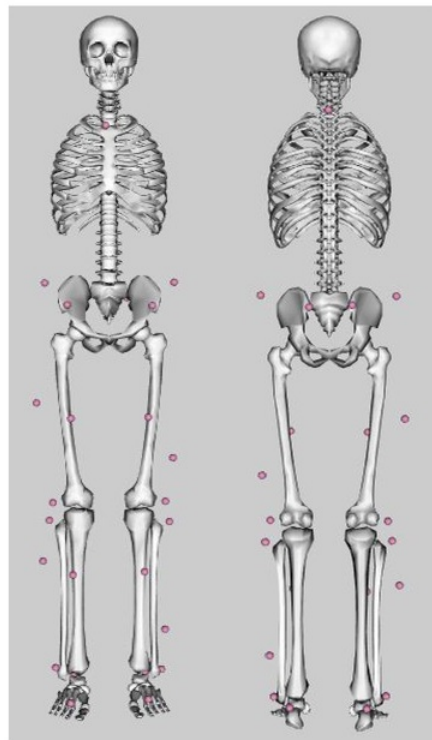


Figure 4.12: Final Vicon Nexus labelled virtual model of subject.

#### 4.4.2 OpenSim

OpenSim is utilised to complete the post processing of the data collection files, visually illustrating the results. Scaling is a process which is an effective tool in OpenSim that optimises the placement of the virtual markers. Scaling accounts for errors made during the experimental marker placement, reducing the effect of the error significantly. The scaling tool requires the mass of the subject and the experimental marker coordinates provided in the static TRC file. The TRC file exported by Vicon Nexus requires format changes, for OpenSim to successfully read the data. The final scaled model is used as the virtual skeleton which OpenSim performs the required calculations on as shown in figure 4.13. Inverse kinematics (IK) is a tool that calculates the joint centres of the hip, knee and ankle from the coordinates of the experimental markers provided in a dynamic TRC file. The IK tool formulates the joint angles of the hip, knee and ankle from the joint centres, yielding a motion file with the required results. The inverse dynamics (ID) tool is utilised within OpenSim to compute the moments experienced by the knee joint, by inputting both the IK motion and GRF files.



**Figure 4.13:** Final scaled OpenSim model.

## 4.5 Data Processing Automation

### 4.5.1 Matlab

Custom written scripts in Matlab are created to reduce the time taken to process the data collected and increase the efficiency of these tedious operations. The code shown in appendix A.2 converts the original TRC file exported from Vicon Nexus into the appropriate format for OpenSim to read. The changes include renaming the header line which includes the subject's name and the name of the markers, to only the name of the markers whilst also saving the file as a new file with the same file extension. This Matlab program reduces the processing time significantly, as the manual method would require the operator to edit each file in Notepad++ followed by saving each individual file as a new file.

The CSV files exported by Vicon Nexus require a file extension conversion as well as a number of other complex alterations. OpenSim can not read CSV files and hence the unique Matlab program converts the CSV file into a motion file (MOT). The GRF files are developed by using a uniquely written Matlab script shown in appendix A.3 and A.4. The GRF file is created using the force plate data within the CSV file recorded by Vicon Nexus. All forces measured by the force plate is firstly extracted from the CSV file to the new GRF file in specified column locations. The centre of pressure (CoP) data is then copied over in specific column locations as well as being converted into SI units through mathematical operations. The moments calculated are placed in the GRF file in designated columns while also being converted into SI units. Time is calculated within the Matlab code using mathematical methods which computes a specific time interval for each GRF file depending on the frame numbers and copies this data into the GRF file in the first column. The headers of the GRF file are in accordance with the OpenSim format requirements also executed in the Matlab script. Finally, the coordinate systems are transformed between local and global using mathematical transformations in Matlab and applying them to the appropriate data in the newly created GRF file.

The results obtained by OpenSim after executing the IK and ID processes create mot and sto files respectively, which include the final formatted data of each trial. In each file for both IK and ID, three out of the exported twenty-eight columns are required for statistical analysis which include knee flexion, knee rotation and knee abduction. Completing this manually is a timely process which requires copying and pasting each column to a separate spreadsheet. The custom Matlab script written shown in appendix A.8 executes this command for every file present in the folder, reducing the chance of human error and increasing the efficiency of the task dramatically. In addition, the code also calculates the gait cycle percentage automatically through mathematical operations, rather than having to manually obtain these results. Moreover, certain columns of data require to be multiplied by negative one for directional purposes, this is also included in the code which employs this command for each file. This Matlab code exports the

data into a single Microsoft Excel spreadsheet which contains a custom macro, using the in-built visual basic for applications (VBA) software. This macro employs the following operations, changes the title of the graphs, formats the axis of the graphs and its limits, deletes empty series where less than 10 trials are conducted and copies all the final graphs into a summary tab.

## **4.6 Signal Processing**

### **4.6.1 Butterworth Filter**

#### **TRC File**

Appendix A.6 illustrate a custom built Matlab program which inputs the numerical coordinates of the TRC file and outputs a TRC file with filtered numerical coordinates. The filter implemented is a fourth order low pass Butterworth filter with a cut off frequency of 6 Hz and sampling rate of 250 Hz, shown in appendix A.5.

#### **GRF File**

Appendix A.7 displays a uniquely built Matlab program which inputs the GRF's of the CSV file and outputs a MOT file with the filtered GRF's. The filter implemented is a fourth order low pass Butterworth filter with a cut off frequency of 300 Hz and sampling rate of 1000 Hz.

## 4.7 Flow Chart

The flow chart illustrated in figure 4.13 displays the complete list of steps required for this study. This includes the functions, files, and automations required to obtain the final results.



**Figure 4.14:** Process flow chart which displays all the steps taken to complete the gait data collection and analysis of a single subject.



# Chapter 5

## Results

In this chapter, the results of five healthy participants and five OA patients are illustrated and statistically analysed. The results comprise of the data collected in the gait laboratory for the OA and healthy subjects which include walking, stair ascent and stair descent trials. Vicon Nexus, OpenSim and custom built Matlab scripts enabled the knee flexion joint angles and joint moments to be calculated and presented accordingly. For the purpose of this study the OA affected group's data is compared to the healthy subject's data through statistical analysis. This investigation will determine if a statistical difference is evident in terms of KFA and KFM between the OA and healthy subjects, for the gait events completed. The data selected for analysis is comprised of the knee which is affected for OA patients, while the left knee data is utilised for the healthy participants. Selecting the left knee side only for control participants is a common method utilised, due to a symmetric data set demonstrated by both knee sides of the healthy cohort.

The graphs for each subjects KFA and KFM can be seen in appendix C. The plots display a number of trials for each subject, meaning the subject performed the same gait event in the same manner multiple times to demonstrate validity and authenticity of the results. The plots demonstrate consistency, evident by the overlapping of the curves for each subjects trials shown in appendix C. As a result of this, one trial was chosen for each plot to be statistically analysed [16,24]. The selected trial for each subjects data set is a clear representation of all the data collected. The characteristic trial is extracted from the  $n$  trials recorded for each unique subject for that specific gait event. Average curves are created in the results section for both IK and ID data which contain one curve for each subject, with the patients denoted by a black line and the participants by an orange line. Similar studies perform the same analysis of results by choosing a single representative curve from each subjects data and superimposing it on a single graph [16,24]. This serves as a visual aid to which clear distinctions or similarities can be observed between the OA and control groups.

The statistical analysis was computed using the statistics program Minitab. Levene's test was used for each sample comparison in order to determine if an equal variance could be assumed between the two groups data. If Levene's test produced a p-value of ( $p \leq 0.05$ ) the data is said to be statistically different in terms of variances and hence equal variances could not be assumed and vice versa. An independent Two-Sample T-Test was performed for each group comparison, to compare the population means between the OA and control group. The null hypothesis for each case is that there is no difference between the population means. The option to assume equal variances or not assume equal variances was dictated by the previous Levene's test p-value outcome. Column charts visually display the statistical results found in the tables which include the mean (max, min and RoM) represented by the blue and orange bars while the standard deviation (SD) is shown by the error bars. For clarity, statistically significant p-values are denoted by bold font in the statistical tables and a red asterisks in the column graphs.

## 5.1 Inverse Kinematics

The inverse kinematic results obtained are displayed and analysed in terms of the gait activities which were undertaken by the subjects in the gait laboratory. The IK results produced after processing the subjects data are displayed as graphs which plot the KFA measured in degrees on the y-axis against the gait cycle (%) or stance phase (%) on the x-axis. Table 5.1-5.3 convey the statistical outcomes calculated for the OA group compared to the healthy (control) group. The KFA determined during walking, step up and step down trials for OA and healthy subjects is the common variable which is being compared for statistical significant differences. KFA is separated into three quantitative values which include the global maximum (max), global minimum (min) and range of motion (RoM) which are extracted from the average curve plots. Figure 5.1 identifies the regions where the max and min are located as well as how the RoM is calculated. The quantitative variables are all measured in degrees.

### 5.1.1 Walking

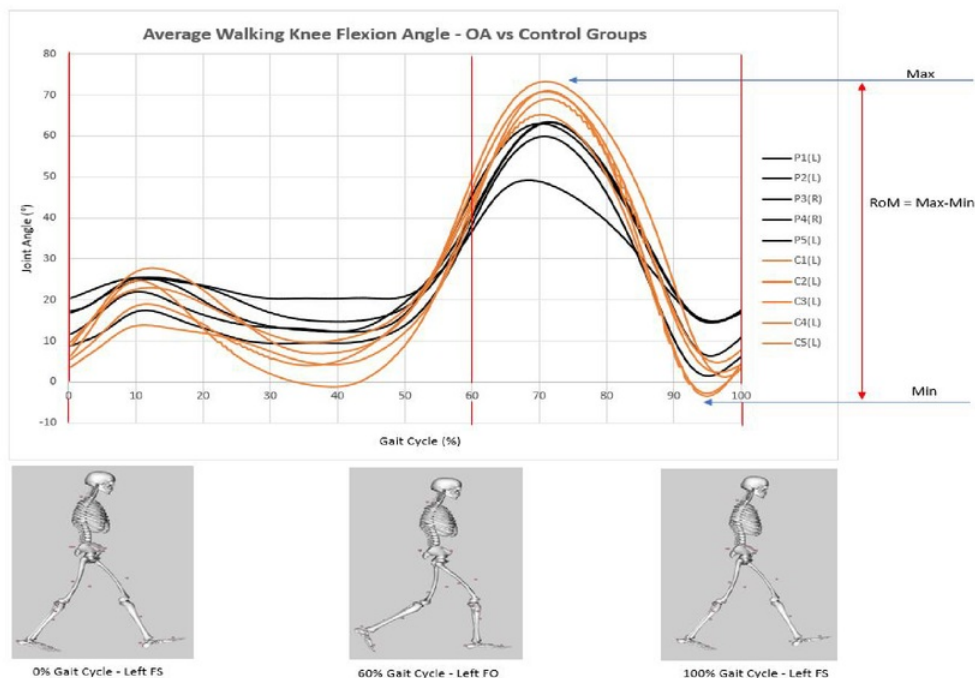
The average walking plot shown in figure 5.1 is made up of a single characteristic walking trial from the graphs shown in appendix C.1.1 for each subject. Figure 5.1 displays the KFA measured from 0-100% of the complete gait cycle. The gait cycle is defined in IK walking trials to be from FS until FS with the same leg. The skeleton models shown at the bottom of figure 5.1 signify the events taking place at 0, 60 and 100 % of gait cycle. Table 5.1 presents a statistical difference between max, min and RoM for OA against control walking trials. This is shown by the p-values to all be below the 0.05 significance level. The null hypothesis can be rejected and thus a statistical difference is evident between OA and control subjects in terms of the walking KFA calculated. The 95% confidence intervals do not contain the null value (0) which also confirms a statistically significant difference between OA and healthy subjects in terms of KFA in all three cases. Visually



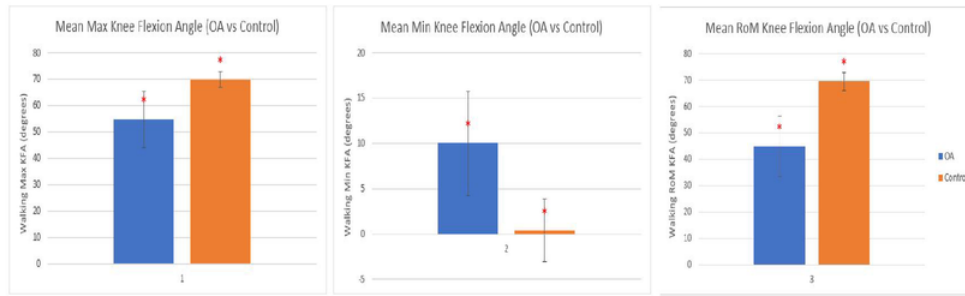
it can also be seen that there is a clear difference in the results when referring to figure 5.1, as the black lines are clearly below the orange lines at the maximum flexion point and higher at the minimum flexion or maximum extension point. The column charts in figure 5.2 also display the calculated mean and SD for both OA and control groups to be very different for the three quantitative variables.

**Table 5.1:** Comparison of walking KFA characteristics between OA and control subjects. A bold font p-value signifies statistical significance.

Variable	OA (n=5)		Control (n=5)		Mean difference (95% CI)	p-value
	Mean	SD	Mean	SD		
Knee Flexion Angle (KFA)						
Max (degrees)	54.80	10.70	69.84	2.95	-15.08 (-26.57, -3.59)	0.016
Min (degrees)	10.00	5.75	0.38	3.47	9.62 (2.69, 16.55)	0.013
Range of motion (degrees)	44.80	11.40	69.46	3.40	-24.70 (-36.94, -12.47)	0.002



**Figure 5.1:** Walking KFA plot for OA vs Control subjects. Contains one representative walking trial from each subject. Skeleton models demonstrate the gait events occurring at 0, 60 and 100% of gait cycle, indicated by red lines. Orange lines represent control data while the black lines denote OA data. Displays the max, min and RoM regions.



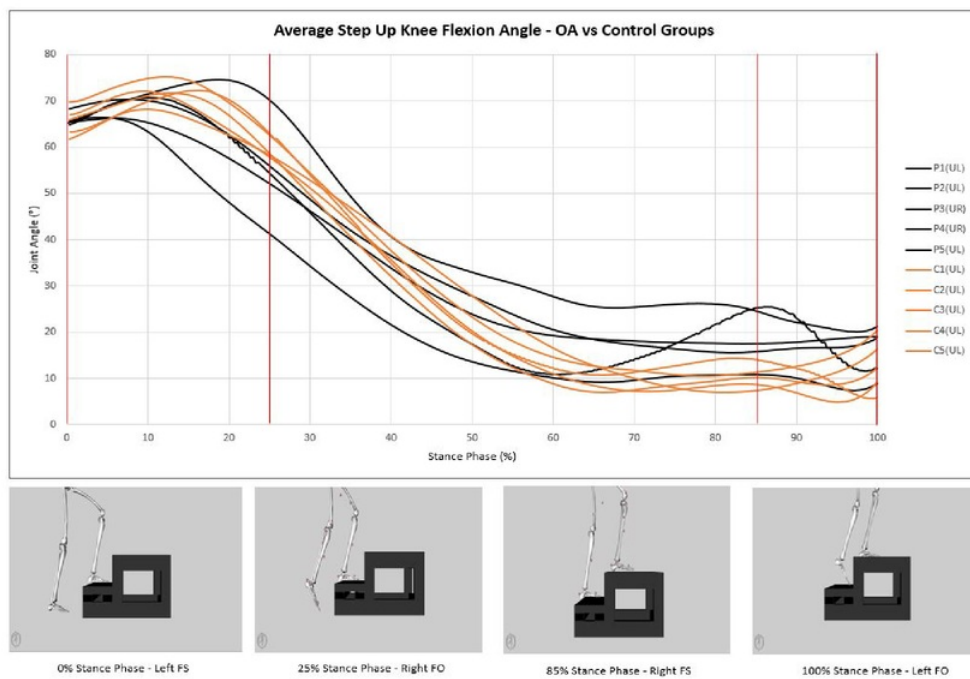
**Figure 5.2:** Mean and SD of walking KFA for OA and control individuals. Mean is represented by the rectangle box and SD is shown by an error bar. Red asterisk denotes statistical significance. OA and control subjects are identified as the blue and orange box, respectively.

### 5.1.2 Stair Ascent

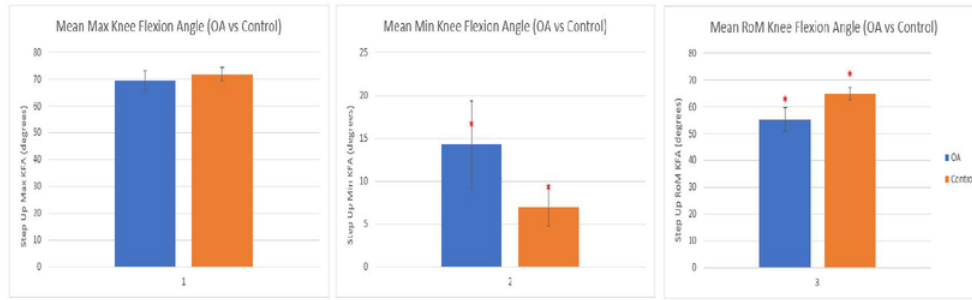
The average stair ascent plot shown in figure 5.3 displays one selected step up trial from each of the five OA and five control subjects shown in appendix C.1.2. The characteristic plot measures the KFA from 0-100% of the stance phase. The stance phase defined in the stepping up trials consists of the subjects data collected from FS until FO of the same leg. The skeleton models shown at the bottom of figure 5.3 signify the events taking place at 0, 25, 85 and 100 % of stance phase. Table 5.2 displays a statistical difference between the stepping up KFA min and RoM calculated for OA individuals compared with control participants. This variation is justified with the min and RoM p-value to be both below the 0.05  $\alpha$  level. Furthermore, the 95% CI's for both min and RoM do not contain the null value which also resembles a strong statistical difference. No significant difference is shown however for the max KFA between OA and control subjects, evident by the p-value exceeding the 0.05 significance level and the 95%CI (-6.66, 2.24) containing the null value. This means that the null hypothesis for stepping up KFA min and RoM can be rejected and thus a statistically significant difference is evident between OA and control subjects. The null hypothesis for the max KFA however is not rejected, meaning there is no significant difference between groups in terms of max KFA for stair ascent trials. Visually it can further be viewed that there is a clear difference in the results when referring to figure 5.3, the black lines are clearly above the orange lines at the minimum flexion point. The column charts in figure 5.4 also display the calculated mean and SD for both OA and control groups to be noticeably different for the KFA min and RoM, however very similar for max KFA.

**Table 5.2:** Comparison of stepping up KFA characteristics between OA and control subjects. A bold font p-value signifies statistical significance.

Variable	OA (n=5)		Control (n=5)		Mean difference (95% CI)	p-value
	Mean	SD	Mean	SD		
Knee Flexion Angle (KFA)						
Max (degrees)	69.67	3.53	71.88	2.49	-2.21 (-6.66, 2.24)	0.285
Min (degrees)	14.29	5.11	6.96	2.14	7.33 (1.62, 13.04)	<b>0.018</b>
Range of motion (degrees)	55.38	4.44	64.92	2.37	-9.54 (-14.73, -4.35)	<b>0.003</b>



**Figure 5.3:** Stair Ascent KFA plot for OA vs Control subjects. Contains one representative stepping up trial from each subject. Skeleton models demonstrate the gait events occurring at 0, 25, 85 and 100% of stance phase, indicated by red lines. Orange lines represent control data while the black lines denote OA data.



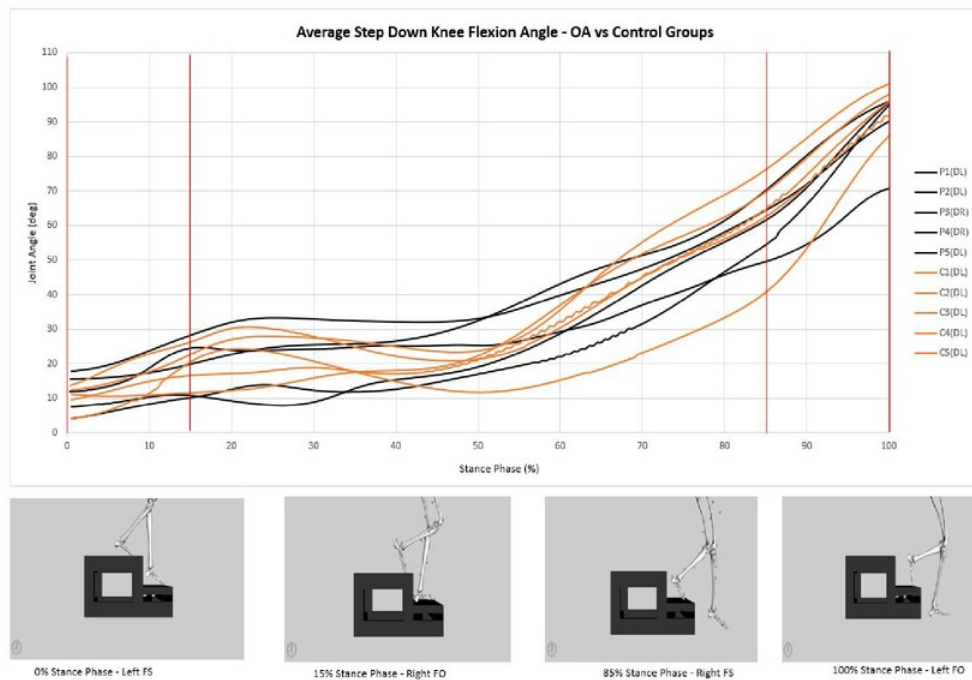
**Figure 5.4:** Mean and SD of stepping up KFA for OA and control individuals. Mean is represented by the rectangle box and SD is shown by an error bar. Red asterisk denotes statistical significance. OA and control subjects are identified as the blue and orange box, respectively.

### 5.1.3 Stair Descent

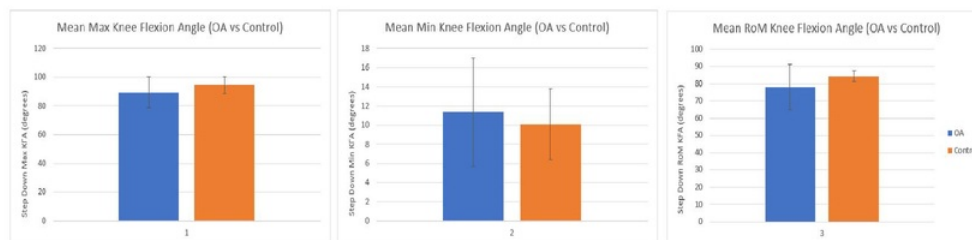
The representative stair descent plot shown in figure 5.5 displays one selected step up trial from each of the five OA and five control subjects shown in appendix C.1.3. The characteristic plot measures the KFA from 0-100% of the stance phase. The stance phase defined in the stepping down trials is made up of the subjects data collected from FS until FO of the same leg. The skeleton models shown at the bottom of figure 5.5 signify the events taking place at 0, 15, 85 and 100 % of stance phase. Table 5.3 displays no statistical difference between max, min and RoM for OA against control walking trials with a p-value greater than 0.05 for all three cases. In addition, the 95% CI's for KFA max, min and RoM contain the null value hence also resembling an insignificant difference between groups. The null hypothesis is not rejected, meaning there is no significant difference between groups in terms of max, min and RoM KFA for stepping down trials. Figure 5.5 demonstrates a fairly consistent set of curves for both OA and control subjects in terms of shape and range. This further portrays that no important differences can be drawn from stair descent trials in terms of KFA for OA and control groups. The column charts in figure 5.6 also display the calculated mean and SD for both OA and control groups to be very similar for the three quantitative variables.

**Table 5.3:** Comparison of stepping down KFA characteristics between OA and control subjects. A bold font p-value signifies statistical significance.

Variable	OA (n=5)		Control (n=5)		Mean difference (95% CI)	p-value
	Mean	SD	Mean	SD		
Knee Flexion Angle (KFA)						
Max (degrees)	89.4	10.8	94.53	5.81	-5.14 (-17.74, 7.47)	0.375
Min (degrees)	11.35	5.64	10.08	3.71	1.28 (-5.68, 8.24)	0.683
Range of motion (degrees)	78.00	13.00	84.45	3.23	-6.42 (-20.24, 7.41)	0.316



**Figure 5.5:** Stair Descent KFA plot for OA vs Control subjects. Contains one representative stepping down trial from each subject. Skeleton models demonstrate the gait events occurring at 0, 25, 75 and 100% of stance phase, indicated by red lines. Orange lines represent control data while the black lines denote OA data.



**Figure 5.6:** Mean and SD of stepping down KFA for OA and control individuals. Mean is represented by the rectangle box and SD is shown by an error bar. Red asterisk denotes statistical significance. OA and control subjects are identified as the blue and orange box, respectively.

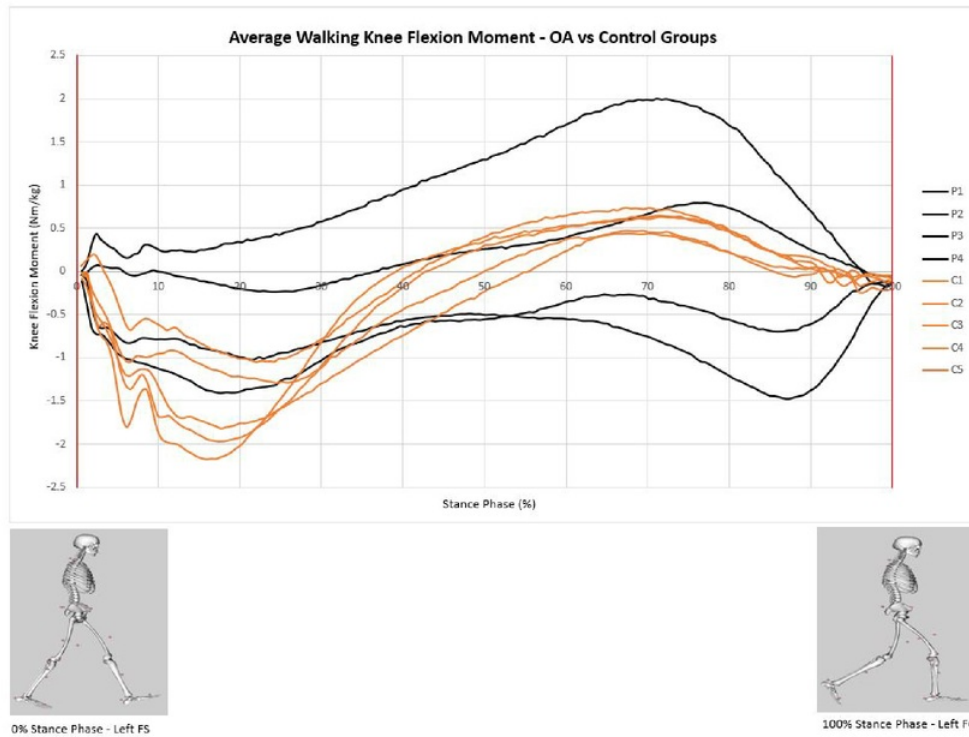
## 5.2 Inverse Dynamics

The ID results obtained are displayed and analysed in terms of the gait activities which were undertaken by the subjects in the gait laboratory. The ID results obtained after processing the subjects data is displayed as graphs which plots the KFM measured in (Nm) on the y-axis against the stance phase percentage on the x-axis. The moments calculated have been normalised to account for the subjects bodyweight by dividing the patients moment by body mass in kgs, hence the KFM is represented as Nm/kg. The stance phase percentage for stair ascent and stair descent comprise of the same gait events illustrated in the IK section. The ID results included one less OA patient due to the subjects force plate measurements not being sufficient for analysis. This means there are four OA patients being compared with five healthy participants for ID walking, stair ascent and stair descent only. The results obtained in the ID section are only visually comparable as any standard statistical method would create an inaccurate representation of the meaning of the results. This is due to the peaks and troughs of the data occurring at very different stance phase percentages. As a result of this, using normal statistical functions would not be able to compare the areas of interest accurately. Therefore complex statistics is required in the future to provide statistical results which accurately reflect the data and any correlations or differences.

### 5.2.1 Walking

The average walking plot shown in figure 5.7 contains one selected walking trial from each of the four OA and five control subjects displayed in appendix C.2.1. The plot measures the KFM from 0-100% of stance phase. The stance phase for ID walking includes the data collected between the initial FS and FO of the same leg. The skeleton models in figure 5.7 denote the two distinct gait events which occur at 0 and 100% of stance phase. In reference to figure 5.7 it is evident that the control group share a very similar KFM throughout the walking gait activity. The peaks and troughs occurring at the same stance phase percentages for control subjects further demonstrates consistency among the cohort. Conversely, within the OA group large disparities are seen in terms of KFM for their corresponding walking trials, visible by the peaks and troughs appearing at difference stance phase percentages. The phase difference of events is noticeably seen among the OA and control groups with the max and min occurring at different percentages of the stance phase.

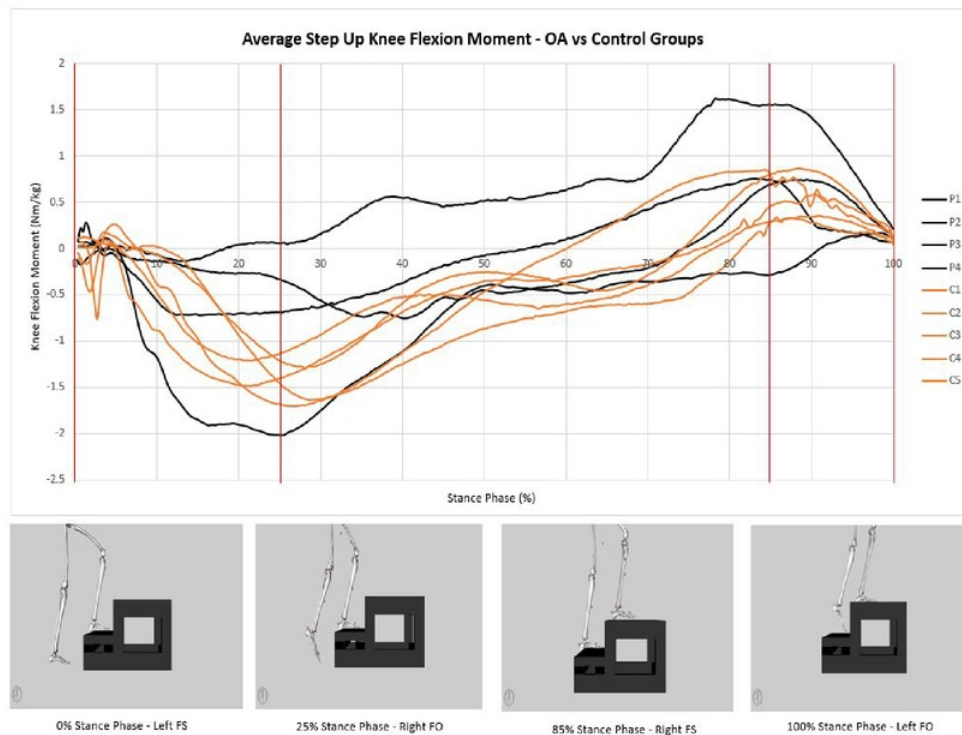




**Figure 5.7:** Walking KFM plot for OA vs Control subjects. Contains one representative walking trial from each subject. Skeleton models demonstrate the gait events occurring at 0 and 100% of stance phase, indicated by red lines. Orange lines represent control data while the black lines denote OA data.

### 5.2.2 Stair Ascent

The representative stair ascent plot shown in figure 5.8 displays one selected stepping up trial from each of the four OA and five control subjects displayed in appendix C.2.2. The plot measures the KFM from 0-100% of the stance phase defined in the IK stair ascent section. In reference to figure 5.8 it is evident that the control groups KFM is similar for the majority of the stance phase. Differences are visible when identifying the peaks and troughs of the control groups data, as they occur at different stance phase percentages. Similarly, within the OA group large fluctuations can also seen in terms of KFM for their corresponding stair ascent trials. The peaks and troughs of the OA patients data curves are also very dissimilar in terms of magnitude. The phase difference of events is clearly seen between the OA and control groups, with the max and min occurring at different percentages of the stance phase.

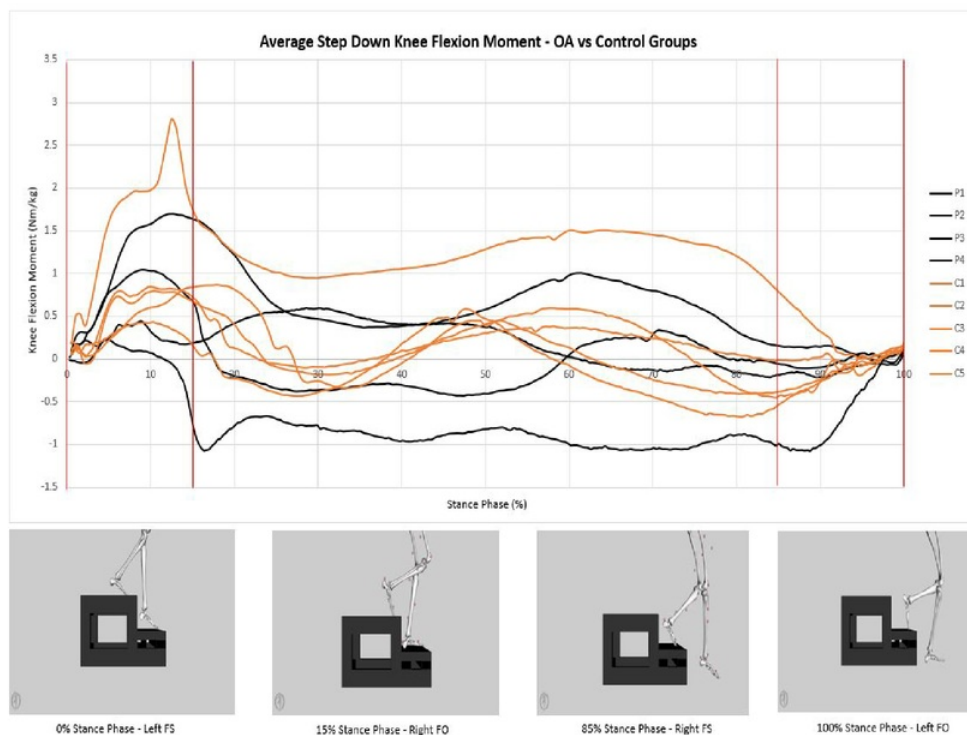


**Figure 5.8:** Stair Ascent KFM plot for OA vs Control subjects. Contains one representative stepping up trial from each subject. Skeleton models demonstrate the gait events occurring at 0, 25, 85 and 100% of stance phase, indicated by red lines. Orange lines represent control data while the black lines denote OA data.



### 5.2.3 Stair Descent

The characteristic stair descent plot shown in figure 5.9 shows one selected stepping down trial from each of the four OA and five control subjects displayed in appendix C.2.2. The plot measures the KFM from 0-100% of the stance phase defined in the IK stair descent section. In reference to figure 5.9 it is evident that the control groups KFM is similar for the duration of the stance phase. The main difference in the control data refers to the curve with a peak of 2.8 Nm/kg which appears to be an outlier. Within the OA group however, large fluctuations are seen in terms of KFM for their corresponding stair descent trials. The peaks and troughs of the OA patients data curves are also very dissimilar in terms of magnitude. The phase difference of events is clearly visible between the OA and control groups, with the max and min occurring at different percentages of the stance phase.



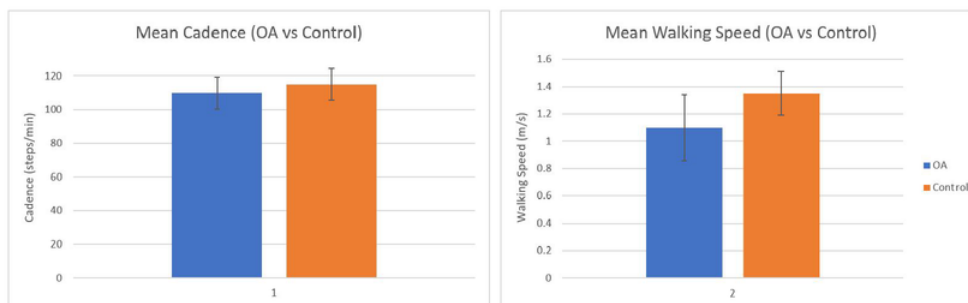
**Figure 5.9:** Stair Descent KFM plot for OA vs Control subjects. Contains one representative stepping down trial from each subject. Skeleton models demonstrate the gait events occurring at 0, 15, 85 and 100% of stance phase, indicated by red lines. Orange lines represent control data while the black lines denote OA data.

### 5.3 Temporal Spatial Parameters

The temporal spatial parameters (TSPs) or spatial temporal parameters (STPs) investigated in this study include the cadence and walking speed measured in (steps/min) and (m/s) respectively. The cadence and walking speed displayed no significant difference between the OA and control groups, demonstrated by the p-values exceeding the 0.05 level, shown in table 5.4. In addition, the 95% CI's for both cadence and walking speed contain the null value, meaning the null hypothesis is not rejected. As a result, no statistical difference is established between the OA and control groups TSPs recorded for walking trials. Figure 5.10 further conveys the similar outcomes of the mean and SD in terms of cadence and walking speed for OA and control individuals.

**Table 5.4:** Comparison of walking TSPs between OA and control subjects. A bold font p-value signifies statistical significance.

Variable	OA (n=5)		Control (n=5)		Mean difference (95% CI)	p-value
	Mean	SD	Mean	SD		
Walking						
Cadence (steps/min)	109.77	9.21	115.10	9.46	-5.34 (-18.95, 8.27)	0.392
Walking Speed (m/s)	1.10	0.24	1.35	0.16	-0.26 (-0.55, 0.03)	0.075



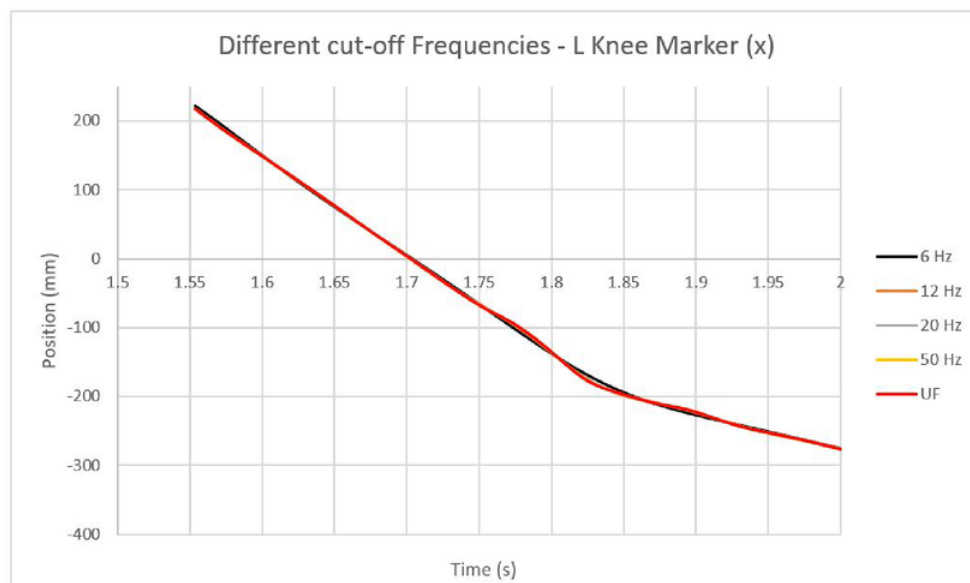
**Figure 5.10:** Mean and SD of walking TSPs for OA and control individuals. Mean is represented by the rectangle box and SD is shown by an error bar. Red asterisk denotes statistical significance. OA and control subjects are identified as the blue and orange box, respectively.

## 5.4 Signal Processing

### 5.4.1 Marker Trajectories

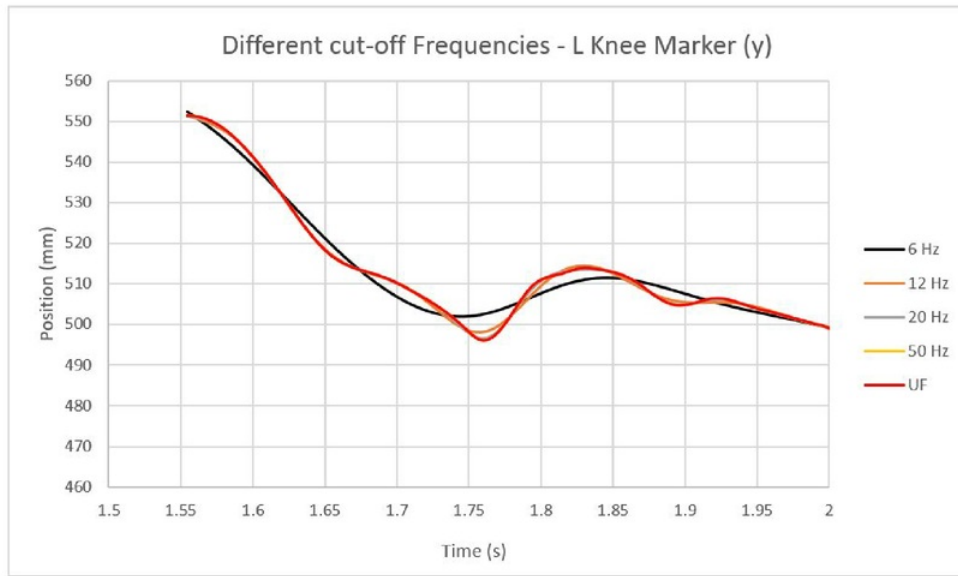
The TRC file exported from Vicon Nexus contains the marker trajectory data as three-dimensional cartesian coordinates denoted by (x, y, z) for each body marker. The left knee marker is plotted in figure 5.11-5.13 in terms of its x, y, z coordinates, which compares the position in millimetres (mm) of the body marker on the y-axis opposed with time in seconds (s) on the x-axis. The data is filtered using a 4th-order low-pass Butterworth filter uniquely designed in Matlab with the code shown in appendix A.5. The BW filter is set at various cut-off frequencies which include 6Hz, 12Hz, 20Hz and 50 Hz. The curves shown illustrate different cut-off frequencies plotted with the original unfiltered marker trajectories denoted by (UF) in the graphs. For each plot the same file was used to show any comparisons or similarities between the filter cut-off frequencies and the original marker positions.

Figure 5.11 displays no real difference in results in terms of the x position of the left knee marker between the filtered data and the UF data. This is evident by the overlap of the curves in figure 5.11 which demonstrate almost identical results for the same data set either being filtered at different frequencies or not filtered at all.



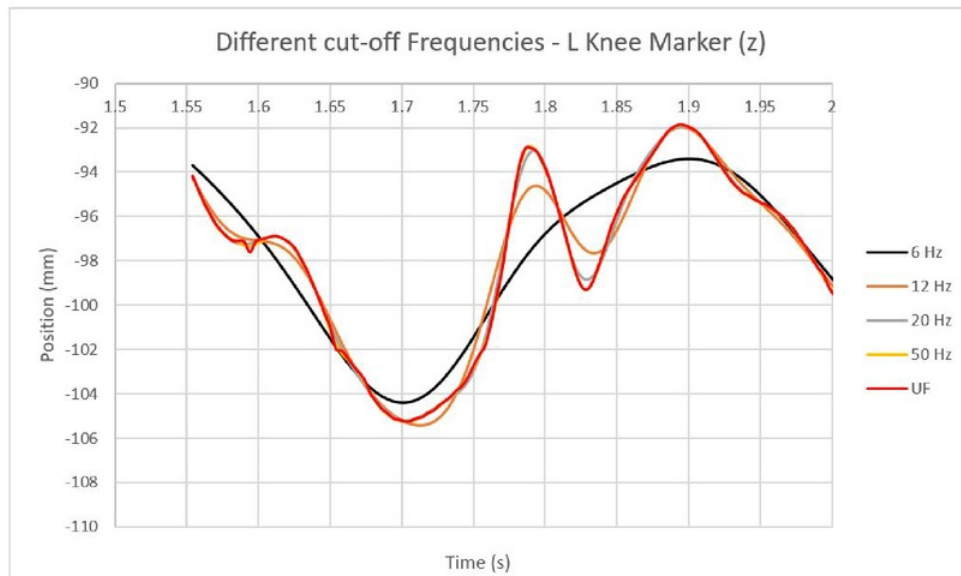
**Figure 5.11:** Plot of filtered vs UF marker trajectory data in the x direction at different cut-off frequencies.

Figure 5.12 demonstrates a minimal difference in results in terms of the y position of the left knee marker when the data is passed through the BW filter at 12 Hz compared to the UF data. An increased difference is shown between the 6 Hz filtered data and the UF data. The 6 Hz  $f_c$  demonstrates a much more smooth curve with different magnitude peaks and troughs. The  $f_c$  set at 20 and 50 Hz displays no sign of difference to the UF curve.



**Figure 5.12:** Plot of filtered vs UF marker trajectory data in the y direction at different cut-off frequencies.

Figure 5.13 demonstrates a more noticeable difference in the results in terms of the z position of the left knee marker when the data is passed through the BW filter at 12 Hz compared to the UF data. A large distinction can be seen between the 6 Hz filtered data and the UF data. The 6 Hz filtered data presents a much smoother curve, with different values for the peaks and troughs as opposed to the UF curve. The 20 Hz filtered data shows a slight difference in the peaks and troughs, while the 50 Hz filtered data portrays no sign of differences between the UF data.

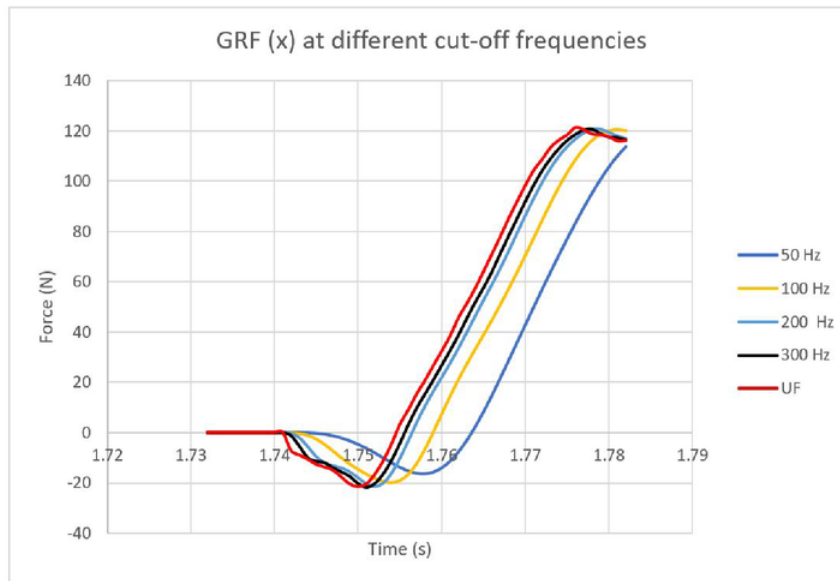


**Figure 5.13:** Plot of filtered vs UF marker trajectory data in the z direction at different cut-off frequencies.

### 5.4.2 Ground Reaction Forces

The CSV file exported from Vicon Nexus contains the force plate data which includes the reaction forces, CoP and moments in the x, y and z directions. A custom built Matlab code shown in appendix A.7 converts this CSV file to a GRF file as well as including a 4th order low-pass BW filter. Figure 5.14-5.16 convey the GRF's measured in Newtons (N) on the y-axis against the time measured in seconds (s) on the x-axis. The BW filter is set at various cut-off frequencies which include 50Hz, 100Hz, 200Hz and 300 Hz. The curves shown display different cut-off frequencies plotted with the original unfiltered GRF data denoted by (UF) in the graphs. For each plot the same file was used to show any comparisons or similarities between the filter cut-off frequencies and the unfiltered GRF data.

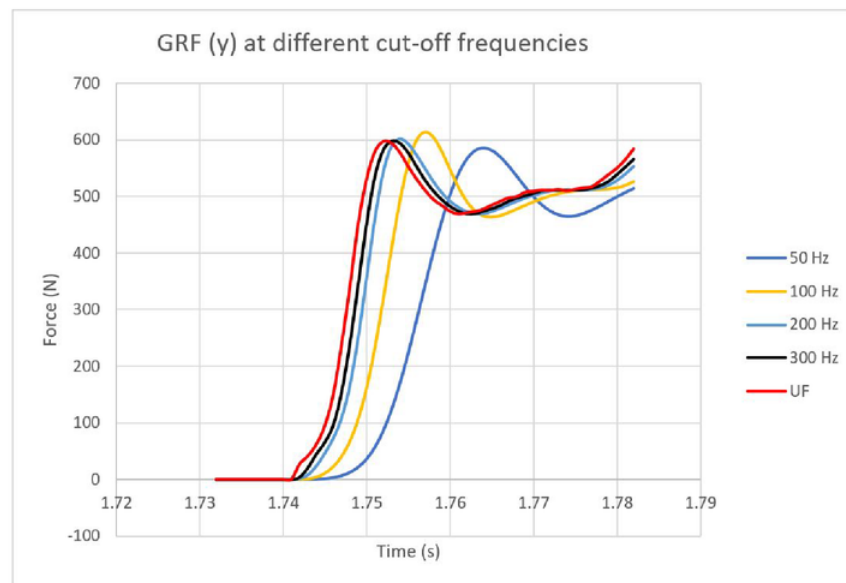
Figure 5.14 displays a close correlation between a large cut-off frequency and the UF data in terms of GRF's in the x direction. This is shown in reference to figure 5.14 by comparing the 300 Hz curve against the UF curve. Conversely, as the  $f_c$  is decreased, the filtered data curves move further and further away from the original UF GRF data curve, evident by the 50 and 100 Hz plots. The shape of the curve is also clearly different between the 50 - 200 Hz data and the UF data. The shape of the 300 Hz curve is very similar to the UF curve, however is more smooth in oscillating regions.



**Figure 5.14:** Plot of filtered vs UF GRF data in the x direction at different cut-off frequencies.

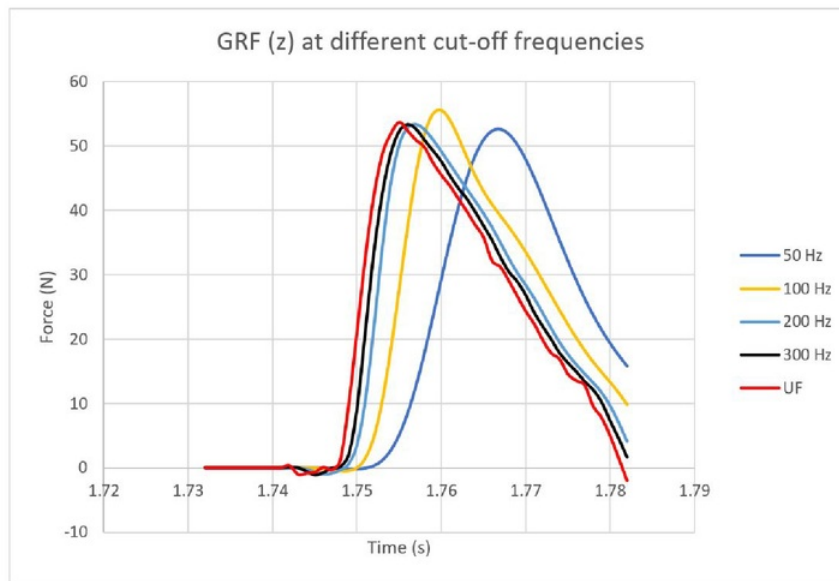


Figure 5.15 displays a close relationship between a large cut-off frequency and the UF data in terms of GRF's in the y direction. Conversely, as the cut-off frequency is decreased, the filtered data curves move further and further away from the original UF GRF data curve, evident by the 50 and 100 Hz plots. The shape of the curve is also clearly different between the 50 - 200 Hz data and the UF data. This is shown by the oscillating regions of the UF data being completely smoothened out in the 50-100 Hz data plots. The shape of the 300 Hz curve is very similar to the UF curve, however is more smooth in oscillating regions.



**Figure 5.15:** Plot of filtered vs UF GRF data in the y direction at different cut-off frequencies.

Figure 5.16 displays a close relationship between a large cut-off frequency and the UF data in terms of GRF's in the z direction. Conversely, as the cut-off frequency is decreased, the filtered data curves move further and further away from the original UF GRF data curve, evident by the 50 and 100 Hz plots. The shape of the curve is also clearly different between the 50 - 200 Hz data and the UF data. This is shown by the oscillating regions of the UF data being completely smoothened out in the 50-100 Hz data plots. The shape of the 300 Hz curve is very similar to the UF curve, however is more smooth in oscillating regions.



**Figure 5.16:** Plot of filtered vs UF GRF data in the z direction at different cut-off frequencies.



# Chapter 6

## Discussion

### 6.1 Walking

The results displayed in figure 5.1 and 5.7 portray the average KFA and KFM of the knee during walking trials. The positive axis is defined as flexion while the negative axis is identified by extension moments and joint angles. Figure 3.1 is comprised of the stance phase (60%) and swing phase (40%) which makes up the complete gait cycle. Joint angles for walking trials are determined by investigating the complete gait cycle. The moments however are calculated from the events which occur in the stance phase, shown in figure 5.7.

FS or initial contact occurs at 0-2% of gait cycle. Figure 5.1 demonstrates a starting KFA of between 5-10 degrees for healthy participants while for OA patients it lies in a higher range of 10-20 degrees. The foot flat or loading response phase occurs at about 2-12% of the gait cycle. The KFA is shown in figure 5.1 to have a magnitude of approximately 15-28 degrees and 18-25 degrees for control and OA subjects respectively. The midstance phase comprises of the knee beginning to extend shortly after flexing at its max point in the foot flat stage. This is indicated by an extending knee angle in figure 5.1 between 12-31% of the gait cycle for healthy subjects while occurring at an earlier stage for OA subjects. FO is during terminal stance phase occurs at an estimated range of 31-50% of the the gait cycle, demonstrates the knee starting to flex again. This is evident by a positive slope in the curve as well as a KFA of approximately 5-10 degrees for healthy participants. The pre-swing phase which is signified at the 50-62 % stage of the gait cycle consists of the FO event. The FO event in figure 5.1 illustrates a KFA of approximately 40-50 degrees and 35-40 degrees for control and OA subjects respectively. The initial swing phase occurs at approximately 62-75% of the gait cycle which conveys in figure 5.1 the KFA to increase to a range of 65-73 degrees and 50-63 degrees for control and OA subjects respectively. This difference in maximum KFA is shown to be statistically significant from table 5.1, with a p-value less than 0.05. The mid swing phase occurs at an estimated range of 75-87% of the gait cycle which shows the maximum KFA to come to an end. The knee then starts to extend after this maximum flexion point, hence the negative

slope of the curve in figure 5.1. The terminal swing phase is approximately from 87-100% of the gait cycle. The final gait event of FS occurs at the end point of the terminal swing phase. The KFA during this phase is approximately 25-35 degrees for both healthy and OA subjects. The knee is then extended until the final FS when the knee flexes again. The maximum extension angle or minimum flexion angle displayed at approximately 95% during the terminal swing phase is shown to be significantly different between OA and control subjects. This is demonstrated by a p-value below the 0.05 significance level for min KFA in table 5.1. As a result, the KFA RoM is also shown to be statistically different between the OA and healthy individuals referring to figure 5.1 and table 5.1.

The walking KFM graph in figure 5.7 displays a distinct variance between the way the control participants walk as opposed to the OA patients. The control subjects data curves can be viewed to be consistent across the duration of the stance phase, however the OA patients present a fairly dissimilar trend to one another. The control participants demonstrate an initial knee extension moment upon initial FS. This extension moment increases for the control group during the loading phase, where the transfer of weight naturally causes an extension moment. Conversely, the OA group demonstrate a mixed response when nearing the loading phase, whereby performing a transfer of weight forcing the subject to have an extended knee moment is uncomfortable or painful. Figure 5.7 shows the knee extension moment to be much smaller in magnitude for OA patients compared to control participants. This means the OA affected patient is slightly flexing to reduce the amount of weight transfer to the affected knee. This in turn results in a limp like gait where the OA patients knee is only slightly extending. This change in gait pattern could potentially be related to a slower walking speed and cadence for OA patients compared to healthy participants, shown in table 5.4.

## 6.2 Stair Ascent

The results displayed in figure 5.3 and 5.8 portray the average KFA and KFM of the knee during stair ascent trials. The positive axis is taken to be flexion while the negative axis is identified by extension moments and joint angles. The stair ascent trials comprise of the stance phase, that is the first 60% of the gait cycle shown in figure 3.1. The stance phase is made up of the events shown in figure 3.1 which are used to analyse the KFA and KFM of the stepping up trials.

Left FS is shown in figure 5.3 to have a starting KFA of between 62-70 degrees for healthy participants and OA patients. The large KFA is due to the subject having to flex there left leg as it elevates to reach the first step. The graph displays a knee extension angle at approximately the 15% mark of stance phase. This is a result of the lifting of the right foot up until right FO at the 25% stance phase point. During this period the left leg extends so the right leg can elevate to the top step and make FS, shown at 85% of stance phase. Finally, left FO indicates where the KFA begins to increase. Figure 5.3

demonstrates a consistent data set between OA and healthy participants. This means the stair ascent data is insufficient in providing biomechanical differences between OA and control individuals. The KFM plot displayed in figure 5.8 also shows a consistent set of results for both OA and control subjects. During the loading phase an inflection point is evident where the knee extension moment changes to become a KFM. This is due to the left leg extending as the right FO is in motion, followed by the left leg flexing for the right leg to reach the top step for FS. The extension moment is shown to be much less during this phase for the knee OA patients. Again this is due to the transfer of weight causing pain or discomfort, forcing the patient to develop a limp or slight flexion to relieve the affected OA knee side from an increased load. Finally, a KFM is seen as right FS occurs, followed by another inflection point at 85% stance phase which shows the final knee extension moment as the left foot reaches FO.

### 6.3 Stair Descent

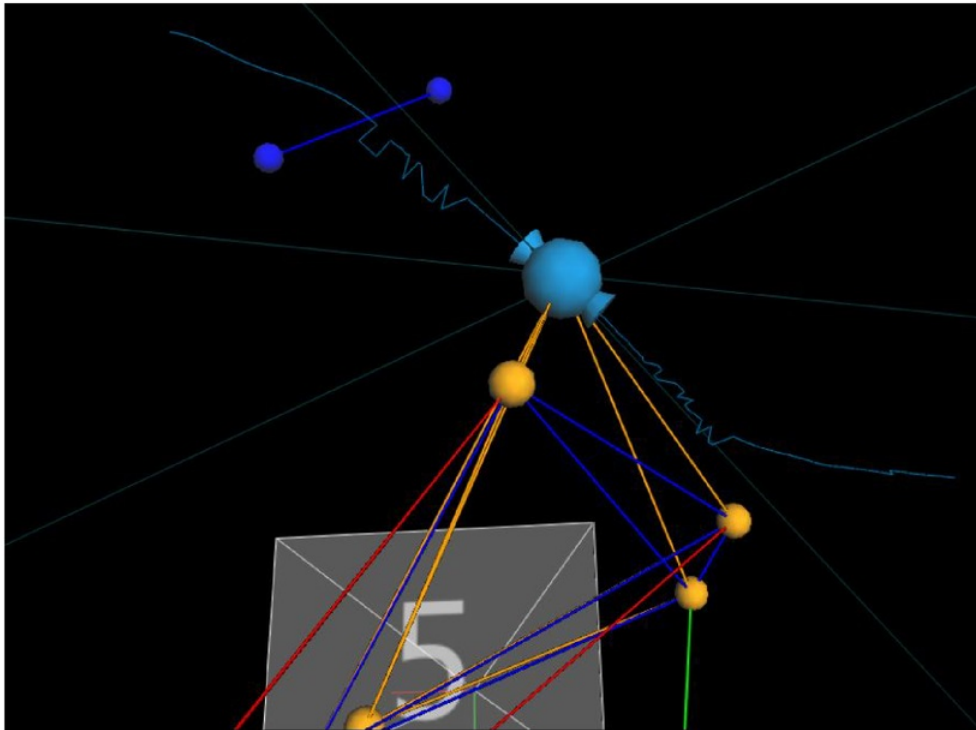
The results displayed in figure 5.5 and 5.9 portray the average KFA and KFM of the knee during stair descent trials. The positive axis is taken to be flexion while the negative axis is identified by extension moments and joint angles. The stair descent trials comprise of the stance phase, that is the first 60% of the gait cycle shown in figure 3.1. The stance phase is made up of the events in figure 3.1 which are used to analyse the KFA and KFM of the stepping down trials.

Left FS is shown in figure 5.5 to have a starting KFA of between 5-18 degrees for healthy participants and OA patients. This is a result of the flexion of the knee when stepping down in order for the left leg to make contact with the first step known as left FS. The KFA then begins to increase after the right FO event at 15%. This is due to the left leg flexing as the right foot moves to make contact with the ground. The right FS event which takes place at 85% of stance phase is shown by figure 5.5 to further increase KFA. The range of KFA at the 85% mark is approximately 40-75 degrees for both OA and healthy subjects. Finally, left FO denotes the maximum KFA as all the weight is transferred to the right leg. The KFA at left FO ranges from 70 - 100 degrees for both groups. The KFM displayed in figure 5.9 demonstrates the control individuals to have a consistent set of data. On the other hand, the OA patients can be seen to have dissimilarities in KFM, particularly in the magnitude of the troughs and peaks. The healthy participants are shown to have a KFM upon left FS, followed by an inflection point at the right FO event which occurs at approximately 15% of stance phase. When right FO occurs the left leg begins to flex in order for the right leg to make contact with the ground from the first step. The KFM is shown for OA patients to have a similar magnitude to the control participants. This is expected, as during the loading phase when the left foot is flat the left knee experiences a greater load, as the weight transfers from the right side to the left. As a result, the patient prefers to flex as extending the leg on the side of the OA affected knee would increase pain and discomfort.

## 6.4 Signal Processing

### 6.4.1 Butterworth Filter

Clinical studies have demonstrated mixed responses in terms of the correct filters and  $f_c$  to use when filtering marker trajectory and GRF data due to differences in gait equipment or data collection techniques. The Butterworth filter is utilised in this study for its unique frequency response of making the 0 Hz -  $f_c$  at -3dB as flat as mathematically possible, eliminating any oscillating regions. To determine the most effective BW filter type a range of  $f_c$  were selected from a number of studies. The range of  $f_c$  for marker trajectory data and GRF data is dissimilar due to the outcomes required from each set of data. Higher  $f_c$  were set for GRF data in order to preserve the details which occur in the raw data. Conversely, the range of  $f_c$  for marker trajectory data was selected to be lower due to the primary significance being to flatten the data as much as possible.

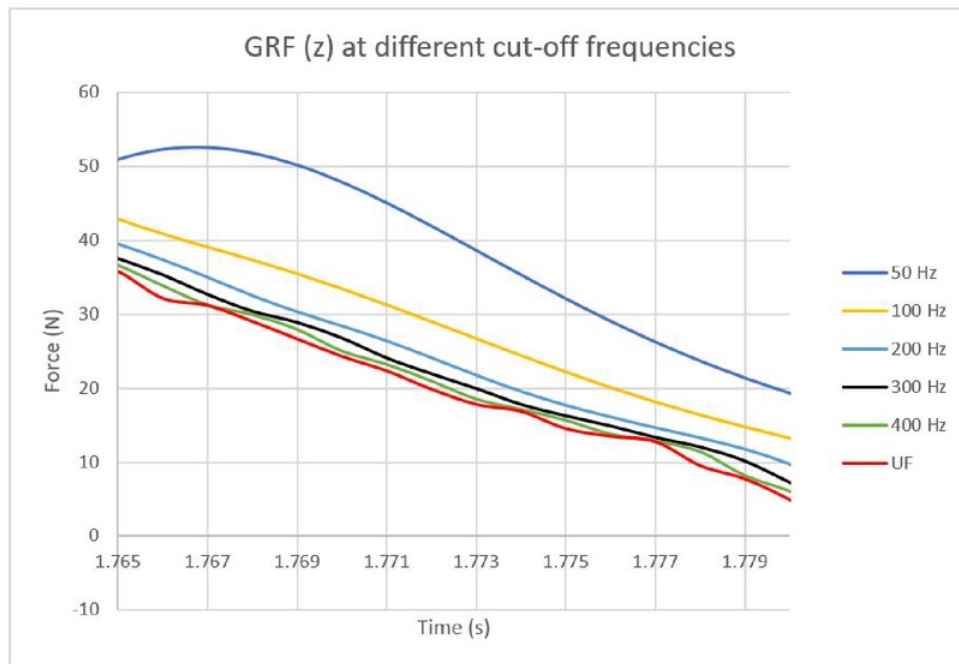


**Figure 6.1:** Vicon Nexus displaying a rippled or zig-zag like marker trajectory.

Marker trajectory data is obtained via an infrared motion capture system at a frequency of 250Hz. A single body marker trajectory is obtained by at least two IR cameras at any given time. Each camera has a tolerance for error which is improved with correct calibration. Although this error is small, a BW filter with the correct  $f_c$  can compensate for the error. Soft tissue is another source of error or extra noise which can become quite problematic. STA is the primary cause of error for optoelectronic gait capture techniques. Soft tissue movement causes the body marker to move through vibrations. The oscillation of soft tissue causes the motion capture cameras to track a rippled or zig-zag like trajectory of the marker as shown in figure 6.1. As a result of STA the error of the position tracked is increased and hence a filter is required with a suitable  $f_c$  to reduce it. The marker trajectory data displays a number of peaks and troughs in figure 5.13. The regions of vibration as shown in figure 5.13 are not of great importance due to their small difference in amplitude. This means if a marker trajectory is filtered the position will be slightly different to the UF marker trajectory at a time where oscillations are evident. The marker trajectory data is analysed in terms of the whole gait cycle. As a result, if the marker changes position due to the filter, it will be for a negligible amount of the complete gait cycle. Also, the joint centre calculations in OpenSim use a number of different marker locations to find the required joint centre. This means if one marker is slightly shifted in one direction as shown in figure 5.12-5.13 after filtering, then the final joint centre calculation will not be significantly affected.

Figure 5.11 demonstrates no real difference between the filtered data sets and the UF data curve. This is due to the UF waveform having a smooth and almost linear curve which requires minimal noise filtering. Figure 5.12 displays an UF curve that is comprised of data which oscillates regularly. The higher  $f_c$  values show minimal difference in the resultant curve compared to the UF curve. On the other hand, the curve with the  $f_c$  set at 6 Hz conveys a substantial difference to the UF data. The shape and direction is similar as is required however the ripples in the UF data is reduced greatly, displaying a smooth and flat data curve. Figure 5.13 illustrates a much more noticeable difference with the filtered data and UF data. The plot shows a clear distinction between the data filtered at 12 Hz  $f_c$ , due to the much more irregular shape and larger oscillating magnitudes of the UF data. The filter with  $f_c$  of 12 Hz still follows most ripples which the UF data portrays, however decreases the amplitude of them moderately. Conversely, the 6 Hz  $f_c$  filter completely eliminates the rippled regions of the UF data, creating a smooth and flat frequency response. As a result, a 4th-order low-pass BW filter set with a  $f_c$  of 6Hz is optimal, demonstrated in figures 5.12-5.13. The code which includes the marker trajectory BW filter is presented in appendix A.5. In reference to figures 5.12-5.13 the oscillating regions are clearly shown to be completely smooth with the data being filtered with a 6Hz  $f_c$  compared to the UF data curve. Subsequently, this means the zig-zag trajectory shown in figure 6.1 will become a smooth line which optimise's the outcome of the final IK and ID results.

GRF data is collected at a frequency of 1000 Hz by Kistler force plates. The force plates are very sensitive and hence pick up a large amount of external noise which include fans, floor vibrations, loud noises and industrial machines. The correct layout of the gait laboratory and mounting of the force plates ensures minimal external noise is produced. The threshold set for the force plates is 20N, meaning any force below 20N is not exported. Dissimilar from marker trajectory data, the events which occur in the GRF data are very important. The time at which the events occur signify the start and end time for a gait cycle. Subsequently, if the data is shifted making an event occur at a different time point by even one frame (0.001s) compared to the UF data, the data collected will be mismatched. This shift is evident in figures 5.14-5.16 where the low  $f_c$  filter values demonstrate a dramatic phase difference. As an example, referring to figure 5.16 the peak of approximately 54 N which occurs at 1.755s for UF data occurs at 1.767 seconds for the data filtered with a 50 Hz  $f_c$ . This shift of 0.012s is not significant in terms of analysing GRF data only, however when pairing with IK data, problems arise. The IK and ID tool in OpenSim is dependent on a start and end time which defines the gait cycle or stance phase for the event. This means if the above time difference of 0.012s occurs due to the low filter  $f_c$ , the marker trajectory data will no longer match the GRF data collected. Consequently, incorrect results will be produced which will be impractical for use. For this reason the  $f_c$  is set at 300 Hz due to figures 5.14-5.16 illustrating the minimal phase difference between the 300 Hz and UF data curves. Figure 6.2 displays an additional  $f_c$  of 400Hz plotted among the other  $f_c$  values and unfiltered data. This graph demonstrates that the higher the  $f_c$  the more closely the filtered curve aligns with the UF data curve. However, increasing the  $f_c$  value reduces the accuracy of the curve, as more noise passes through the filter. This is evident in reference to figure 6.2 as the green curve displays an increased region of the data to be rippled compared to the black line. As a result, the 300 Hz curve displays the best compromise in terms of gait events and phase difference. The code which includes the GRF BW filter is presented in appendix A.7. Setting the  $f_c$  at 300 Hz for GRF data improves the results output by the ID tool in OpenSim, hence enhancing the knee flexion moments calculated.



**Figure 6.2:** Plot of filtered vs UF GRF data in the z direction at different cut-off frequencies over a short time frame.

## 6.5 Data Processing

The processing of data in this study plays a large role in terms of formatting and manipulating the information to produce the correct results. This research paper contains three unique custom Matlab scripts which were designed to minimise the human error involved in manual data processing techniques by automating them.

Appendix A.2 shows the custom Matlab code written which automates the processing of TRC files. The code reduces the time taken significantly compared to completing the task manually which consists of changing the header names and saving each file as a new file with a new name. When there are in excess of 30-60 files per subject, errors are of increased risk due to fatigue and repetition of the same task.

Appendix A.3-A.4 displays the unique Matlab program constructed to automate the conversion of a CSV file to a MOT file containing only the GRF data. This piece of code executes a number of tedious and mathematical tasks which include, extracting the GRF data from the CSV file to the newly created MOT file, converting the global coordinate system in Vicon Nexus to the global coordinate system in OpenSim and then inverting the global coordinate system, mathematical operations convert the units to SI units, mathematically calculates the time for each unique file from the frame number, changes the names and format of the header and saves the new file with a MOT extension. Manually, this task would take hours to create one file let alone the average of 60 files per subject which would take days. The risk of human error is also substantial with many tedious and small tasks required to create the big picture.

Appendix A.8 demonstrates the specifically designed Matlab script which is the final processing stage of data shown in figure 4.13. The code performs numerous tasks which consist of the following, extracts data from the final formatted IK and ID files into a new excel spreadsheet, mathematically calculates the gait cycle percentage, multiplies the data depending on the input by negative one for coordinate system purposes and normalises the moment data by dividing the moment by the subjects body mass. Human error is a large possibility in this circumstance as hundreds of columns need to be extracted between files and placed in certain column locations. Furthermore, individually multiplying columns by negative one is also problematic if done manually as the wrong column could easily be multiplied, producing the wrong results. Manually calculating the gait cycle percentage is another large task that requires a great deal of time as this needs to be completed for each file. The code reduces all these possibilities of error and increases the efficiency of presenting the results significantly.



## 6.6 Problems and Solutions

This study comprises of methods and techniques which are novel in terms of producing the unique results for this investigation. Problems have emerged at various points of the research process which required solutions to improve and obtain the required outcomes. Issues which have been experienced throughout the study include the incorrect setup of the gait laboratory, the anatomical placement of body markers on the subject, mixing up the local and global coordinate systems in different software platforms, gap filling markers with various marker trajectories, not filtering marker trajectory and GRF data, using the scaling tool technique in OpenSim incorrectly, gait times implemented in the IK and ID OpenSim tool, incorrect multipliers for flexion, abduction and rotation, incorrect use of marker trajectory filter and the graphing of results. For each of the problems stated, solutions have emerged making the procedure a much more fluent and accurate set of steps.

The gait laboratory comprises of a vast amount of variables which need to be taken into account when setting it up for the collection of subject gait data. Problems encountered during the setting up of the gait laboratory were primarily due to the team being unfamiliar of the software settings. The dimensions of the force plate and their corresponding location in space were incorrect for a number of subjects. This was only identified when a Vicon Nexus specialist provided the team with a face to face tutorial of how to correctly input the system parameters. Another key issue was the 8 force pins per force plate were mixed up meaning the data collected was inhibited in certain directions. This was fixed by spending a day in the gait laboratory where each setting detail of Vicon Nexus and Bioware were checked and addressed if incorrect.

The placement of skin markers on anatomical locations has been a consistent problem throughout the study. The main reason is due to the patients containing a large soft tissue percentage which makes locating bony landmarks through palpating even more of a challenge. Developing a protocol which contained techniques for the subject and person marking increased the accuracy of marker placement towards the latter end of the study.

Utilising the programs Vicon Nexus and OpenSim also demonstrated problematic, as each program had a unique way of defining certain characteristics such as the coordinate system. While OpenSim utilised the International Society of Biomechanics coordinate system, Vicon Nexus presented a different local and global coordinate system for GRF and marker trajectory data respectively. This was transformed a number of times incorrectly due to misunderstanding the coordinate system Vicon Nexus was actually using for each component. Subsequently, understanding the direction and meaning of the GRF resultant vector lead to the correct transformation solution.

The marker trajectories shown in Vicon Nexus require a gap fill function when the markers position is missing for more than one frame. At the beginning of the study the missing

marker trajectory would be filled with any marker on the segment, not knowing the implications this would cause. At a later stage, the results of IK were shown to be dissimilar to the general findings. This problem was fixed by locating a marker on the same segment which shared a very similar trajectory to the missing marker. The gap fill function produced much smoother and accurate marker trajectories when the correct marker was chosen. Resultantly, precise IK results were produced which aligned with the general findings.

Initially, the marker trajectory and GRF data was not filtered during the process. This demonstrated large variations in the final processed IK and ID data. Custom filters were designed in Matlab which filtered the appropriate data. The filtering methods improved the results significantly, as the plots displayed similar characteristics to other clinical studies.

The scaling tool in OpenSim was and still is perhaps the most problematic process of the study. The scaling of the subject in the early stages of the study was completed with minimal knowledge of what the implications were of moving virtual markers. It became clear when the results were constantly different from general findings that scaling played a significant role. New techniques and methods were implemented in the scaling process which profoundly changed the results. After the successful scaling of a subject there was a clear comparison seen between the old scaled model results and the optimised scaled model results.

The IK and ID tool within OpenSim requires a start and end time which defines the gait cycle or stance phase under investigation. During the early stages of the study, the times input into the tools were obtained from visual observation of gait events in Vicon Nexus. This yielded a number of errors in the data causing important results to be inhibited. This was solved by utilising a feature in Vicon Nexus which allows for the force plates to detect gait events. Subsequently, Vicon Nexus exported the exact time at which the events occurred. As a result, this improved the outcome significantly with the graphs displaying similar trends and features to the general findings.

## 6.7 Limitations

The limitations of this study are carried over from similar gait analysis research restrictions. Time is the primary limitation experienced throughout this study. This study was dependent on the amount of subjects willing to participate. Subsequently, bookings which took weeks of notice were required and hence a study of this scope needs the appropriate time to accommodate. The facilities such as the gait laboratory also required bookings as it is a shared space and challenging to find a free slot. The sample size was another restriction which coincided with having a short time frame and a lack of patients and participants available for investigation. Statistical analysis could only be performed for a small number of null hypothesis as the sample size was too small for thorough statistical functions. Common statistical tests could not be utilised due to the small sample size, hence making the presentation of results and determining similarities or differences between groups challenging. The portable stair case utilised comprised of only one step which could mount a portable force plate, limiting the gait analysis for stepping trials to only the stance phase. Increasing the number of steps which can mount portable force plates would allow for a complete gait cycle of gait data to be collected. This limitation restricted different understandings and comparisons from being determined in terms of stepping activities for OA and control subjects. The process of marking up is a challenging task due to the soft tissue palpitations which has greatly limited the data. Many of the subjects investigated contained high percentages of soft tissue. As a result, the increased soft tissue the harder for the anatomical location to be defined and for the marker to represent the bony landmark position. Not having access to clustered markers or virtual markers significantly limited the data collected. The alternate marker methods can provide improved marker trajectories which are closer to the anatomical location of interest. These methods are superior especially when high percentage soft tissue subjects are involved, as finding bony landmarks is a challenge for even experienced clinicians. Restricted to only eight IR motion capture cameras was another constraint which effected the outcomes of the results. Increasing the number of cameras provides an increased accuracy, as more cameras will be able to identify a single marker, hence producing a lower tolerance for marker trajectory error. The gait laboratory used for the study also served as a constraint. The dimensions of the laboratory and the positioning of the key components in the room forced cameras to be placed in undesirable positions. Furthermore, the gait laboratory was a shared space which meant each time data was to be collected, important components would be moved around or changed. This limited the consistency of results produced and lead to increased errors as other users of the gait lab unknowingly changed significant configuration files and camera positions. The Gait2392 model was another limitation in terms of its default dimensions and characteristics.



## Chapter 7

### Conclusion

In conclusion, this study presents various biomechanical differences between knee OA and healthy individuals. Statistical differences were apparent for both the walking and stair ascent trials, which displayed knee OA patients to have a greater KFA min and a smaller RoM in relation to control participants. The stepping down trials presented no significant differences between OA and control subjects in terms of KFA. The KFM were found to be consistent across all types of gait activities for control subjects. Conversely, the KFM for OA patients was dissimilar across the three activities in relation to the magnitude and locations of the peaks and troughs. Limiting the sample results to only investigate flexion/extension in terms of KFA and KFM reduced the number of potential biomechanical differences that could be determined between knee OA and healthy subjects. Analysing the adduction and rotation joint angles and moments of subjects is proposed for future work, which may bring about new understandings of the biomechanical differences between knee OA and healthy subjects. The custom built BW filters with cutoff frequencies 6Hz for marker trajectory data and 300Hz for GRF data exhibited a major improvement in IK and ID results. This was shown by the changes in signal characteristics such as flattening of the peaks and troughs for marker trajectory data and filtering out noise for GRF data, while maintaining a close phase difference in gait events. The automation of data processing through unique Matlab scripts further provided more accurate results while decreasing the human error and increasing efficiency.



## Chapter 8

### Future Work

The future work is aligned with eliminating the limitations associated with this study. This includes primarily ensuring enough time is set for collecting and analysing the data. A large sample size is also preferred for a study such as this. The increased data from an increased sample size would make the statistics more representative of the actual results obtained. In addition, more statistical analysis could be conducted which require larger sample sizes producing various outcomes which would demonstrate statistical significance or insignificant findings. Relationships between variables is also an important characteristic to determine the biomechanical differences between OA and healthy knee joints, which is useful with large population groups. Complex statistical tests are also required to be implemented in future studies for data such as the ID results presented, where the curves were inconsistent and beyond the scope of basic statistical tests. The knee joint angles and moments in terms of abduction/adduction and internal/external rotation are important key components which can identify a range of characteristics which flexion/extension can not demonstrate. Investigating these different variables can lead to a number of unique understandings about the potential biomechanical differences between OA and control subjects. Further advancements are also required in the automation of scaling the virtual model. Automating the scaling process has the potential to improve the outcomes significantly, especially in terms of adduction and rotation results. Importing the actual dimensions of the lower extremities of the body would allow a virtual model to be created which more accurately represents the subject under investigation. The individual would undergo various MRI scans of different parts of the lower extremities such as the pelvis and femur, where these files would be directly imported into OpenSim. This will further optimise the scaling process as less scaling will need to be done for each subject due to the correct model being utilised which resembles their actual body dimensions. Future advancements have the potential to build upon this study and provide the scientific community with different key understandings of how the biomechanical characteristics can be used to investigate real world problems such as knee OA.





# Appendix A

## Data Processing Automation

### A.1 Overview

This section displays the custom built Matlab programs which are responsible for automating the data processing and post processing stages. These unique codes perform complex mathematical manipulations and transformations from various coordinate systems. In addition, the signal processing custom Matlab scripts are also displayed in this section which comprise of the various filters used in order to obtain the correct results.

### A.2 TRC File - Automated File Format Reconstruction

```
% TRC automation
%
% Author: James Naim
%
% Code written in Matlab 2017a
%
% Imports original TRC file , changes row 4 headers and saves new
    TRC filename_processed
%
% Import the TRC file called mainOutput
function mainOutput = TRC_Automation()

% Initialize variables.
delimiter = '\t';

startRow = 6;
```

[illegible]

```

Numbers = table(Text{1:end-1});

% Initialize variables.
delimiter = '\t';

startRow1 = 1;
endRow1 = 5;

% Extract header data from each TRC file in the selected
  folder
fileID(f)=fopen(string(L1(f)));
Text=textscan(fileID(f), formatSpec, endRow1(1)-startRow1(1)
  +1, 'Delimiter', delimiter, 'TextType', 'string', '
  HeaderLines', startRow1(1)-1, 'ReturnOnError', false, '
  EndOfLine', '\r\n');
$f_c$lose(fileID(f));
Header = table(Text{1:end-1});

%Create final variable by combining Header and Numbers
mainOutput1=vertcat(Header,Numbers);
mainOutput2=table2array(mainOutput1);

% Change Column Headings
B=[cellstr('Frame#'),cellstr('Time'),cellstr('C7'),cellstr
(''),cellstr(''),cellstr('CLAV'),cellstr(''),cellstr(''),
cellstr('LASI'),cellstr(''),cellstr(''),cellstr('RASI'),
cellstr(''),cellstr(''),cellstr('LPSI'),cellstr(''),
cellstr(''),cellstr('RPSI'),cellstr(''),cellstr(''),
cellstr('LTOR'),cellstr(''),cellstr(''),cellstr('RTOR'),
cellstr(''),cellstr(''),cellstr('LTHI'),cellstr(''),
cellstr(''),cellstr('LKNE'),cellstr(''),cellstr(''),
cellstr('LTIB'),cellstr(''),cellstr(''),cellstr('LANK'),
cellstr(''),cellstr(''),cellstr('LHEE'),cellstr(''),
cellstr(''),cellstr('LTOE'),cellstr(''),cellstr(''),
cellstr('LQUA'),cellstr(''),cellstr(''),cellstr('LFIB'),
cellstr(''),cellstr(''),cellstr('LSHI'),cellstr(''),
cellstr(''),cellstr('RTHI'),cellstr(''),cellstr(''),
cellstr('RKNE'),cellstr(''),cellstr(''),cellstr('RTIB'),
cellstr(''),cellstr(''),cellstr('RANK'),cellstr(''),
cellstr(''),cellstr('RHEE'),cellstr(''),cellstr(''),
cellstr('RTOE'),cellstr(''),cellstr(''),cellstr('RQUA'),
cellstr(''),cellstr(''),cellstr('RFIB'),cellstr(''),
cellstr(''),cellstr('RSHI'),cellstr(''),cellstr('')];

```

```
mainOutput2(4,:)=B';

% Selecting the TRC file to be processed
filename2=char(filename1(1,f));
F2=strsplit(filename2, '. ');
filename3=char(F2(1,1));
exportfile=strcat(filename3, '_Processed ', '.trc ');
fileID(f)=fopen(char(exportfile), 'w');

% Creating new TRC file
[rows, cols]=size(mainOutput2);
for i=1:rows
    for j=1:cols
        fprintf(fileID(f), '%s\t', mainOutput2{i, j});
    end
    fprintf(fileID(f), '\n');
end
end
fprintf('Thank you, processing is complete. \n');
end
```

```
% CSV to GRF Converter Automated
%
% Author: James Naim
%
% Code written in Matlab 2017a
%
% Import the CSV file called data
function data = CSV_GRF_Converter_Automation_Unfiltered()

% Initialize variables.
delimiter = ',';

startRow = 1;
endRow = inf;

% Number of columns of importfile
formatSpec = '%s%s%s%s%s%s%s%s%s%s%s%s%s%s%s%s%s%s%s%s%s%s[s\n\r]';
fprintf('Choose the directory where the files to be processed are located in!\n');
% Open required directory with CSV files inside
directory = uigetdir('');
% List all files with .CSV extension in the directory selected
G= dir(fullfile(directory,'*.CSV'));

% Number of CSV files
nTrials = size(G);
fileCount = nTrials(1,1);
P=fileCount;

% Listing files in the directory
G1=struct2cell(G);
L=(G1(1,:));
L1=transpose(L);

% Selecting filename of the TRC file to be processed in the directory chosen
```

```

fprintf('Choose the directory which the processed files should
be saved in!\n');
directory1 = uigetdir('');
filename= dir(fullfile(directory1, '*.CSV'));
filename1=struct2cell(filename);

% Columns with required data
x = [3 5 4 9 11 10 20 22 21 26 28 27 37 39 38 43 45 44 6 8 7 23
     25 24 40 42 41];

% Moment and distance converted to metres
x1 = [4 5 6 10 11 12 16 17 18 19 20 21 22 23 24 25 26 27];

% New matrix with zeros in column 1
c1 = [ 2 3 4 5 6 7 8 9 10 11 12 13 14 15 16 17 18 19 20 21 22 23
     24 25 26 27 28];

fprintf('Processing! \n');

% Extract data from each file in the selected directory
for f=1:P
    fileID(f)=fopen(string(L1(f)));
    Text = textscan(fileID(f), formatSpec, endRow(1)-startRow(1)
        +1, 'Delimiter', delimiter, 'TextType', 'string', '
        ReturnOnError', false, 'EndOfLine', '\r\n');
    $f_c$fclose(fileID(f));
    data1 = double([Text{1:end-1}]);

    filename2=char(filename1(1,f));
    F2=strsplit(filename2, '.');
    filename3=char(F2(1,1));

    % Size of input file (data1) array
    E = size(data1);
    Rowz = E(1,1);

    % Variable A1 assigned as the 1st vector from CSV file which
    contains frame numbers
    k1 = 1;
    for i=1:Rowz
        A1(k1,1) = data1(i,1);
        k1=k1+1;
    end

```

```

% Finding the start row number for numerical data
A2=isfinite(A1); % 1 if num, 0 if char vector
A3=find(A2,inf,'first'); % Row number for every 1 found
numStart(1,1) = A3(4,1); % Starting row for numerical values

% Force, Moment and Distance vectors of the CSV file
for i=1:Rowz
    for j=1:length(x)
        A6(i,j) = data1(i,x(j));
    end
end

% Finding the end row number for numerical data
z1=0;
for z2=numStart:Rowz
    if z1==0
        if isnan(A1(z2,1))
            numEnd(1,1) = z2-1;
            z1 = 1;
        end
    end
end

% Data extract from CSV file to new array A7 with numerical
data only
z3 = 1;
for z4=numStart:numEnd
    A7(z3,:) = A6(z4,:);
    z3=z3+1;
end

% Number of rows with numerical data
rowC=numEnd-numStart+1;

% Size of A7 array
E1=size(A7);
Rowz1=E1(1,1);

for i=1:Rowz1
    for j=3:3:27
        A7(i,j)=A7(i,j)*-1;
    end
end

```

```

end

for i=1:Rowz1
    for j=x1
        A7(i,j)=A7(i,j)/1000;
    end
end

% Creating Header of zeros [6 x 28] matrix
A8 = zeros(Rowz1+6,28);

% Vector of zeros to be filled with frame number
frameNumber = zeros(Rowz1,1);

% Frame number vector
z5 = 1;
for i = numStart:numEnd
    frameNumber(z5,1) = A1(i,:);
    z5=z5+1;
end

% Time vector
for i = 1:length(frameNumber)
    Time(i,1) = (4*(frameNumber(1,1) - 1) + i-1)/1000;
end

% Filling A8[:,1] with time
z6 = 1;
for j = 7:Rowz1+6
    A8(j,1)=Time(z6,1);
    z6=z6+1;
end

% Filling A8 columns 2-28 for all rows of size (A7) with
    data from A7
z7 =1;
for j = 7:Rowz1+6
    A8(j,c1)=A7(z7,:);
    z7=z7+1;
end

% Change Column Headings
rowCount = num2str(rowC);

```



```

nRow = strcat('nRows=',rowCount);
Header1 =[cellstr(filename3), cellstr(''),cellstr(''),
cellstr(''),cellstr(''),cellstr(''),cellstr(''),cellstr(''),cellstr(''),
cellstr(''),cellstr(''),cellstr(''),cellstr(''),cellstr(''),
cellstr(''),cellstr(''),cellstr(''),cellstr(''),cellstr(''),cellstr(''),
cellstr(''),cellstr(''),cellstr(''),cellstr(''),cellstr(''),cellstr(''),
cellstr(''),cellstr(''),cellstr(''))
cellstr(nRow), cellstr(''),cellstr(''),cellstr(''),
cellstr(''),cellstr(''),cellstr(''),cellstr(''),
cellstr(''),cellstr(''),cellstr(''),cellstr(''),
cellstr(''),cellstr(''),cellstr(''),cellstr(''),
cellstr(''),cellstr(''),cellstr(''),cellstr(''),
cellstr(''),cellstr(''),cellstr(''),cellstr(''))
cellstr('nColumns=28'), cellstr(''),cellstr(''),cellstr(''),
cellstr(''),cellstr(''),cellstr(''),cellstr(''),cellstr(''),
cellstr(''),cellstr(''),cellstr(''),cellstr(''),
cellstr(''),cellstr(''),cellstr(''),cellstr(''),
cellstr(''),cellstr(''),cellstr(''),cellstr(''),
cellstr(''),cellstr(''),cellstr(''),cellstr(''))
cellstr('inDegrees=yes'), cellstr(''),cellstr(''),
cellstr(''),cellstr(''),cellstr(''),cellstr(''),
cellstr(''),cellstr(''),cellstr(''),cellstr(''),
cellstr(''),cellstr(''),cellstr(''),cellstr(''),
cellstr(''),cellstr(''),cellstr(''),cellstr(''),
cellstr(''),cellstr(''),cellstr(''),cellstr(''),
cellstr(''))
cellstr('endheader'), cellstr(''),cellstr(''),cellstr(''),
cellstr(''),cellstr(''),cellstr(''),cellstr(''),cellstr(''),
cellstr(''),cellstr(''),cellstr(''),cellstr(''),
cellstr(''),cellstr(''),cellstr(''),cellstr(''),
cellstr(''),cellstr(''),cellstr(''),cellstr(''),
cellstr(''))
cellstr('time'),cellstr('1_ground_force_vx'),cellstr('1
_ground_force_vy'),cellstr('1_ground_force_vz'),
cellstr('1_ground_force_px'),cellstr('1
_ground_force_py'),cellstr('1_ground_force_pz'),
cellstr('2_ground_force_vx'),cellstr('2
_ground_force_vy'),cellstr('2_ground_force_vz'),

```

```

        cellstr('2_ground_force_px '), cellstr('2
        _ground_force_py '), cellstr('2_ground_force_pz '),
        cellstr('3_ground_force_vx '), cellstr('3
        _ground_force_vy '), cellstr('3_ground_force_vz '),
        cellstr('3_ground_force_px '), cellstr('3
        _ground_force_py '), cellstr('3_ground_force_pz '),
        cellstr('1_ground_torque_x '), cellstr('1
        _ground_torque_y '), cellstr('1_ground_torque_z '),
        cellstr('2_ground_torque_x '), cellstr('2
        _ground_torque_y '), cellstr('2_ground_torque_z '),
        cellstr('3_ground_torque_x '), cellstr('3
        _ground_torque_y '), cellstr('3_ground_torque_z ') ]];

% Creating a string cell array containing A8
data2 = string(A8);

% Copying the headings (Header1) into first 6 rows of data2
z8 = 1;
for i=1:6
    data2(i,:)=Header1(z8,:);
    z8=z8+1;
end

% Clearing variables to refresh data exported for each file
clear A1 A2 A3 A6 A7 A8

% Selecting the MOT file to be processed and exported as
filename_GRF.mot
exportfile=strcat(filename3,'_GRF.mot');
fileID(f)=fopen(char(exportfile),'w');

% Creating new MOT file with all the data stored in data2
array
[rows,cols]=size(data2);
for i=1:rows
    for j=1:cols
        fprintf(fileID(f),'%s\t',data2(i,j));
    end
    fprintf(fileID(f),'\n');
end
end
fprintf('Thank you, processing is complete. \n');
end

```

```
% CSV to GRF Converter Automated
%
% Changes FP CS and CoP GS to match OpenSim GS
%
% Author: James Naim
%
% Code written in Matlab 2017a
%
% Import the CSV file called data
function data = CSV_GRF_Converter_Automation_Filtered()

% Initialize variables.
delimiter = ',';

startRow = 1;
endRow = inf;

% Number of columns of importfile
formatSpec = '%s%s%s%s%s%s%s%s%s%s%s%s%s%s%s%s%s%s%s%s%s%s%s%s';
formatSpec = formatSpec + ['\n\r'];
fprintf('Choose the directory where the files to be processed
are located in!\n');
% Open required directory with CSV files inside
directory = uigetdir('');
% List all files with .CSV extension in the directory selected
G= dir(fullfile(directory,'*.CSV'));

% Number of CSV files
nTrials = size(G);
fileCount = nTrials(1,1);
P=fileCount;

% Listing files in the directory
G1=struct2cell(G);
L=(G1(1,:));
L1=transpose(L);

% Selecting filename of the TRC file to be processed in the
```

```

    directory chosen
fprintf('Choose the directory which the processed files should
    be saved in!\n');
directory1 = uigetdir('');
filename= dir(fullfile(directory1, '*.CSV'));
filename1=struct2cell(filename);

% Columns with required data
x = [3 5 4 9 11 10 12 14 13 18 20 19 21 23 22 27 29 28 6 8 7 15
    17 16 24 26 25];

% Moment and distance matrix needed to be converted to metres
x1 = [4 5 6 10 11 12 16 17 18 19 20 21 22 23 24 25 26 27];

% Centre of Pressure new z coordinate to multiply by -1
x2 = [6 12 18];

% Force Vector new x and y coordinate to multiply by -1
x3 = [1 2 7 8 13 14];

% Moment Vector new x and y coordinate to multiply by -1
x4 = [19 20 22 23 25 26];

% New matrix with zeros in column 1
c1 = [ 2 3 4 5 6 7 8 9 10 11 12 13 14 15 16 17 18 19 20 21 22 23
    24 25 26 27 28];

fprintf('Processing! \n');

% Extract data from each file in the selected directory
for f=1:P
    fileID(f)=fopen(string(L1(f)));
    Text = textscan(fileID(f), formatSpec, endRow(1)-startRow(1)
        +1, 'Delimiter', delimiter, 'TextType', 'string', '
        ReturnOnError', false, 'EndOfLine', '\r\n');
    $f_c$close(fileID(f));
    data1 = double([Text{1:end-1}]);

    filename2=char(filename1(1,f));
    F2=strsplit(filename2, '.');
    filename3=char(F2(1,1));

    % Size of input file (data1) array

```

```

E = size(data1);
Rowz = E(1,1);

% Variable A1 assigned as the 1st vector from CSV file which
% contains frame numbers
k1 = 1;
for i=1:Rowz
    A1(k1,1) = data1(i,1);
    k1=k1+1;
end

% Finding the start row number for numerical data
A2=isfinite(A1); % 1 if num, 0 if char vector
A3=find(A2,inf,'first'); % Row number for every 1 found
numStart(1,1) = A3(4,1); % Starting row for numerical values

% Force, Moment and Distance vectors of the CSV file
for i=1:Rowz
    for j=1:length(x)
        A6(i,j) = data1(i,x(j));
    end
end

% Finding the end row number for numerical data
z1=0;
for z2=numStart:Rowz
    if z1==0
        if isnan(A1(z2,1))
            numEnd(1,1) = z2-1;
            z1 = 1;
        end
    end
end

% Data extract from CSV file to new array A7 with numerical
% data only
z3 = 1;
for z4=numStart:numEnd
    A7(z3,:) = A6(z4,:);
    z3=z3+1;
end

% Number of rows with numerical data

```

```

rowC=numEnd-numStart+1;

% Size of A7 array
E1=size(A7);
Rowz1=E1(1,1);

% Multiply COP new z coordinate by -1
for i=1:Rowz1
    for j=x2
        A7(i,j)=A7(i,j)*-1;
    end
end

% Multiply new x and y coordinate for F and M by -1
for i=1:Rowz1
    for j=x3
        A7(i,j)=A7(i,j)*-1;
    end
    for k=x4
        A7(i,k)=A7(i,k)*-1;
    end
end

% Converting Centre of Pressure and Moment to SI Units
for i=1:Rowz1
    for j=x1
        A7(i,j)=A7(i,j)/1000;
    end
end

% Creating Header of zeros [6 x 28] matrix
A8 = zeros(Rowz1+6,28);

% Vector of zeros to be filled with frame number
frameNumber = zeros(Rowz1,1);

% Frame number vector
z5 = 1;
for i = numStart:numEnd
    frameNumber(z5,1) = A1(i,:);
    z5=z5+1;
end

```

```
% Time vector
for i = 1:length(frameNumber)
    Time(i,1) = (4*(frameNumber(1,1) - 1) + i-1)/1000;
end

% Filling A8[:,1] with time
z6 = 1;
for j = 7:Rowz1+6
    A8(j,1)=Time(z6,1);
    z6=z6+1;
end

% Filling A8 columns 2–28 for all rows of size (A7) with
data from A7
z7 =1;
for j = 7:Rowz1+6
    A8(j,c1)=A7(z7,:);
    z7=z7+1;
end

% Change Column Headings
rowCount = num2str(rowC);
nRow = strcat('nRows=',rowCount);
Header1 =[cellstr(filename3), cellstr(''),cellstr(''),
cellstr(''),cellstr(''),cellstr(''),cellstr(''),cellstr('')
cellstr(''),cellstr(''),cellstr(''),cellstr(''),cellstr(''),
cellstr(''),cellstr(''),cellstr(''),cellstr(''),cellstr(''),
cellstr(''),cellstr(''),cellstr(''),cellstr(''),cellstr(''),
cellstr(''),cellstr(''),cellstr(''))
cellstr(nRow), cellstr(''),cellstr(''),cellstr(''),
cellstr(''),cellstr(''),cellstr(''),cellstr(''),
cellstr(''),cellstr(''),cellstr(''),cellstr(''),
cellstr(''),cellstr(''),cellstr(''),cellstr(''),
cellstr(''),cellstr(''),cellstr(''),cellstr(''),
cellstr(''),cellstr(''),cellstr(''),cellstr(''),
cellstr(''),cellstr(''),cellstr(''),cellstr(''),
cellstr('nColumns=28'), cellstr(''),cellstr(''),cellstr(''),
cellstr(''),cellstr(''),cellstr(''),cellstr(''),cellstr(''),
cellstr(''),cellstr(''),cellstr(''),cellstr(''),
cellstr(''),cellstr(''),cellstr(''),cellstr(''),
cellstr(''),cellstr(''),cellstr(''),cellstr(''),
cellstr(''),cellstr(''),cellstr(''),cellstr(''),
```

```

        cellstr(''),cellstr(''),cellstr(''),cellstr('')
cellstr('inDegrees=yes'), cellstr(''),cellstr(''),
        cellstr(''),cellstr(''),cellstr(''),cellstr(''),
        cellstr(''),cellstr(''),cellstr(''),cellstr(''),
        cellstr(''),cellstr(''),cellstr(''),cellstr(''),
        cellstr(''),cellstr(''),cellstr(''),cellstr(''),
        cellstr(''),cellstr(''),cellstr(''),cellstr(''),
        cellstr(''),cellstr(''),cellstr(''),cellstr(''),
        cellstr('')
cellstr('endheader'), cellstr(''),cellstr(''),cellstr
(''),cellstr(''),cellstr(''),cellstr(''),cellstr(''),
        cellstr(''),cellstr(''),cellstr(''),cellstr(''),
        cellstr(''),cellstr(''),cellstr(''),cellstr(''),
        cellstr(''),cellstr(''),cellstr(''),cellstr(''),
        cellstr(''),cellstr(''),cellstr(''),cellstr(''),
        cellstr(''),cellstr(''),cellstr(''),cellstr('')
cellstr('time'),cellstr('1_ground_force_vx'),cellstr('1
_ground_force_vy'),cellstr('1_ground_force_vz'),
        cellstr('1_ground_force_px'),cellstr('1
_ground_force_py'),cellstr('1_ground_force_pz'),
        cellstr('2_ground_force_vx'),cellstr('2
_ground_force_vy'),cellstr('2_ground_force_vz'),
        cellstr('2_ground_force_px'),cellstr('2
_ground_force_py'),cellstr('2_ground_force_pz'),
        cellstr('3_ground_force_vx'),cellstr('3
_ground_force_vy'),cellstr('3_ground_force_vz'),
        cellstr('3_ground_force_px'),cellstr('3
_ground_force_py'),cellstr('3_ground_force_pz'),
        cellstr('1_ground_torque_x'),cellstr('1
_ground_torque_y'),cellstr('1_ground_torque_z'),
        cellstr('2_ground_torque_x'),cellstr('2
_ground_torque_y'),cellstr('2_ground_torque_z'),
        cellstr('3_ground_torque_x'),cellstr('3
_ground_torque_y'),cellstr('3_ground_torque_z')];

% Creating a string cell array containing A8
data2 = string(A8);

% Copying the headings (Header1) into first 6 rows of data2
z8 = 1;
for i=1:6
    data2(i,:)=Header1(z8,:);
    z8=z8+1;

```



```
end

% Clearing variables to refresh data exported for each file
clear A1 A2 A3 A6 A7 A8

% Selecting the MOT file to be processed and exported as
filename_GRF.mot
exportfile=strcat(filename3, '_GRF.mot');
fileID(f)=fopen(char(exportfile), 'w');

% Creating new MOT file with all the data stored in data2
array
[rows, cols]=size(data2);
for i=1:rows
    for j=1:cols
        fprintf(fileID(f), '%s\t', data2(i, j));
    end
    fprintf(fileID(f), '\n');
end
end
fprintf('Thank you, processing is complete. \n');
end
```

[illegible]

```
% Import file selected into table
dataFilter = table(dataArray{1:end-1});

% Convert file selected data into array
dataIn = table2array(dataFilter);

% Filter the dataIn using a rational transfer function defined
% by the numerator and denominator coefficients b and a.
dataFilter = filter(b,a,dataIn);

dataFilter=filtfilt(b, a, dataIn);

figure(1);
plot(dataIn)
hold on;
plot(dataFilter)
hold off;
legend('show');
end
```

[illegible]

```
Rowz=G(1,1);
Col=G(1,2);

% Copying filtered TRC file into original TRC file from (6,3)
    till (inf,inf)
for i = 6:Rowz
    for j = 3:Col
        mainOutput2(i,j) = mainOutput1(i-5,j-2);
    end
end

%Creating new TRC file
[rows,cols]=size(mainOutput2);
exportfile=strcat(filename, '_processed ', '.TRC');
fileID=fopen(char(exportfile), 'w');
for k=1:rows
    for m=1:cols
        fprintf(fileID, '%s\t', mainOutput2{k,m});
    end
    fprintf(fileID, '\n');
end
end

% NaN or gaps in TRC file will break code, need full frame to
    full frame in Vicon to fix this
```

```
% CSV to GRF Converter Automated
%
% Changes coordinate systems, converts to SI units and extracts
    relevant data
%
% Author: James Naim
%
% Code written in Matlab 2017a
%
% Import the CSV file called data
function data = CSV_GRF_Converter_Automation_Unfiltered_BWFilter
    ()

% Initialize variables.
delimiter = ',';

startRow = 1;
endRow = inf;

% Cutoff frequency
$f_c$ = 300;
% Try $f_c$ = 50, 100, 200, 300 & 400
% Sample rate
fs = 1000;
% Order of filter
n = 4;
% Try n=2
% Normalised cutoff frequency
Wn = $f_c$/(fs/2);

% [b,a] = butter(n,Wn,f_type), n = Order of filter , Wn =
    normalised cutoff freq, f_type = filter type
[b,a] = butter(n,Wn,'low');

% Number of columns of importfile
formatSpec = '%s%s%s%s%s%s%s%s%s%s%s%s%s%s%s%s%s%s%s%s%s%s'
    '%s%s%s%s%s%s%s%s%s%s%s%s%s%s%s%s%s%s%s%s%s%s'
    '\r';
fprintf('Choose the directory where the files to be processed
    are located in!\n');
```

```

% Open required directory with CSV files inside
directory = uigetdir('');
% List all files with .CSV extension in the directory selected
G= dir(fullfile(directory, '*.CSV'));

% Number of CSV files
nTrials = size(G);
fileCount = nTrials(1,1);
P=fileCount;

% Listing files in the directory
G1=struct2cell(G);
L=(G1(1,:));
L1=transpose(L);

% Selecting filename of the TRC file to be processed in the
  directory chosen
fprintf('Choose the directory which the processed files should
  be saved in!\n');
directory1 = uigetdir('');
filename= dir(fullfile(directory1, '*.CSV'));
filename1=struct2cell(filename);

% Columns with required data
x = [3 5 4 9 11 10 20 22 21 26 28 27 37 39 38 43 45 44 6 8 7 23
     25 24 40 42 41];

% Moment and distance matrix needed to be converted to metres
x1 = [4 5 6 10 11 12 16 17 18 19 20 21 22 23 24 25 26 27];

% Centre of Pressure new z coordinate to multiply by -1
x2 = [6 12 18];

% Force Vector new x and y coordinate to multiply by -1
x3 = [1 2 7 8 13 14];

% Moment Vector new x and y coordinate to multiply by -1
x4 = [19 20 22 23 25 26];

% New matrix with zeros in column 1
c1 = [ 2 3 4 5 6 7 8 9 10 11 12 13 14 15 16 17 18 19 20 21 22 23
      24 25 26 27 28];

```

```

fprintf('Processing! \n');

% Extract data from each file in the selected directory
for f=1:P
    fileID(f)=fopen(string(L1(f)));
    Text = textscan(fileID(f), formatSpec, endRow(1)-startRow(1)
        +1, 'Delimiter', delimiter, 'TextType', 'string', '
        ReturnOnError', false, 'EndOfLine', '\r\n');
    $f.c$lose(fileID(f));
    data1 = double([Text{1:end-1}]);

    filename2=char(filename1(1,f));
    F2=strsplit(filename2, '.');
    filename3=char(F2(1,1));

    % Size of input file (data1) array
    E = size(data1);
    Rowz = E(1,1);

    % Variable A1 assigned as the 1st vector from CSV file which
        contains frame numbers
    k1 = 1;
    for i=1:Rowz
        A1(k1,1) = data1(i,1);
        k1=k1+1;
    end

    % Finding the start row number for numerical data
    A2=isfinite(A1); % 1 if num, 0 if char vector
    A3=find(A2,inf,'first'); % Row number for every 1 found
    numStart(1,1) = A3(4,1); % Starting row for numerical values

    % Force, Moment and Distance vectors of the CSV file
    for i=1:Rowz
        for j=1:length(x)
            A6(i,j) = data1(i,x(j));
        end
    end

    % Finding the end row number for numerical data
    z1=0;
    for z2=numStart:Rowz
        if z1==0

```



```

        if isnan(A1(z2,1))
            numEnd(1,1) = z2-1;
            z1 = 1;
        end
    end
end

% Data extract from CSV file to new array A7 with numerical
% data only
z3 = 1;
for z4=numStart:numEnd
    A7(z3,:) = A6(z4,:);
    z3=z3+1;
end

% Number of rows with numerical data
rowC=numEnd-numStart+1;

% Size of A7 array
E1=size(A7);
Rowz1=E1(1,1);

% Multiply COP new z coordinate by -1
for i=1:Rowz1
    for j=x2
        A7(i,j)=A7(i,j)*-1;
    end
end

% Multiply new x and y coordinate for F and M by -1
for i=1:Rowz1
    for j=x3
        A7(i,j)=A7(i,j)*-1;
    end
    for k=x4
        A7(i,k)=A7(i,k)*-1;
    end
end

% Converting Centre of Pressure and Moment to SI Units
for i=1:Rowz1
    for j=x1
        A7(i,j)=A7(i,j)/1000;
    end
end

```

```
        end
    end

    % Filter the dataIn using a rational transfer function
    % defined by the numerator and denominator coefficients b
    % and a.
    A7 = filter(b,a,A7);

    % Creating Header of zeros [6 x 28] matrix
    A8 = zeros(Rowz1+6,28);

    % Vector of zeros to be filled with frame number
    frameNumber = zeros(Rowz1,1);

    % Frame number vector
    z5 = 1;
    for i = numStart:numEnd
        frameNumber(z5,1) = A1(i,:);
        z5=z5+1;
    end

    % Time vector
    for i = 1:length(frameNumber)
        Time(i,1) = (4*(frameNumber(1,1) - 1) + i-1)/1000;
    end

    % Filling A8[:,1] with time
    z6 = 1;
    for j = 7:Rowz1+6
        A8(j,1)=Time(z6,1);
        z6=z6+1;
    end

    % Filling A8 columns 2-28 for all rows of size (A7) with
    % data from A7
    z7 =1;
    for j = 7:Rowz1+6
        A8(j,c1)=A7(z7,:);
        z7=z7+1;
    end

    % Change Column Headings
    rowCount = num2str(rowC);
```

```

nRow = strcat('nRows=',rowCount);
Header1 =[cellstr(filename3), cellstr(''),cellstr(''),
cellstr(''),cellstr(''),cellstr(''),cellstr(''),cellstr(''),cellstr(''),
cellstr(''),cellstr(''),cellstr(''),cellstr(''),cellstr(''),
cellstr(''),cellstr(''),cellstr(''),cellstr(''),cellstr(''),cellstr(''),
cellstr(''),cellstr(''),cellstr(''),cellstr(''),cellstr(''),cellstr(''),
cellstr(''),cellstr(''),cellstr(''))
cellstr(nRow), cellstr(''),cellstr(''),cellstr(''),
cellstr(''),cellstr(''),cellstr(''),cellstr(''),
cellstr(''),cellstr(''),cellstr(''),cellstr(''),
cellstr(''),cellstr(''),cellstr(''),cellstr(''),
cellstr(''),cellstr(''),cellstr(''),cellstr(''),
cellstr(''),cellstr(''),cellstr(''),cellstr(''))
cellstr('nColumns=28'), cellstr(''),cellstr(''),cellstr(''),
cellstr(''),cellstr(''),cellstr(''),cellstr(''),cellstr(''),
cellstr(''),cellstr(''),cellstr(''),cellstr(''),
cellstr(''),cellstr(''),cellstr(''),cellstr(''),
cellstr(''),cellstr(''),cellstr(''),cellstr(''),
cellstr(''),cellstr(''),cellstr(''),cellstr(''))
cellstr('inDegrees=yes'), cellstr(''),cellstr(''),
cellstr(''),cellstr(''),cellstr(''),cellstr(''),
cellstr(''),cellstr(''),cellstr(''),cellstr(''),
cellstr(''),cellstr(''),cellstr(''),cellstr(''),
cellstr(''),cellstr(''),cellstr(''),cellstr(''),
cellstr(''),cellstr(''),cellstr(''),cellstr(''),
cellstr(''))
cellstr('endheader'), cellstr(''),cellstr(''),cellstr(''),
cellstr(''),cellstr(''),cellstr(''),cellstr(''),cellstr(''),
cellstr(''),cellstr(''),cellstr(''),cellstr(''),
cellstr(''),cellstr(''),cellstr(''),cellstr(''),
cellstr(''),cellstr(''),cellstr(''),cellstr(''),
cellstr(''))
cellstr('time'),cellstr('1_ground_force_vx'),cellstr('1
_ground_force_vy'),cellstr('1_ground_force_vz'),
cellstr('1_ground_force_px'),cellstr('1
_ground_force_py'),cellstr('1_ground_force_pz'),
cellstr('2_ground_force_vx'),cellstr('2
_ground_force_vy'),cellstr('2_ground_force_vz'),

```

```

        cellstr('2_ground_force_px '), cellstr('2
        _ground_force_py '), cellstr('2_ground_force_pz '),
        cellstr('3_ground_force_vx '), cellstr('3
        _ground_force_vy '), cellstr('3_ground_force_vz '),
        cellstr('3_ground_force_px '), cellstr('3
        _ground_force_py '), cellstr('3_ground_force_pz '),
        cellstr('1_ground_torque_x '), cellstr('1
        _ground_torque_y '), cellstr('1_ground_torque_z '),
        cellstr('2_ground_torque_x '), cellstr('2
        _ground_torque_y '), cellstr('2_ground_torque_z '),
        cellstr('3_ground_torque_x '), cellstr('3
        _ground_torque_y '), cellstr('3_ground_torque_z ') ];

% Creating a string cell array containing A8
data2 = string(A8);

% Copying the headings (Header1) into first 6 rows of data2
z8 = 1;
for i=1:6
    data2(i,:)=Header1(z8,:);
    z8=z8+1;
end

% Clearing variables to refresh data exported for each file
clear A1 A2 A3 A6 A7 A8

% Selecting the MOT file to be processed and exported as
filename_GRF.mot
exportfile=strcat(filename3, '_GRF.mot');
fileID(f)=fopen(char(exportfile), 'w');

% Creating new MOT file with all the data stored in data2
array
[rows,cols]=size(data2);
for i=1:rows
    for j=1:cols
        fprintf(fileID(f), '%s\t', data2(i,j));
    end
    fprintf(fileID(f), '\n');
end
end
fprintf('Thank you, processing is complete. \n');
end

```

```
% Post Processing Automation
%
% Author: James Naim
%
% Code written in Matlab 2017a
%
% Import the IK mot file called dataMother
function dataMother = IK_ID_Automation()

% Initialize variables.
delimiter = '\t';

startRow = 8;
endRow = inf;

% Number of columns of importfile
formatSpec = '%f%f%f%f%f%f%f%f%f%f%f%f%f%f%f%f%f%f%f%f%f%f%f%f'
    '%f%f%f%f[\n\r]';

% IK or ID file for processing
prompt='Would you like to run IK or ID?\n';
answer=input(prompt,'s');
fprintf('Choose the directory which the files for processing are
in!\n');

if string(answer) == 'IK'
    directory = uigetdir('');
    G= dir( fullfile(directory , '*.MOT') );
elseif string(answer) == 'ID'
    directory = uigetdir('');
    G= dir( fullfile(directory , '*.STO') );
end

% Number of IK files
nTrials = size(G);
fileCount = nTrials(1,1);
P=fileCount;

% Listing files in directory
G1=struct2cell(G);
```

```

L=(G1(1,:));
L1=transpose(L);

if string(answer) == 'ID'
    promptn2 = 'What is the subjects body mass in kg? \n';
    Bodymass = input(promptn2);
end

prompt1='Is the file a walking or step trial?\n';
answer1=input(prompt1,'s');

if string(answer1)=='walking'

    % Column Selection for Walking Trials
    prompt2='Which leg do you wish to select , L or R?\n';
    answer2=input(prompt2,'s');

    if string(answer2) == 'R'
        x=11;
        y=12;
        z=13;
    elseif string(answer2) == 'L'
        x=20;
        y=21;
        z=22;
    end

    % Extract data from each file in the selected folder
    for f=1:P
        fileID(f)=fopen(string(L1(f)));
        Text=textscan(fileID(f), formatSpec, endRow(1)-startRow
            (1)+1, 'Delimiter', delimiter, 'TextType', 'string',
            'HeaderLines', startRow(1)-1, 'ReturnOnError', false,
            'EndOfLine', '\r\n');
        $f_c$close(fileID(f));
        dataMother1 = table(Text{1:end-1});

        % Size of array
        E = size(dataMother1);
        Rowz = E(1,1);

        for i=1:Rowz
            % Column Extraction

```

```

        T(i,f) = (100/Rowz)*(i);    %Gait Cycle
        A(i,f) = table2array(dataMother1(i,x)); %Flexion
        B(i,f) = table2array(dataMother1(i,y)); %Rotation
        C(i,f) = table2array(dataMother1(i,z)); %Abduction
    end
end

% Select nonzero values only
A(A==0)=NaN;
B(B==0)=NaN;
C(C==0)=NaN;
T(T==0)=NaN;

% Multipliers for IK
% +ve = Flexion, Internal Rotation and Adduction
if string(answer2) == 'R' && string(answer) == 'IK'
    A=A*-1; % Flexion Right multiply by -1
    B=B*-1; % Rotation Right multiply by -1
elseif string(answer2) == 'L' && string(answer) == 'IK'
    A=A*-1; % Flexion Left multiply by -1
    C=C*-1; % Abduction Left multiply by -1
end

% Multipliers for ID
if string(answer2) == 'R' && string(answer) == 'ID'
    A=A*-1; % Flexion Right multiply by -1
    B=B*-1; % Rotation Right multiply by -1
elseif string(answer2) == 'L' && string(answer) == 'ID'
    A=A*-1; % Flexion Left multiply by -1
    C=C*-1; % Abduction Left multiply by -1
end

% All ID data divided by subjects bodymass in kg
if string(answer) == 'ID'
    A=A/Bodymass;
    B=B/Bodymass;
    C=C/Bodymass;
end

fprintf('Which directory is the graphing template .xslm file
in?\n')

directory1 = uigetdir('');
```

```

filename= dir( fullfile( directory1 , '*.xslm' ) );
filename1=struct2cell(filename);

fprintf('Select the graphing template .xslm file?\n')

filename2=uigetfile(char( fullfile( filename1(1,1) ) ));
ff=fullfile( directory1 , filename2 );

fprintf('Processing...\n');

if string(answer2) == 'R'
    xlsxwrite(ff,T, 'Gait Cycle', 'L3');
    xlsxwrite(ff,A, 'Knee Flexion', 'L3');
    xlsxwrite(ff,B, 'Knee Rotation', 'L3');
    xlsxwrite(ff,C, 'Knee Adduction', 'L3');
elseif string(answer2) == 'L'
    xlsxwrite(ff,T, 'Gait Cycle', 'A3');
    xlsxwrite(ff,A, 'Knee Flexion', 'A3');
    xlsxwrite(ff,B, 'Knee Rotation', 'A3');
    xlsxwrite(ff,C, 'Knee Adduction', 'A3');
end
fprintf('Thank you, come again!\n');
end

if string(answer1) == 'step'

% Column Selection for Stepping Trials
prompt3='Is this a L or R trial? Which leg do you wish to
select, L or R? (Write both answers separated by a
forward slash e.g. L/L or R/R) \n';
answer2=input(prompt3,'s');

if string(answer2) == 'R/R'
    x=11;
    y=12;
    z=13;
elseif string(answer2) == 'L/L'
    x=20;
    y=21;
    z=22;
elseif string(answer2) == 'R/L'
    x=20;
    y=21;

```



```

        z=22;
    elseif string(answer2) == 'L/R'
        x=11;
        y=12;
        z=13;
    end

% Extract data from each file in the selected folder
for f=1:P
    fileID(f)=fopen(string(L1(f)));
    Text=textscan(fileID(f), formatSpec, endRow(1)-startRow
        (1)+1, 'Delimiter', delimiter, 'TextType', 'string',
        'HeaderLines', startRow(1)-1, 'ReturnOnError', false,
        'EndOfLine', '\r\n');
    $f_c$lose(fileID(f));
    dataMother1 = table(Text{1:end-1});

    % Size of array
    E = size(dataMother1);
    Rowz = E(1,1);

    for i=1:Rowz
        % Column Extraction
        T(i,f) = (100/Rowz)*(i);    %Gait Cycle
        A(i,f) = table2array(dataMother1(i,x));    %Flexion
        B(i,f) = table2array(dataMother1(i,y));    %Rotation
        C(i,f) = table2array(dataMother1(i,z));    %Abduction
    end
end

% Select nonzero values only
A(A==0)=NaN;
B(B==0)=NaN;
C(C==0)=NaN;
T(T==0)=NaN;

% Multipliers for IK
if string(answer2) == 'R/R' && string(answer) == 'IK'
    A=A*-1; % Flexion Right trial Right leg multiply by -1
    B=B*-1; % Rotation Right trial Right leg multiply by -1
elseif string(answer2) == 'L/L' && string(answer) == 'IK'
    A=A*-1; % Flexion Left trial Left leg multiply by -1
    C=C*-1; % Abduction Left trial Left leg multiply by -1

```

```

elseif string(answer2) == 'R/L' && string(answer) == 'IK'
    A=A*-1; % Flexion Right trial Left leg multiply by -1
    C=C*-1; % Abduction Right trial Left leg multiply by -1
elseif string(answer2) == 'L/R' && string(answer) == 'IK'
    A=A*-1; % Flexion Left trial Right leg multiply by -1
    B=B*-1; % Rotation Left trial Right leg multiply by -1
end

% Multipliers for ID
if string(answer2) == 'R/R' && string(answer) == 'ID'
    A=A*-1; % Flexion Right trial Right leg multiply by -1
    B=B*-1; % Rotation Right trial Right leg multiply by -1
elseif string(answer2) == 'L/L' && string(answer) == 'ID'
    A=A*-1; % Flexion Left trial Left leg multiply by -1
    C=C*-1; % Abduction Left trial Left leg multiply by -1
elseif string(answer2) == 'R/L' && string(answer) == 'ID'
    A=A*-1; % Flexion Right trial Left leg multiply by -1
    C=C*-1; % Abduction Right trial Left leg multiply by -1
elseif string(answer2) == 'L/R' && string(answer) == 'ID'
    A=A*-1; % Flexion Left trial Right leg multiply by -1
    B=B*-1; % Rotation Left trial Right leg multiply by -1
end

% All ID data divided by subjects bodymass in kg
if string(answer) == 'ID'
    A=A/Bodymass;
    B=B/Bodymass;
    C=C/Bodymass;
end

% Write and save data onto selected Excel template
fprintf('Which directory is the graphing template .xslm file
in?\n')

directory1 = uigetdir('');
filename= dir(fullfile(directory1, '*.xslm'));
filename1=struct2cell(filename);

fprintf('Select the graphing template .xslm file?\n')

filename2=uigetfile(char(fullfile(filename1(1,1)))));
ff=fullfile(directory1, filename2);

```

```
fprintf('Processing...\n');

if string(answer2) == 'R/R'
    xlswrite(ff,T, 'Gait Cycle', 'AH4');
    xlswrite(ff,A, 'Knee Flexion', 'AH4');
    xlswrite(ff,B, 'Knee Rotation', 'AH4');
    xlswrite(ff,C, 'Knee Adduction', 'AH4');
elseif string(answer2) == 'L/L'
    xlswrite(ff,T, 'Gait Cycle', 'A4');
    xlswrite(ff,A, 'Knee Flexion', 'A4');
    xlswrite(ff,B, 'Knee Rotation', 'A4');
    xlswrite(ff,C, 'Knee Adduction', 'A4');
elseif string(answer2) == 'R/L'
    xlswrite(ff,T, 'Gait Cycle', 'W4');
    xlswrite(ff,A, 'Knee Flexion', 'W4');
    xlswrite(ff,B, 'Knee Rotation', 'W4');
    xlswrite(ff,C, 'Knee Adduction', 'W4');
elseif string(answer2) == 'L/R'
    xlswrite(ff,T, 'Gait Cycle', 'L4');
    xlswrite(ff,A, 'Knee Flexion', 'L4');
    xlswrite(ff,B, 'Knee Rotation', 'L4');
    xlswrite(ff,C, 'Knee Adduction', 'L4');
end

fprintf('Thank you, come again!\n');

end
end
```



# Appendix B

## Marker Sets

### B.1 Overview

This section provides the anatomical locations and details of the Hospital Helen Hayes and Modified Helen Hayes marker sets utilised in this study.

### B.2 Helen Hayes

Segment	Marker No.	Marker Label	Definition
Right Foot	1	RMH	Right Metatarsal head 2
Right Foot	2	RH	Right Heel
Right Foot	3	RM	Right Malleolus
Right Tibia	4	RTIBW	Right Tibial wand
Right Femur	5	RFEM	Right Femoral Epicondyle
Right Femur	6	RFEMW	Right Femoral Wand
Pelvis	7	RASIS	Right ASIS
Left Foot	8	LMH	Left Metatarsal head 2
Left Foot	9	LH	Left Heel
Left Foot	10	LM	Left Malleolus
Left Tibia	11	LTIBW	Left Tibial Wand
Left Femur	12	LFEM	Left Femoral Epicondyle
Left Femur	13	LFEMW	Left Femoral Wand
Pelvis	14	LASIS	Left ASIS
Pelvis	15	SAC	Sacrum

## B.3 Modified Helen Hayes

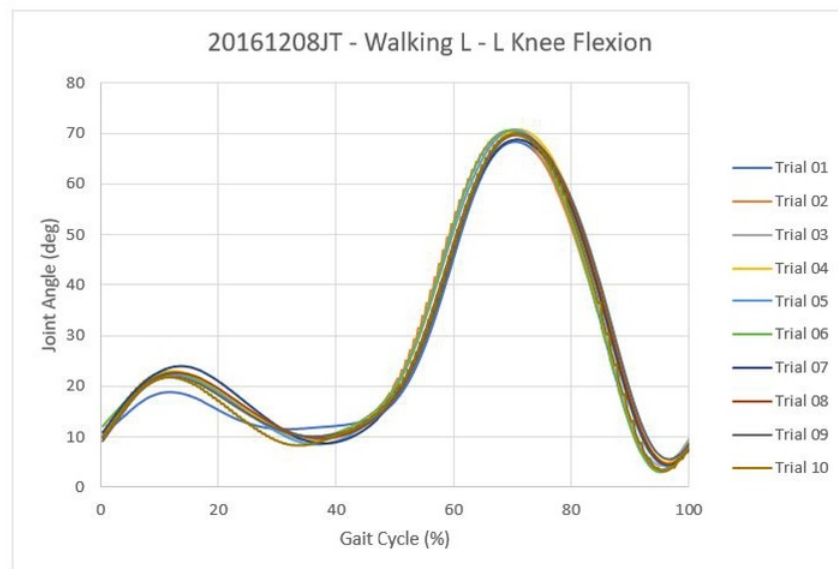
Segment		Marker Label	Definition	Position	Check
Pelvis	1.	RPSI	Right PSIS	Easily found by moving superior and medially with the thumbs from the mid part of the flesh part of the buttocks. Try to feel up and under the PSIS on each side. Located at S2 level	<input type="checkbox"/>
	2.	LPSI	Left PSIS	<sup>A</sup>	<input type="checkbox"/>
	3.	RASI	Right ASIS	From the midline of the thighs move superiorly. The first lump is the ASIS	<input type="checkbox"/>
	4.	LASI	Left ASIS	<sup>A</sup>	<input type="checkbox"/>
	5.	LTOR	Left Torso	Located on the superior iliac crest. Place fingers/hands on waist and move inferiorly. First lump is the iliac crest	<input type="checkbox"/>
	6.	RTOR	Right Torso	<sup>A</sup>	<input type="checkbox"/>
Left Femur	7.	LKNE	Left Knee	On the flexion-extension axis of the knee. Lateral epicondyle	<input type="checkbox"/>
Right Femur	8.	RKNE	Right Knee	On the flexion-extension axis of the knee. Lateral epicondyle	<input type="checkbox"/>
Left Femur	9.	LFIB	Left Fibula	Proximal fibula landmark near the knee	<input type="checkbox"/>
Right Femur	10.	RFIB	Right Fibula	Proximal fibula landmark near the knee	<input type="checkbox"/>
Left Foot	11.	LANK	Left Ankle	Lateral malleolus.	<input type="checkbox"/>
	12.	LHEE	Left Heel	On the calcaneus at the same height above the plantar surface of the foot as the toe marker.	<input type="checkbox"/>
	13.	LTOE	Left Toe	Over second metatarsal head.	<input type="checkbox"/>
Right Foot	14.	RANK	Right Ankle	Lateral malleolus.	<input type="checkbox"/>
	15.	RHEE	Right Heel	On the calcaneus at the same height above the plantar surface of the foot as the toe marker.	<input type="checkbox"/>
	16.	RTOE	Right Toe	Over second metatarsal head	<input type="checkbox"/>
Left Femur	17.	LTHI	Left Thigh	Over the <b>lower</b> lateral 1/3 surface of the left thigh in line with the hip and knee joint centres. The anterior-posterior position of this marker is extremely important. Observe knee flexion/extension to confirm location.	<input type="checkbox"/>
	18.	LQUA	Left Quadriceps	Anterior and middle part of the thigh. Height is not important	<input type="checkbox"/>
Right femur	19.	RTHI	Right Thigh	Over the <b>upper</b> lateral 1/3 surface of the left thigh in line with the hip and knee joint centres. The anterior-posterior position of this marker is extremely important. Observe knee flexion/extension to confirm location.	<input type="checkbox"/>
	20.	RQUA	Right Quadriceps	Anterior and middle part of the thigh. Height is not important	<input type="checkbox"/>
Left Tibia	21.	LTIB	Left Tibia	Over the <b>lower</b> 1/3 surface of the left shank. In line with the knee and ankle joint centres. The anterior-posterior position is critical.	<input type="checkbox"/>
	22.	LSHI	Left Shin	On the ridge of the shin. Height is not important	<input type="checkbox"/>
Right Tibia	23.	RTIB	Right Tibia	Over the <b>upper</b> 1/3 surface of the left shank. In line with the knee and ankle joint centres. The anterior-posterior position is critical.	<input type="checkbox"/>
	24.	RSHI	Right Shin	On the ridge of the shin. Height is not important, but needs to be same with contralateral leg.	<input type="checkbox"/>
Torso	25.	CLAV	Clavicle	Jugular notch where the clavicles meet the sternum	<input type="checkbox"/>
	26.	C7	Cervical	Located at C7 of Cervical Spine. Run finger down the neck and first large lump is usually the C7	<input type="checkbox"/>
Head (static only)	27.	HEAD	Top of the Head	Most superior point (static only)	<input type="checkbox"/>
	28.	LFHD	Left Front Head		<input type="checkbox"/>

# Appendix C

## Results

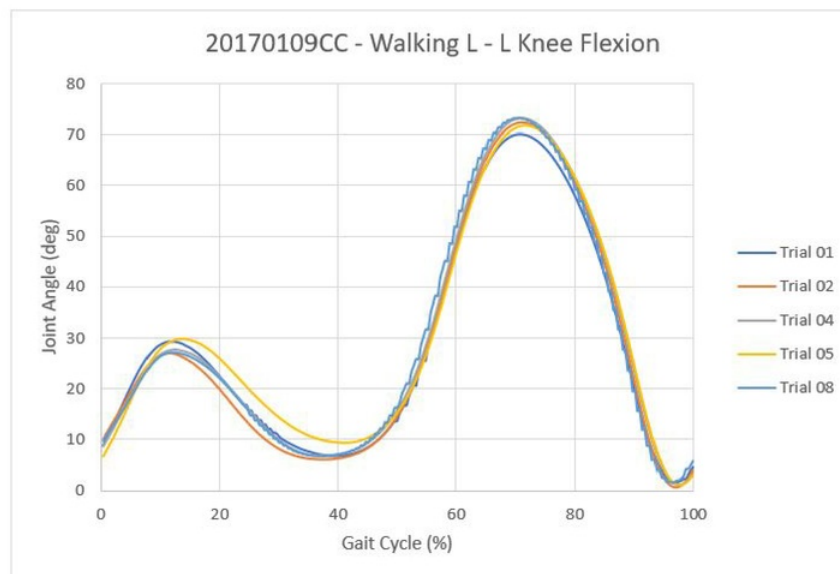
### C.1 Inverse Kinematics

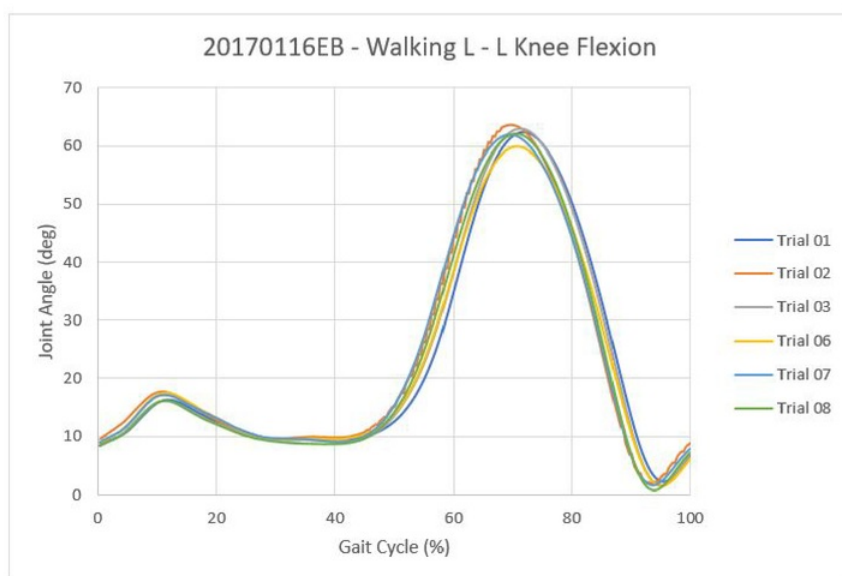
#### C.1.1 Walking



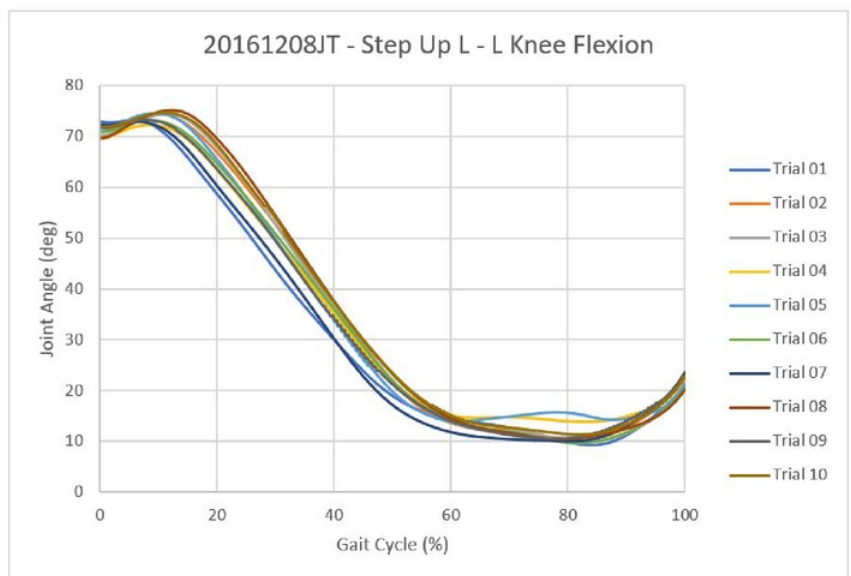


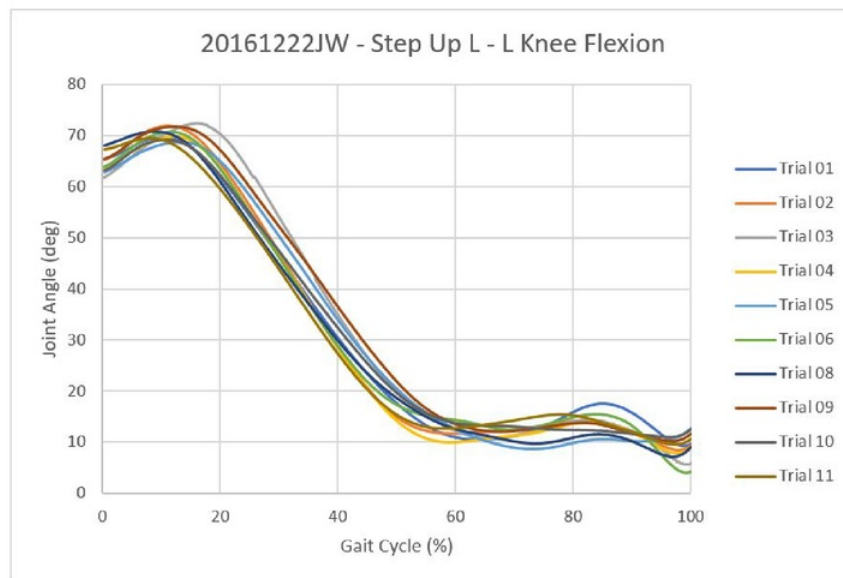


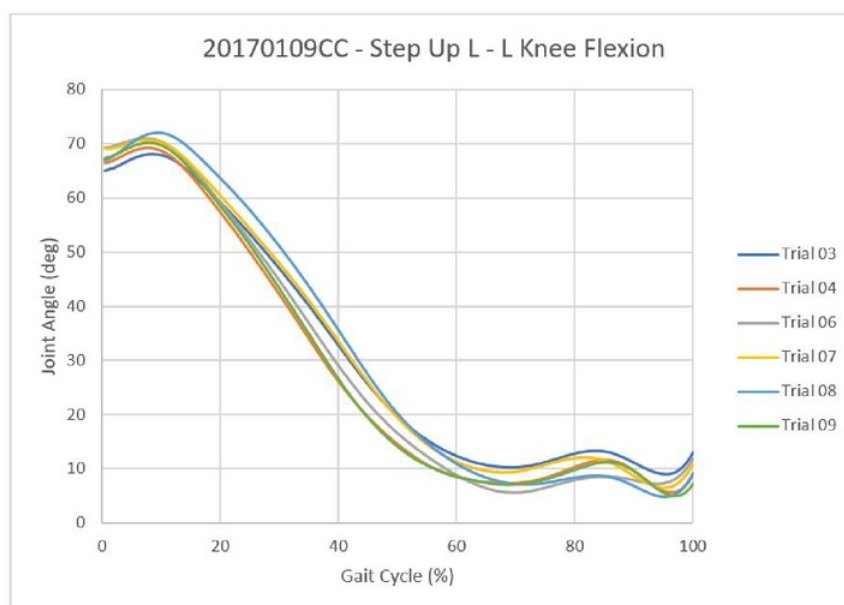
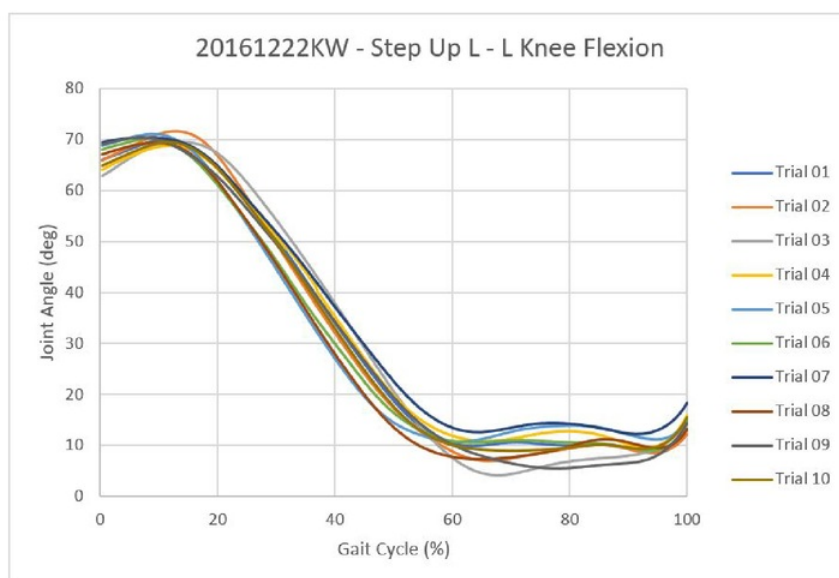


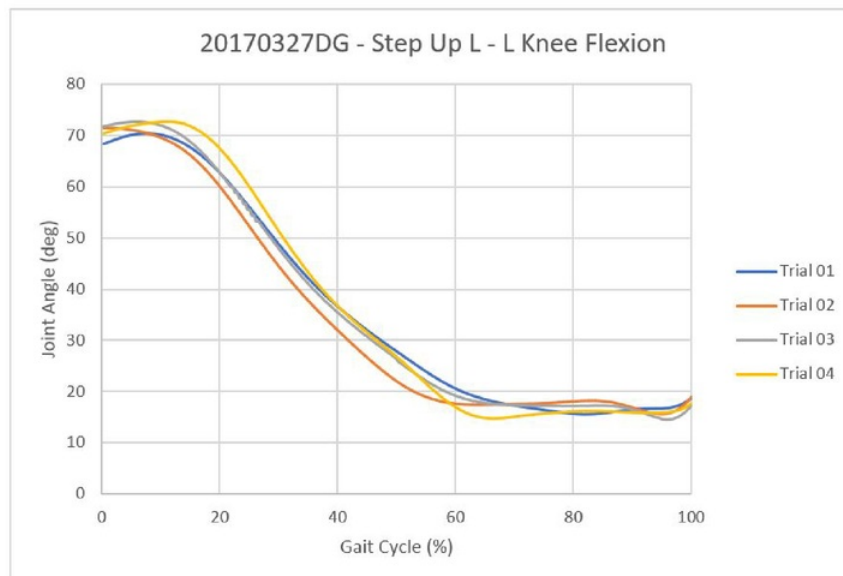
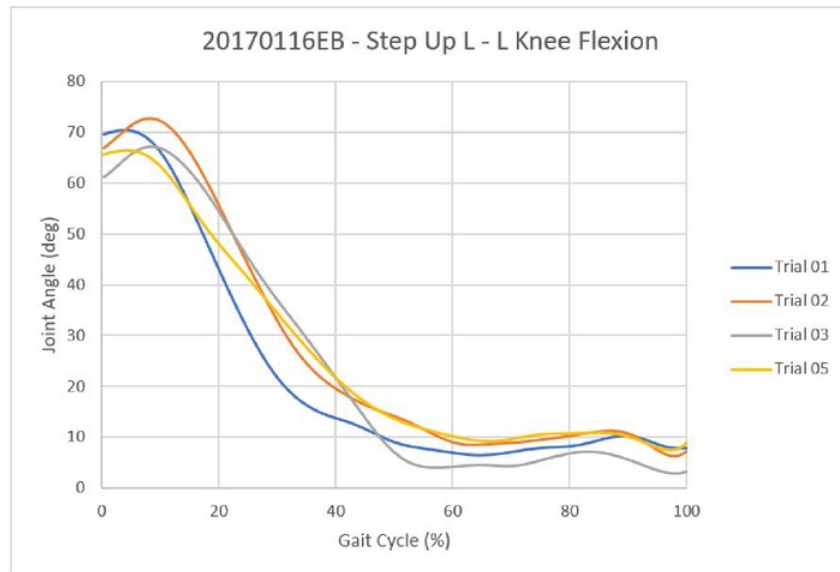


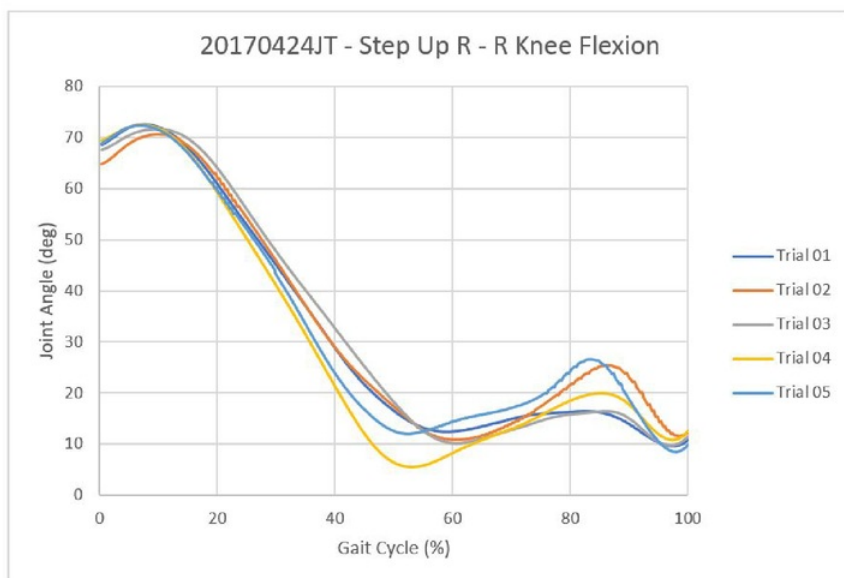




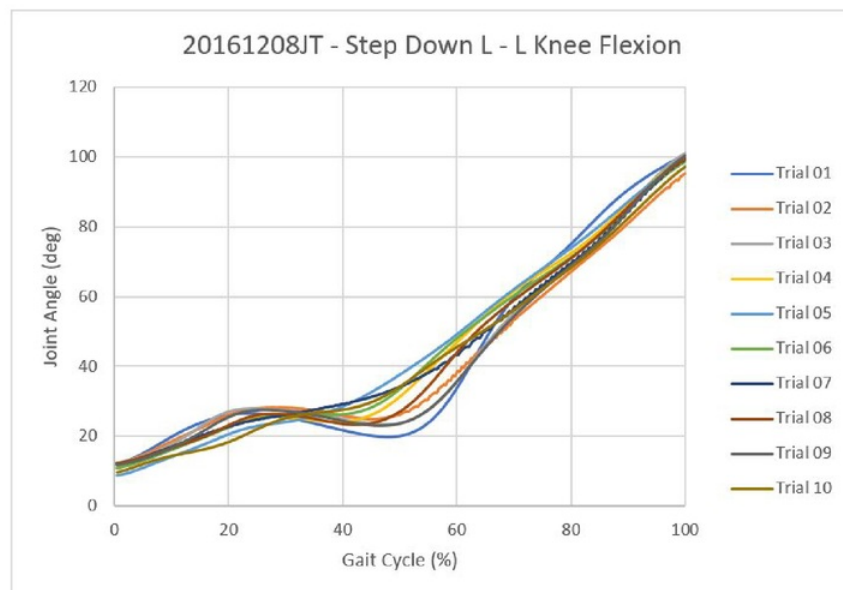
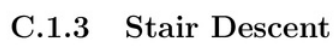


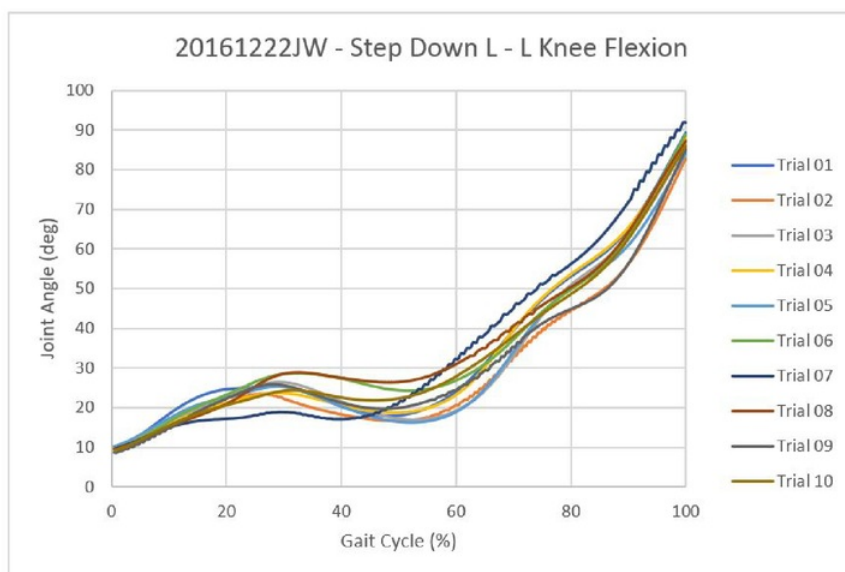
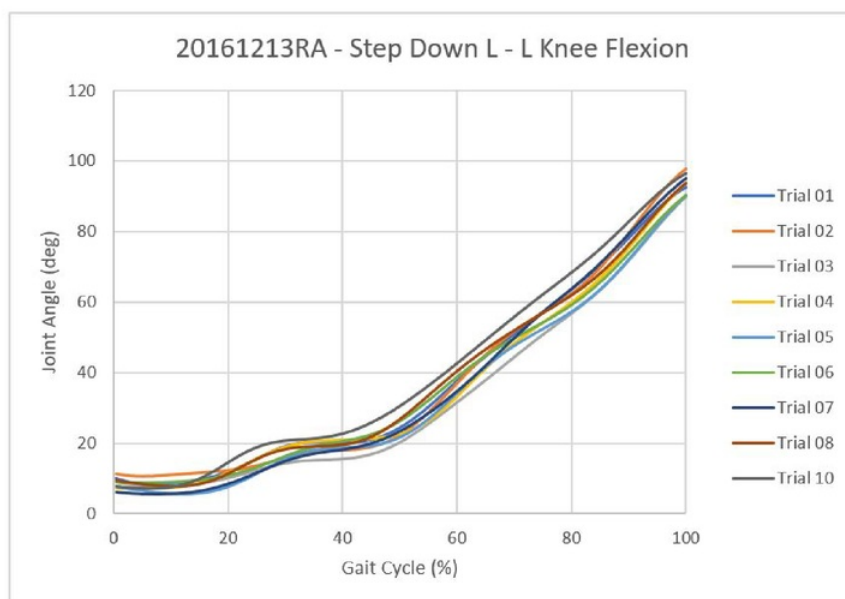














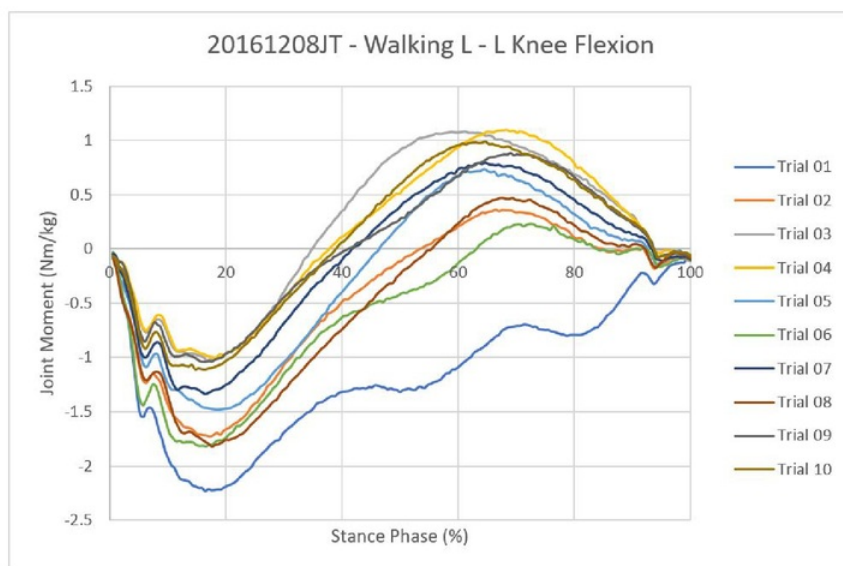


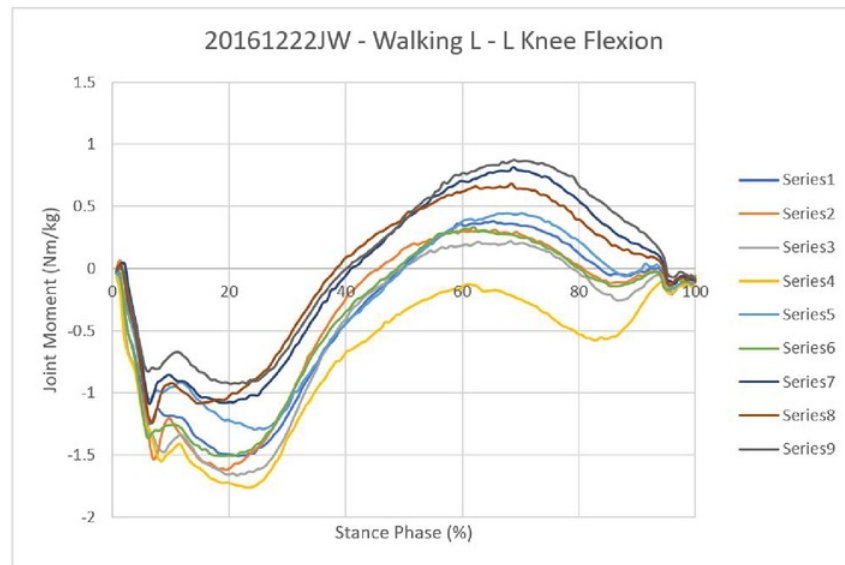


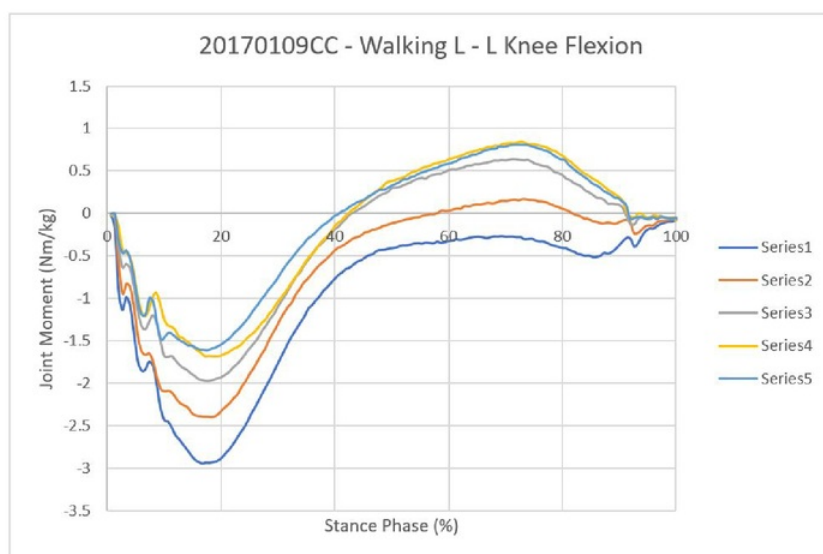
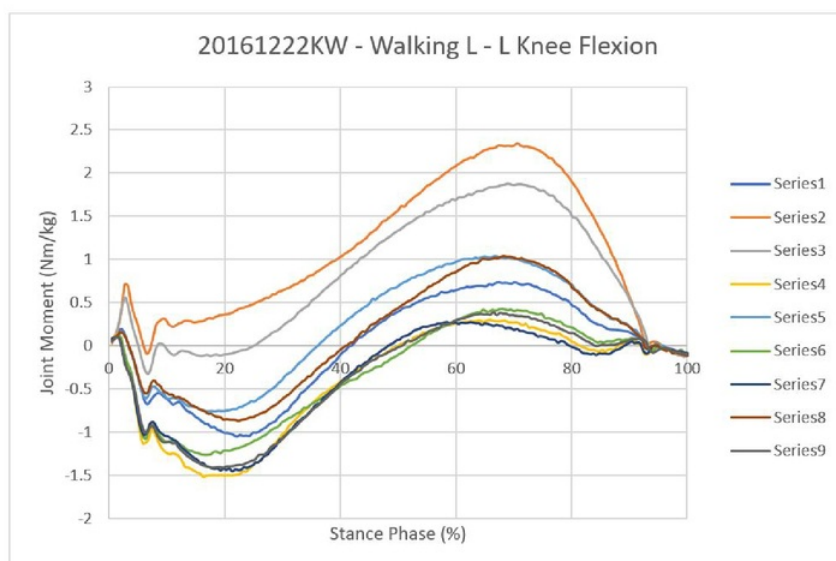


## C.2 Inverse Dynamics

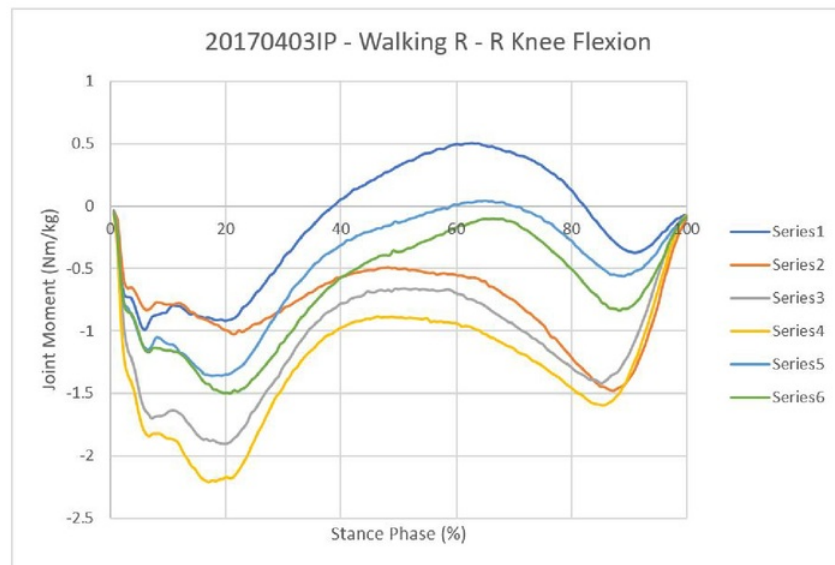
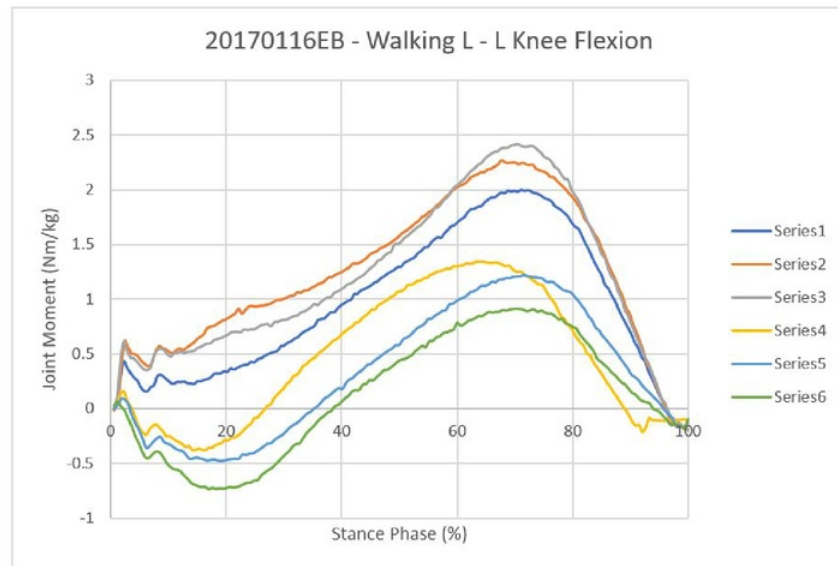
### C.2.1 Walking

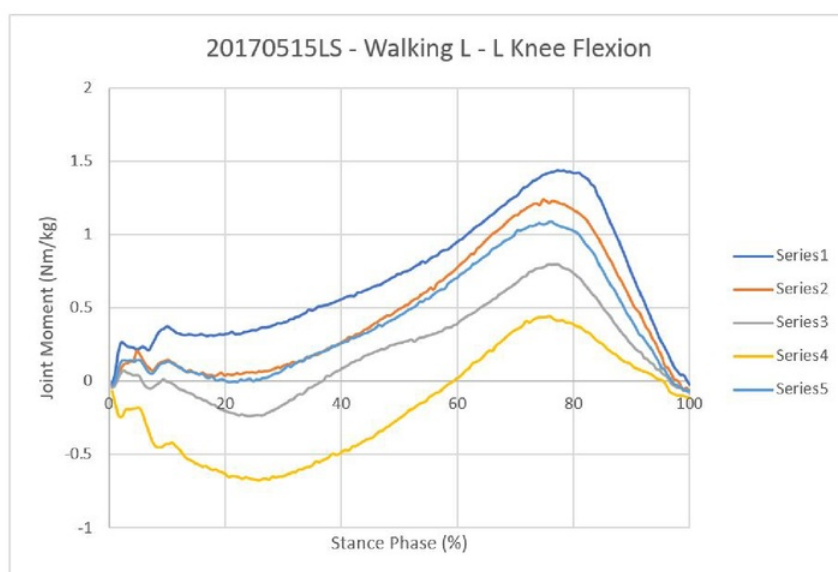
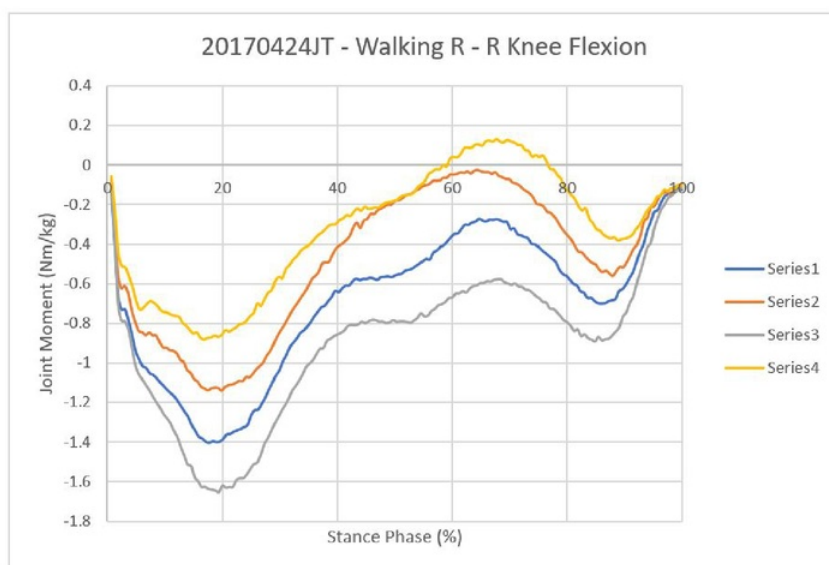




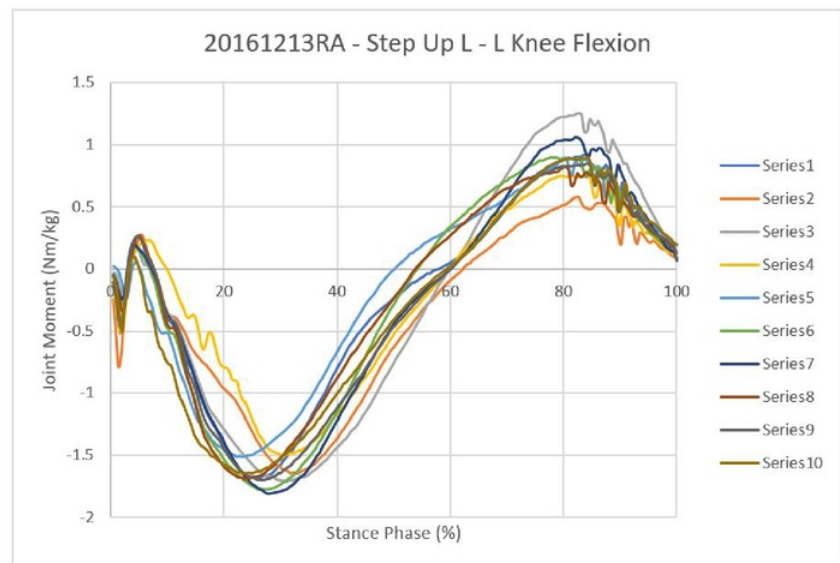
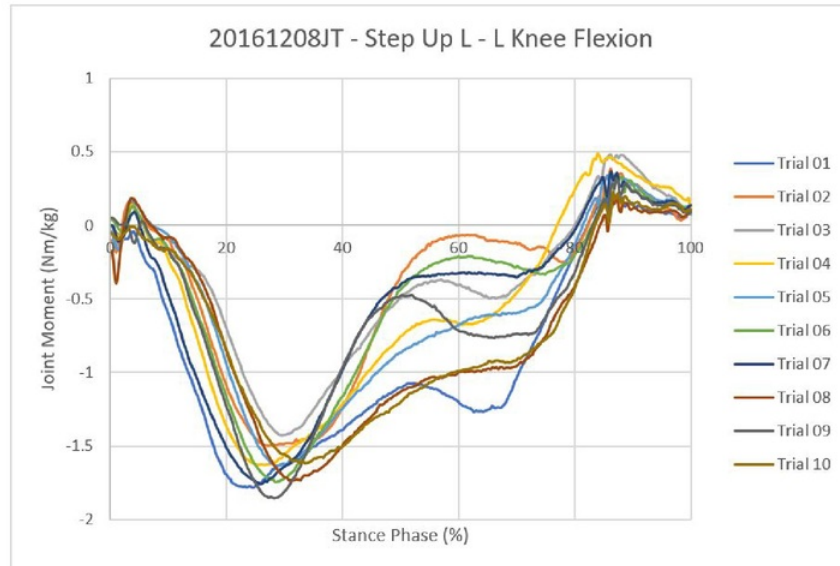


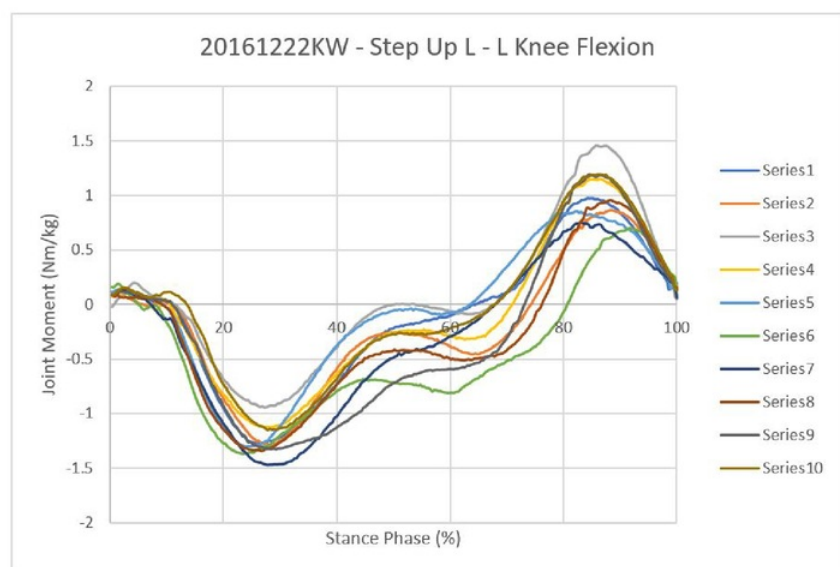
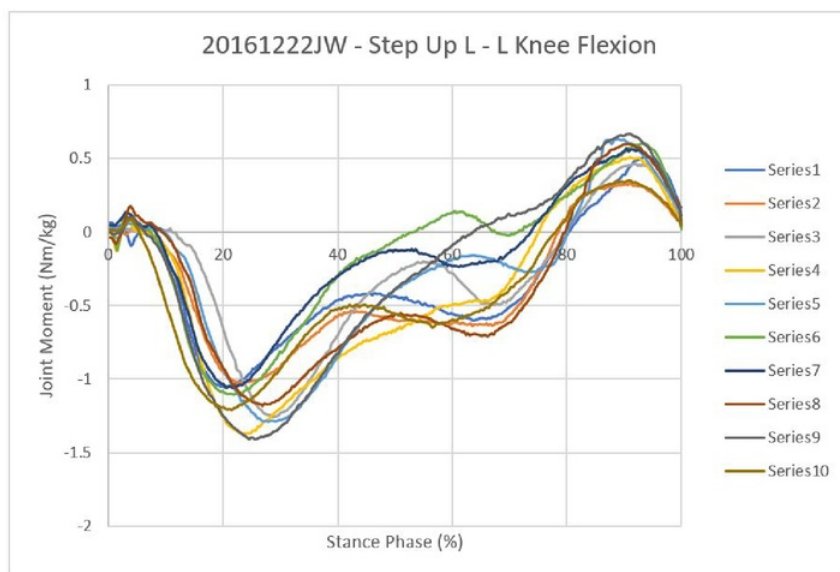


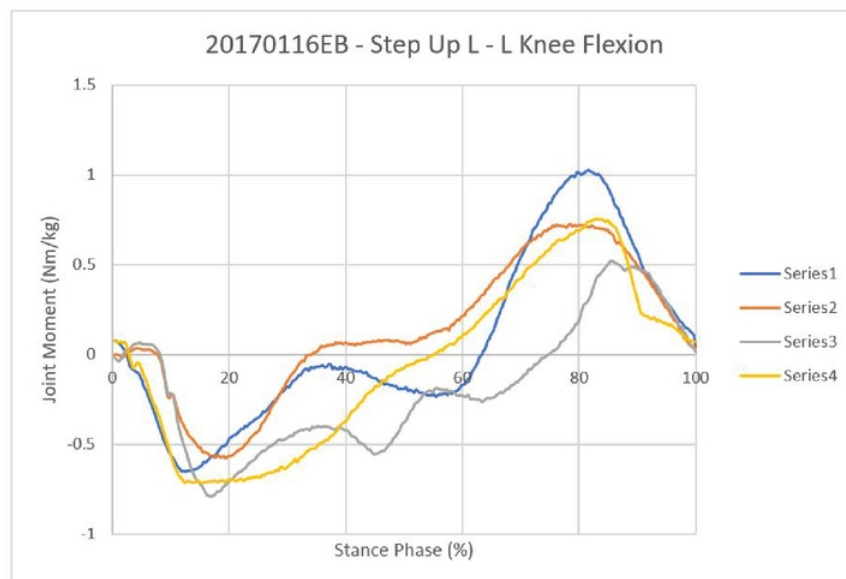
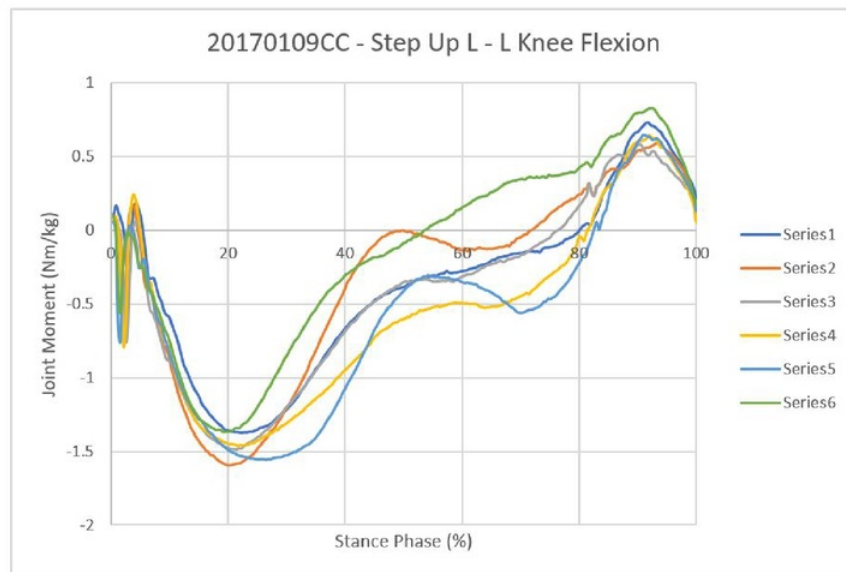


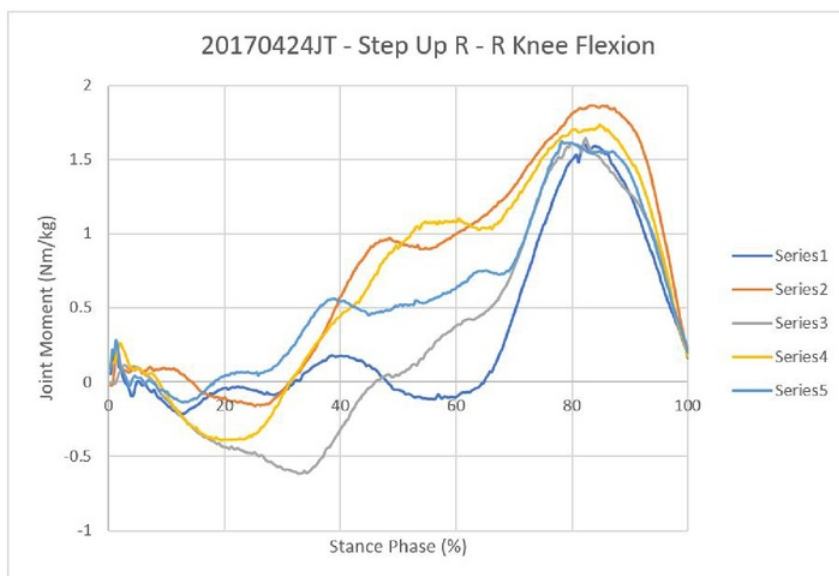
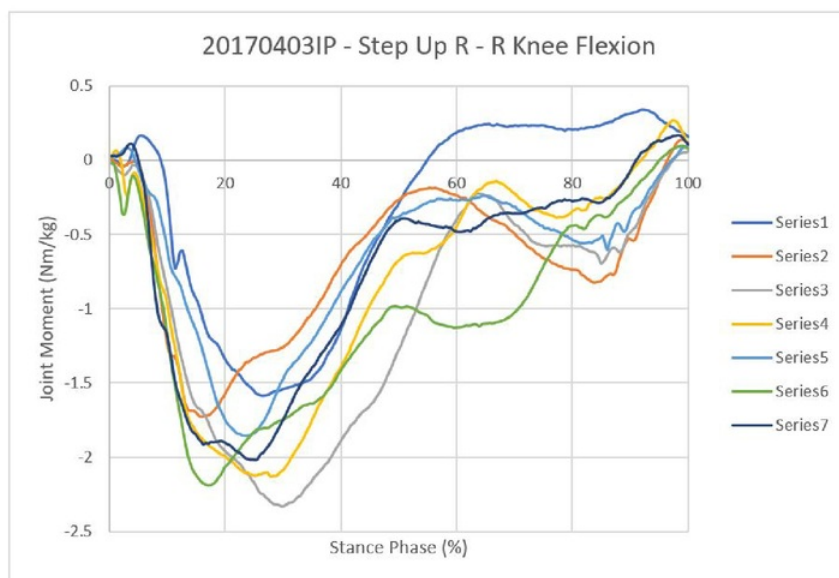


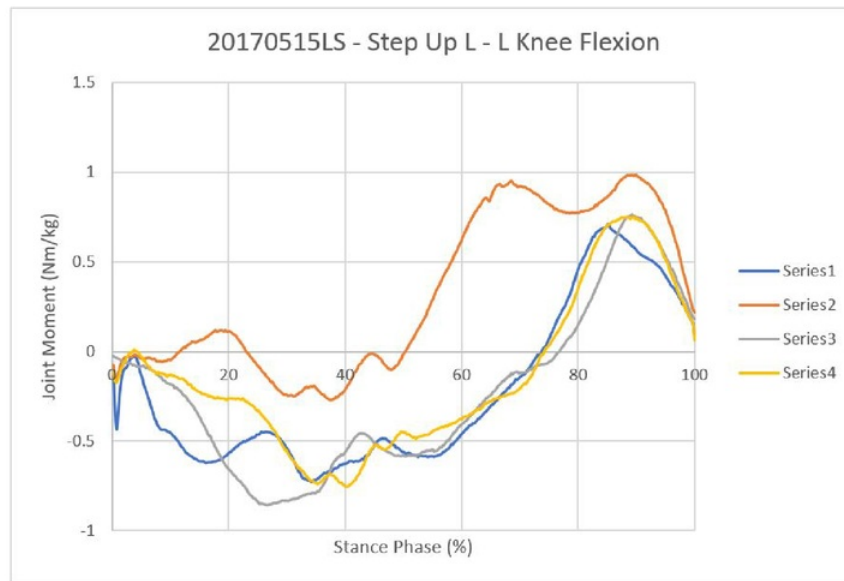
### C.2.2 Stair Ascent



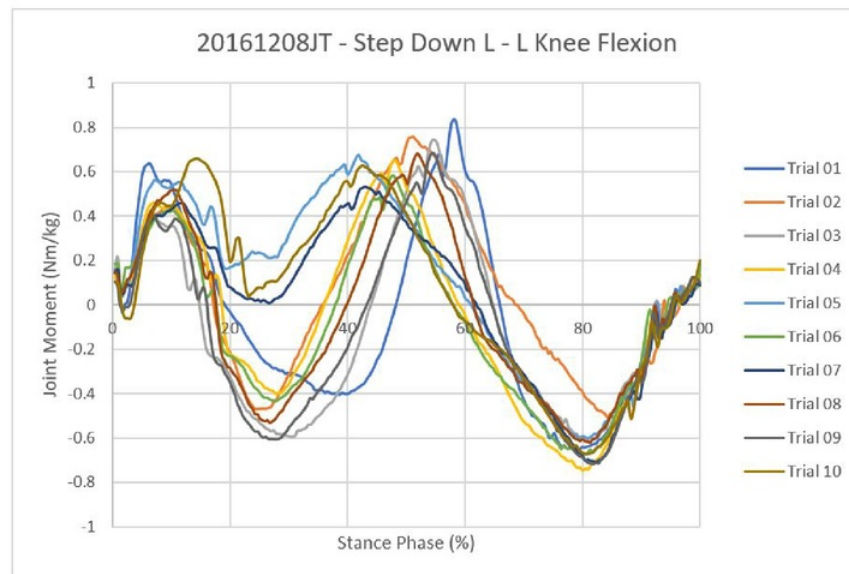


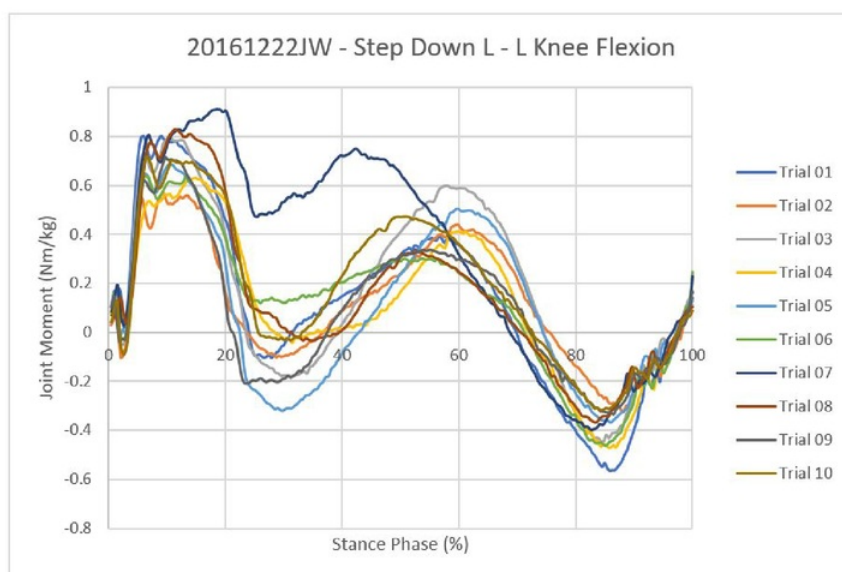
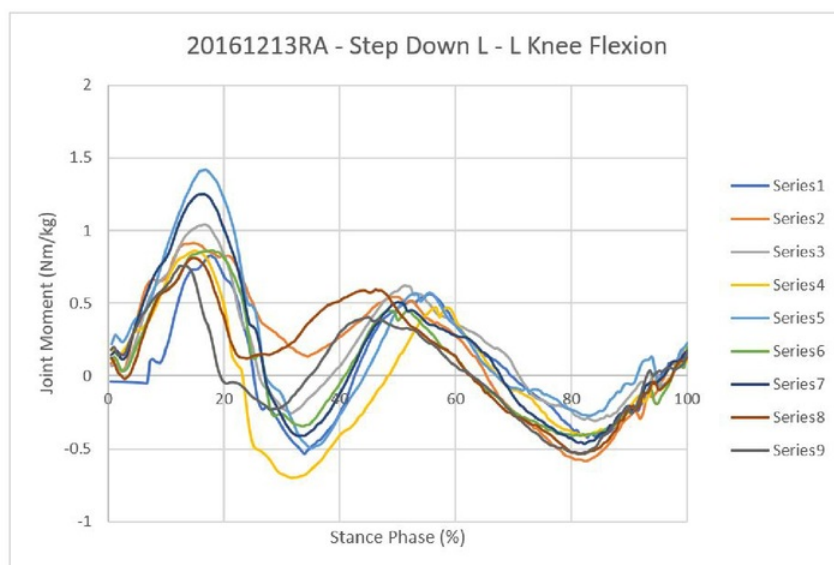




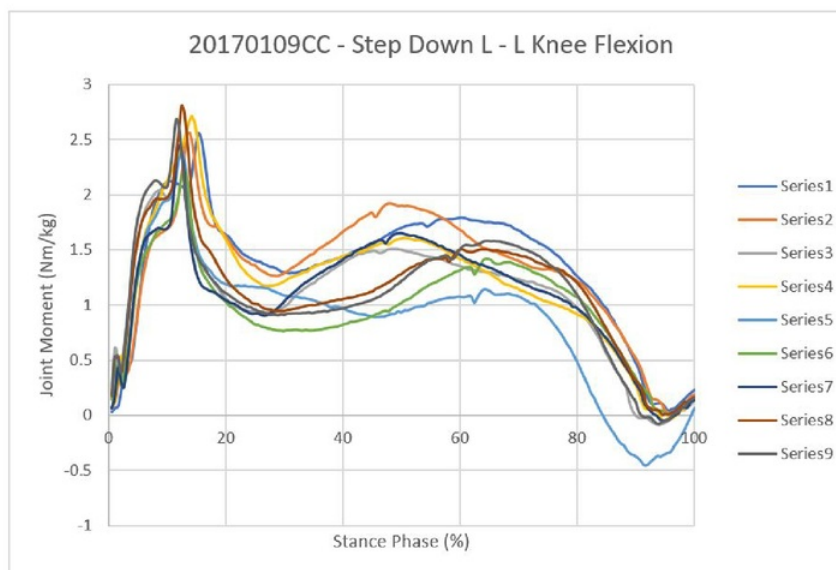
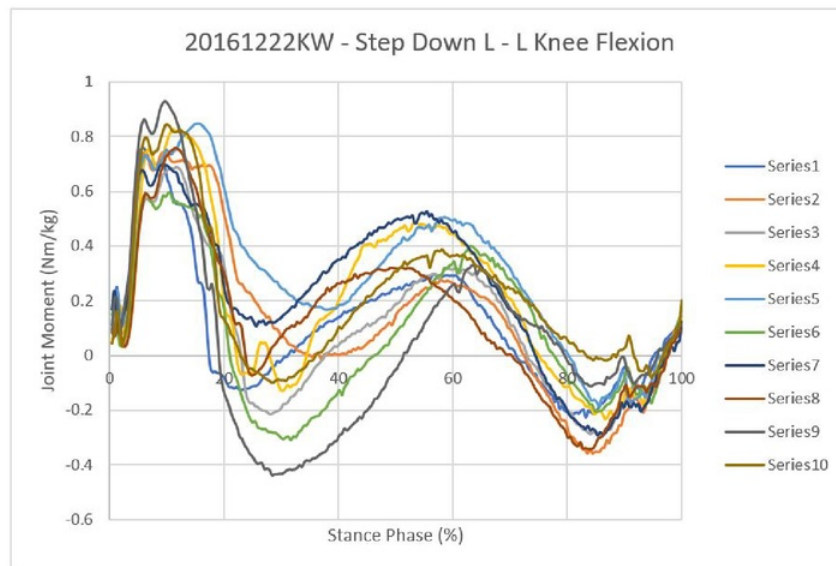


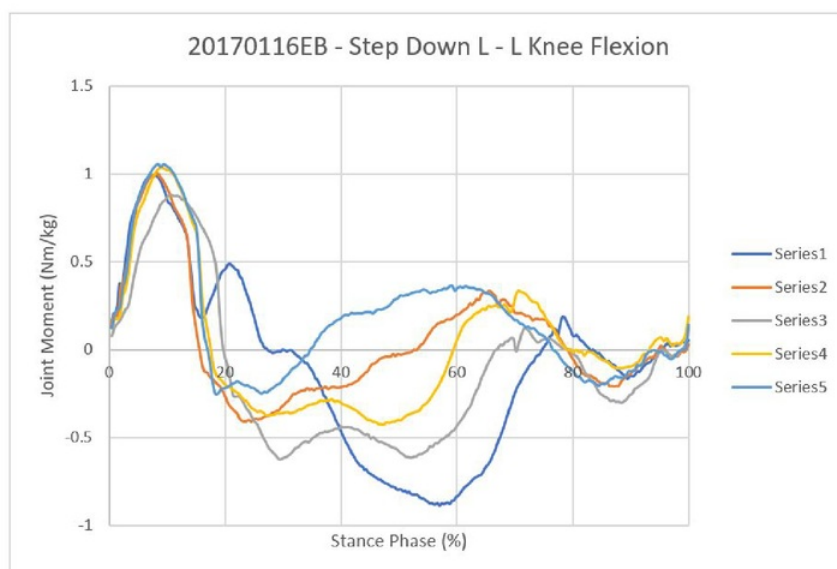
### C.2.3 Stair Descent

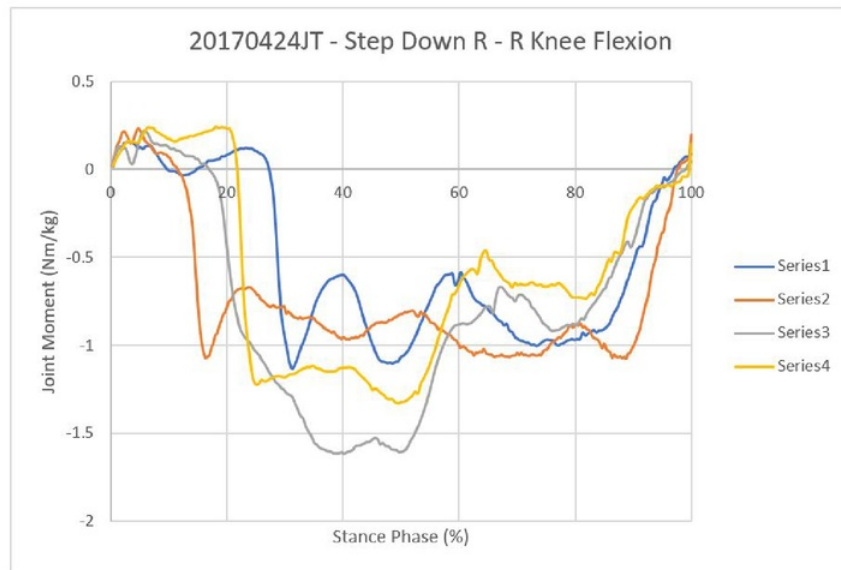














# Appendix D




















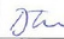
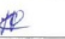



## Attendance Form

### D.1 Overview

This section displays the meetings that occurred with my supervisor.

### D.2 Consultation Meeting Attendance Form

Consultation Meetings Attendance Form

Week	Date	Comments (if applicable)	Student's Signature	Supervisor's Signature
1	4/08/17	* Updated supervisor on my progress report		
2	7/08/17	* Reviewed progress on my code		
3	15/08/17	* Antti's filter discussion		
4	24/08/17	* Discussion of results		
5	28/08/17	* Progress on report & results		
6	5/09/17	* Filter for TRC files		
7	14/09/17	* Results discussion		
8	28/10/17	* Analysing graphs		
9	9/10/17	* Discussion of data		
10	17/10/17	Results (stats)		
11	23/10/17	Results		
12	31/10/17	Discussion		



## Bibliography

- [1] V. Pedroia, J. Haefeli, K. Morioka, H.-L. Teng, L. Nardo, R. B. Souza, A. R. Ferguson, and S. Majumdar, "Mri and biomechanics multidimensional data analysis reveals r2-r1 $\rho$  as an early predictor of cartilage lesion progression in knee osteoarthritis," *Journal of Magnetic Resonance Imaging*, 2017.
- [2] L. F. A. Selistre, S. M. Mattiello, T. H. Nakagawa, G. H. Gonçalves, M. Petrella, and R. K. Jones, "The relationship between external knee moments and muscle co-activation in subjects with medial knee osteoarthritis," *Journal of Electromyography and Kinesiology*, vol. 33, pp. 64–72, 2017.
- [3] M. O'connell, S. Farrokhi, and G. K. Fitzgerald, "The role of knee joint moments and knee impairments on self-reported knee pain during gait in patients with knee osteoarthritis," *Clinical Biomechanics*, vol. 31, pp. 40–46, 2016.
- [4] A. I. of Health and Welfare, "Musculoskeletal fact sheet," 2014.
- [5] M. D. Van Manen, J. Nace, and M. A. Mont, "Management of primary knee osteoarthritis and indications for total knee arthroplasty for general practitioners," *The Journal of the American Osteopathic Association*, vol. 112, no. 11, pp. 709–715, 2012.
- [6] B. Gao, M. L. Cordova, and N. N. Zheng, "Three-dimensional joint kinematics of acl-deficient and acl-reconstructed knees during stair ascent and descent," *Human movement science*, vol. 31, no. 1, pp. 222–235, 2012.
- [7] S. Meireles, F. De Groote, S. Van Rossom, S. Verschueren, and I. Jonkers, "Differences in knee adduction moment between healthy subjects and patients with osteoarthritis depend on the knee axis definition," *Gait & Posture*, vol. 53, pp. 104–109, 2017.
- [8] M. A. Marra, V. Vanheule, R. Fluit, B. H. Koopman, J. Rasmussen, N. Verdon-schot, and M. S. Andersen, "A subject-specific musculoskeletal modeling framework to predict in vivo mechanics of total knee arthroplasty," *Journal of biomechanical engineering*, vol. 137, no. 2, p. 020904, 2015.
- [9] H. Uustal and E. Baerga, "Physical medicine and rehabilitation board review," *Demos Medical Publishing: New York, NY, USA*, 2004.

- [10] J. E. Naili, P. Wretenberg, V. Lindgren, M. D. Iversen, M. Hedström, and E. W. Broström, "Improved knee biomechanics among patients reporting a good outcome in knee-related quality of life one year after total knee arthroplasty," *BMC musculoskeletal disorders*, vol. 18, no. 1, p. 122, 2017.
- [11] L. Sosdian, R. Hinman, T. Wrigley, K. Paterson, M. Dowsey, P. Choong, and K. Bennell, "Quantifying varus and valgus thrust in individuals with severe knee osteoarthritis," *Clinical Biomechanics*, vol. 39, pp. 44–51, 2016.
- [12] D. L. Benoit, D. K. Ramsey, M. Lamontagne, L. Xu, P. Wretenberg, and P. Renström, "Effect of skin movement artifact on knee kinematics during gait and cutting motions measured in vivo," *Gait & posture*, vol. 24, no. 2, pp. 152–164, 2006.
- [13] B. F. Mentiplay, L. G. Perraton, K. J. Bower, Y.-H. Pua, R. McGaw, S. Heywood, and R. A. Clark, "Gait assessment using the microsoft xbox one kinect: Concurrent validity and inter-day reliability of spatiotemporal and kinematic variables," *Journal of biomechanics*, vol. 48, no. 10, pp. 2166–2170, 2015.
- [14] K. Lebel, P. Boissy, H. Nguyen, and C. Duval, "Inertial measurement systems for segments and joints kinematics assessment: towards an understanding of the variations in sensors accuracy," *Biomedical engineering online*, vol. 16, no. 1, p. 56, 2017.
- [15] D. C. Sanchez-Ramirez, B. Malfait, I. Baert, M. van der Leeden, J. van Dieën, W. F. Lems, J. Dekker, F. P. Luyten, and S. Verschueren, "Biomechanical and neuromuscular adaptations during the landing phase of a stepping-down task in patients with early or established knee osteoarthritis," *The Knee*, vol. 23, no. 3, pp. 367–375, 2016.
- [16] A. V. Wiik, A. Aqil, M. Brevadt, G. Jones, and J. Cobb, "Abnormal ground reaction forces lead to a general decline in gait speed in knee osteoarthritis patients," *World journal of orthopedics*, vol. 8, no. 4, p. 322, 2017.
- [17] M. Eltoukhy, J. Oh, C. Kuenze, and J. Signorile, "Improved kinect-based spatiotemporal and kinematic treadmill gait assessment," *Gait & posture*, vol. 51, pp. 77–83, 2017.
- [18] D. Ramsey, P. Wretenberg, D. Benoit, M. Lamontagne, and G. Nemeth, "Methodological concerns using intra-cortical pins to measure tibiofemoral kinematics," *Knee Surgery, Sports Traumatology, Arthroscopy*, vol. 11, no. 5, pp. 344–349, 2003.
- [19] L. Taylor, E. Miller, and K. R. Kaufman, "Static and dynamic validation of inertial measurement units," *Gait & Posture*, 2017.
- [20] B. Müller, W. Ilg, M. A. Giese, and N. Ludolph, "Validation of enhanced kinect sensor based motion capturing for gait assessment," *PloS one*, vol. 12, no. 4, p. e0175813, 2017.



- [21] T. D. Collins, S. N. Ghoussayni, D. J. Ewins, and J. A. Kent, "A six degrees-of-freedom marker set for gait analysis: repeatability and comparison with a modified helen hayes set," *Gait & posture*, vol. 30, no. 2, pp. 173–180, 2009.
- [22] B. K. Madeti, S. R. Chalamalasetti *et al.*, "Biomechanics of knee jointa review," *Frontiers of Mechanical Engineering*, vol. 10, no. 2, pp. 176–186, 2015.
- [23] P. Komdeur, F. E. Pollo, and R. W. Jackson, "Dynamic knee motion in anterior cruciate impairment: a report and case study," *Proceedings (Baylor University. Medical Center)*, vol. 15, no. 3, p. 257, 2002.
- [24] A. Baliunas, D. Hurwitz, A. Ryals, A. Karrar, J. Case, J. Block, and T. Andriacchi, "Increased knee joint loads during walking are present in subjects with knee osteoarthritis," *Osteoarthritis and cartilage*, vol. 10, no. 7, pp. 573–579, 2002.
- [25] K. Manal and W. Rose, "A general solution for the time delay introduced by a low-pass butterworth digital filter: An application to musculoskeletal modeling," *Journal of biomechanics*, vol. 40, no. 3, pp. 678–681, 2007.
- [26] T. N. Babu, T. M. Raj, and T. Lakshmanan, "1267. application of butterworth filter for fault diagnosis on journal bearing," *Journal of VibroEngineering*, vol. 16, no. 3, 2014.
- [27] K. S. Erer, "Adaptive usage of the butterworth digital filter," *Journal of biomechanics*, vol. 40, no. 13, pp. 2934–2943, 2007.
- [28] G. Wang and K. Wang, "Study and design of exponential and butterworth low-pass filters used for digital speckle interference fringe filtering," *Optik-International Journal for Light and Electron Optics*, vol. 124, no. 24, pp. 6713–6717, 2013.
- [29] S. L. Delp, J. P. Loan, M. G. Hoy, F. E. Zajac, E. L. Topp, and J. M. Rosen, "An interactive graphics-based model of the lower extremity to study orthopaedic surgical procedures," *IEEE Transactions on Biomedical engineering*, vol. 37, no. 8, pp. 757–767, 1990.
- [30] D. V. é. l. D ' i a and S. S. M. Guti 'e rrez, "Biomechanics and motor control of human movement," *XIKUA Bolet ' i n Cient ' i from the Upper School of Tlahuelilpan*, vol. 1, no. 1, 2013.